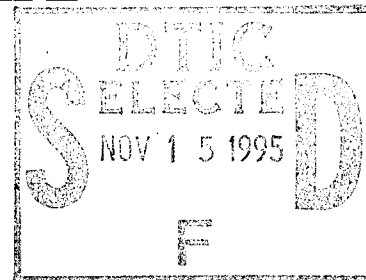# ADVANCED COMPRESSOR FOR LONG LIFE SPACE CRYOCOOLERS

Peter W. Curwen
Warren D. Waldron

Mechanical Technology Inc.
968 Albany-Shaker Road
Latham, New York 12110

DTIC
SELECTE
NOV 1 5 1995
F

19951113 022

November 1994

Final Report

PHILLIPS LABORATORY
Space and Missiles Technology Directorate
AIR FORCE MATERIEL COMMAND
KIRTLAND AIR FORCE BASE, NM 87117-5776

AD NUMBER

AD- B205 080

NEW LIMITATION CHANGE

TO

DISTRIBUTION STATEMENT A -
Approved for public release; Distri-
bution unlimited.

Limitation Code: 1

FROM

DISTRIBUTION STATEMENT -

Limitation Code:

AUTHORITY

Janet E. Mosher, Phillips Lab., Kirtland AFB, N.M.

This final report was prepared by Mechanical Technology Inc., Job Order 21021002. The Laboratory Project Officer-in-Charge was Capt Jeffrey Wiese (VTPT).

This technical report has been reviewed and is approved for publication.

FOR THE COMMANDER

JEFFREY WIESE, Capt, USAF
Project Officer

DAVID KRISTENSEN, Lt Col, USAF
Chief, Space Power and Thermal
Management Division

HENRY L. PUGH, JR., Col, USAF
Director of Space and Missiles Technology

The following notice applies to any unclassified (including originally classified and now declassified) technical reports released to "qualified U.S. contractors" under the provisions of DoD Directive 5230.25, Withholding of Unclassified Technical Data From Public Disclosure.

<u>NOTICE TO ACCOMPANY THE DISSEMINATION OF EXPORT-CONTROLLED TECHNICAL DATA</u>

1. Export of information contained herein, which includes, in some circumstances, release to foreign nationals within the United States, without first obtaining approval or license from the Department of State for items controlled by the International Traffic in Arms Regulations (ITAR), or the Department of Commerce for items controlled by the Export Administration Regulations (EAR), may constitute a violation of law.

2. Under 22 U.S.C. 2778 the penalty for unlawful export of items or information controlled under the ITAR is up to two years imprisonment, or a fine of $100,000, or both. Under 50 U.S.C., Appendix 2410, the penalty for unlawful export of items or information controlled under the EAR is a fine of up to $1,000,000, or five times the value of the exports, whichever is greater; or for an individual, imprisonment of up to 10 years, or a fine of up to $250,000, or both.

3. In accordance with your certification that establishes you as a "qualified U.S. Contractor", unauthorized dissemination of this information is prohibited and may result in disqualification as a qualified U.S. contractor, and may be considered in determining your eligibility for future contracts with the Department of Defense.

4. The U.S. Government assumes no liability for direct patent infringement, or contributory patent infringement or misuse of technical data.

5. The U.S. Government does not warrant the adequacy, accuracy, currency, or completeness of the technical data.

6. The U.S. Government assumes no liability for loss, damage, or injury resulting from manufacture or use for any purpose of any product, article, system, or material involving reliance upon any or all technical data furnished in response to the request for technical data.

7. If the technical data furnished by the Government will be used for commercial manufacturing or other profit potential, a license for such use may be necessary. Any payments made in support of the request for data do not include or involve any license rights.

8. A copy of this notice shall be provided with any partial or complete reproduction of these data that are provided to qualified U.S. contractors.

<u>D E S T R U C T I O N   N O T I C E</u>

For classified documents, follow the procedures in DoD 5200.22-M, Industrial Security Manual, Section II-19 or DoD 5200.1-R, Information Security Program Regulation, Chapter IX. For unclassified, limited documents, destroy by any method that will prevent disclosure of contents or reconstruction of the document.

DRAFT SF 298

1. Report Date (dd-mm-yy) November 1994	2. Report Type Final	3. Dates covered (from... to) 10/91 TO 7/94	
4. Title & subtitle Advanced Compressor for Long-Life Space Cryocoolers		5a. Contract or Grant # F29601-91-C-0112	
		5b. Program Element # 62601F	
6. Author(s) Peter W. Curwen Warren D. Waldron		5c. Project # 2102	
		5d. Task # 10	
		5e. Work Unit # 02	
7. Performing Organization Name & Address Mechanical Technology Incorporated 968 Albany-Shaker Road Latham, New York 12110		8. Performing Organization Report # 94TR37	
9. Sponsoring/Monitoring Agency Name & Address Phillips Laboratory 3550 Aberdeen Ave SE Kirtland AFB, NM 87117-5776		10. Monitor Acronym	
		11. Monitor Report # PL-TR-94-1139	

12. Distribution/Availability Statement
Distribution authorized to U.S. Government Agencies and their contractors only; Critical Technology; November 1994. Other requests shall be referred to AFMC/STI.

13. Supplementary Notes

14. Abstract

The objective of the program was to demonstrate the advantages (high reliability, low weight, and long life) of hermetically sealed diaphragm-type compressors intended for space cryocooler applications. To accomplish this objective, a "proof-of-concept" compressor was designed, built, and tested. The compressor was designed to drive a 30-K, 0.5-W orifice-pulse-tube cryocooler under development by the National Institute of Standards and Technology (NIST). Compressor design requirements were developed around the pulse-tube cryocooler requirements in an effort to optimize overall cryocooler performance.

During the program, excellent test results were obtained. With the compressor operating within 1.2 percent of its design frequency, stroke, mean pressure, pressure amplitude, and phase angle, the pressure volume (pv) power and estimated compressor efficiency exceeded design values by approximately 4 percent.

15. Subject Terms
compressors, cryocooler,

Security Classification of			19. Limitation of Abstract	20. # of Pages	21. Responsible Person (Name and Telephone #)
16. Report Unclassified	17. Abstract Unclassified	18. This Page Unclassified	Limited	142	Capt Jeffrey Wiese (505) 846-2686

CONTENTS

CONTENTS Concluded

iv

FIGURES

FIGURES Concluded

TABLES

1.0 SUMMARY

This report describes the work accomplished by Mechanical Technology Incorporated (MTI) under Contract F29601-91-C-0112 entitled, "Advanced Compressor for Long-Life Cryocoolers." The objective of the overall program was to demonstrate the advantages (high reliability, low weight, and long life) of hermetically sealed diaphragm-type compressors intended for space cryocooler applications. To accomplish this objective, a "proof-of-concept" compressor was designed to meet Phillips Laboratory requirements, then built and tested.

Phillips Laboratory intended that the compressor be utilized to drive a 30-K, 0.5-W orifice-pulse-tube cryocooler that was being designed and built by the National Institute of Standards and Technology (NIST). Thus, the compressor design requirements were developed around the pulse-tube cryocooler requirements in an effort to optimize the overall cryocooler performance. To accomplish this, MTI and NIST worked together to optimize the parameters that affected both the compressor and the pulse tube. The optimization effort concentrated on minimizing electrical input power and compressor weight.

With these requirements defined, a compressor design analysis study was conducted to establish design point conditions for a two-module, back-to-back compressor. The detail design of a proof-of-concept compressor was then completed. This design differed from the conceptual "flight"-type design studied during the aforementioned design analysis effort in that it employed O-ring type seals instead of welded hermetic closures and was of "bar stock" construction. Otherwise, all significant components (motor, diaphragm, bellows, bearings, etc.) were of a basic design consistent with space-flight hardware design.

Following construction of the proof-of-concept unit, the compressor was tested at design point conditions. The orifice-pulse-tube unit for which the compressor was intended was not available for testing. Instead, a "pulse-tube simulator" was employed to load the compressor. This simulator consisted of an aftercooler, a variable orifice, and an appropriate volume. It allowed the compressor to produce the desired pressure amplitude, phase angle, and pressure volume (pv) power when operated at its design stroke and frequency conditions.

Results of the design point tests were excellent. With the compressor operating between 0.5 and 1.2 percent of its design frequency, stroke, mean pressure, pressure amplitude, and phase angle, the pv power and estimated compressor efficiency exceeded design values by ~4 percent. Given these results, the program demonstrated the performance advantages of a diaphragm-type compressor that uses a moving-magnet-type motor contained in an oil-filled cavity. The low-weight characteristic of these machines (compared with conventional Oxford-type compressors) was also demonstrated during the early design analysis phase of the program.

Long life and reliability were demonstrated by means of appropriate industry-accepted design, analysis, and reliability prediction techniques. Actual endurance and other proof-type testing will be required to fully document the compressor's life and reliability potential.

2.0 INTRODUCTION

The objective of the overall program was to design and demonstrate the advantages (high reliability, low weight, long life) of hermetically sealed diaphragm-type compressors intended for space cryocooler applications. The program was divided into two phases. Phase I involved detail design and analysis activities that concluded with a layout design of a pressure-wave generator designed to interface with a 30-K, 0.5-W pulse-tube cryocooler currently being designed by the NIST. Phase II addressed compressor hardware manufacture and test. As summarized below, this report documents the activities performed during the contract.

Section 3.0, Overview of Advanced Compressor Design, presents the compressor concept, the functions of its major components and subassemblies, and the rationale behind its claimed advantages (high reliability, low weight, long life). A flight-type concept is used to describe the compressor design in this section.

Section 4.0, Compressor Specification, discusses development of the final specification and the system optimization (for minimum weight) efforts involved to arrive at the final specification. The principal optimization variables were operating frequency, motor stroke, and motor type (moving and stationary backiron).

Section 5.0, Subsystem and Component Design, discusses the detail design and/or the selection of the major components and subsystems of the compressor. In particular, it addresses procedures for setting allowable design stresses; the design details of the diaphragm, bellows, motor, porting, bearings; and the selection of the hydraulic fluid. This section also includes a comprehensive summary of all pertinent variables (stresses, displacements, volumes, losses, forces, efficiencies, etc.) for each component.

Section 6.0, Proof-of-Concept Compressor Design, describes the breadboard compressor built and tested during Phase II and emphasizes the differences between this unit and the one described in Section 3.0. It also discusses estimated temperature distributions and the instrumentation incorporated into the proof-of-concept compressor. Photographs of compressor hardware are included.

Section 7.0, Compressor Control and Power Electronics, describes the requirements and function of the compressor control system and its various subsystems.

Section 8.0, Test Program, describes the test program, compressor test results, and compares the results with the design predictions.

Section 9.0, Conclusions, presents the significant conclusions of the Design and Test program.

3.0 OVERVIEW OF ADVANCED COMPRESSOR DESIGN

The advanced cryocooler compressor is a positive-displacement gas compressor that can be configured as either a "pressure wave" compressor for regenerative types of cryocoolers, or as a "through-flow" compressor for recuperative cryocoolers. Stirling-cycle and pulse-tube cryocoolers are examples of regenerative cryocoolers in which the time-averaged helium flow at any point in the cycle is zero. Reversed Brayton, Gifford-McMahon, and Joule-Thomson cryocoolers are examples of recuperative cycles where the average helium flow at any point in the cycle is greater than zero. From a design standpoint, a positive-displacement pressure-wave compressor does not require any flow-producing mechanism, such as pressure-actuated valves or timed ports. It is, therefore, a less complex machine than a through-flow compressor, which requires valves or timed ports to provide a unidirectional flow of gas to the cryocooler cycle.

3.1 Features of Advanced Cryocooler Compressor

The compressor concept being developed has the following features in both its pressure-wave and through-flow configurations:

- The helium gas in the cryocooler cycle is hermetically isolated from the compressor drive system. Consequently, the compressor drive system cannot contaminate the helium with particulate matter or condensible outgassing vapors.

- The compressor does not require any dynamic gas seals within the helium environment. The problems associated with wear debris and life in the case of rubbing seals, and long-term stability and alignment in the case of precision noncontacting clearance seals, are thus eliminated.

- A linear electric motor is used to drive the compressor in a "free-piston" manner that eliminates the need for any kinematic drive mechanism between the reciprocating motor plunger and the helium compression chamber. Furthermore, the linear motor's ac power coil is mounted in the motor's stator assembly, thus eliminating flexing power leads such as are required for "moving-coil" types of motors.

- Simple, rugged oil-lubricated journal bearings are used to support the reciprocating motor plunger. Since bearing loads are very small, bearing life in excess of 100,000 hr is predicted. Since there is no mechanical connection of the motor plunger to the compressor's frame, stroke limitations imposed by mechanical spring or flexure support systems are eliminated.

5

○ Like the Oxford and other reciprocating types of compressors, unbalanced axial forces are intrinsic to the basic compression module of the advanced compressor. However, there are no intrinsic unbalanced radial forces or torsional moments associated with the module. The very low levels of residual vibration required for cryogenic sensor applications can be obtained using the "conventional" back-to-back module arrangement in conjunction with demonstrated electronic vibration control techniques. The compressor can also be configured in a single compression-module arrangement as illustrated shortly.

The above features are strongly focused on providing a compressor with very long life at high reliability levels. In addition, the design implementation of these features is strongly focused on achieving a readily manufacturable, minimum-cost compressor system.

3.2 Compressor Description

Figure 1 is a cross section of the advanced compressor concept configured for driving a regenerative Stirling-cycle or pulse-tube cryocooler. The complete compressor consists of two identical pressure-wave compression modules in back-to-back arrangement for cancellation of first-order unbalanced vibration forces[1]. In the arrangement shown, the two modules share a common compression space; however, the design can also be applied to separated compression spaces. For a pulse-tube cryocooler, the pulse-tube assembly can be directly mounted to the compressor center body as described in Section 6.0 for the Phase II proof-of-concept compressor. In the case of split-Stirling cryocoolers, transfer lines from the compression space would generally be connected to back-to-back displacers.

The compressor shown in Figure 1 consists of two linear-motor-driven, hydraulically actuated, valveless diaphragm compressor modules that function together to generate the helium pressure wave. Welded static seal joints are used throughout to obtain hermetic containment of both the cryocooler helium gas and the hydraulic fluid within the compressor drive modules. Figure 1 is thus representative of a flight-rated design. However, the proof-of-concept compressor that was built and tested in Phase II utilized static O-ring seals for ease of assembly, development modification, and posttest inspections. The degree of hermeticity achieved with O-ring seals will approach that of a welded design, at least for the purposes of laboratory characterization testing.

---

[1]First-order axial vibration forces are canceled by minimizing the magnitude of the difference in the two reciprocating plunger masses at assembly and ensuring that the two plungers operate with identical amplitudes 180 deg out of phase. As is discussed in Section 7.0, the control system has been designed to control both the difference in plunger amplitude and the phase between the two plungers so as to control the first harmonic of axial vibration. Angular vibration is minimized by controlling the amount of coaxial offset between the two plungers during the manufacturing process. There are no inherent time-dependent radial forces that would cause a radial vibration component.

6
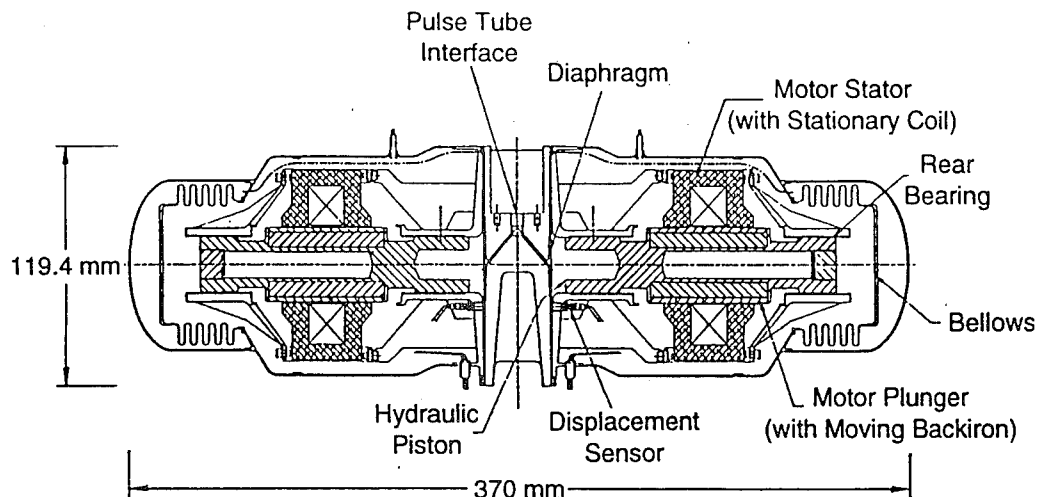
Figure 1. Cross Section of the Advanced Compressor for Regenerative Cryocoolers (Two-Module, Back-to-Back Arrangement)

Figure 2 is a cross-section view of a single-module compressor arrangement that uses a hydraulically coupled counterbalance mass to cancel the momentum of the compressor's reciprocating plunger assembly. This arrangement may have significant cryocooler interfacing and packaging advantages in some applications. This counterbalance-mass technique was used successfully in a 60-Hz hydraulically coupled free-piston Stirling engine/compressor development. However, as with the back-to-back two-module arrangement, electronic vibration control techniques would still be needed to achieve the extremely low levels of residual vibration required for many cryogenic sensor applications.

3.2.1 Method of Helium Compression

Elastic deflection of metallic diaphragms is used to obtain positive-displacement compression of the helium in each compressor module. This method of compression has the following important advantages: (1) hermetic separation is achieved between the helium gas and the drive system hydraulic fluid and (2) dynamic seals are totally eliminated within the helium system[2].

Design of the diaphragms is described in Subsection 5.2. The diaphragms are electron-beam welded to the compressor center body to achieve the hermetic seal. The compressor center body and the two diaphragms can be cleaned and vacuum baked both prior to and following the electron-beam welding process.

---

[2]The diaphragm is fabricated from wrought PH 15-8 Mo. Wrought materials are not known to allow helium or oil permeation unless there are material defects such as tears and porosity that actually form a "tunnel" of sufficient size to permit fluid flow. The final step in the diaphragm fabrication process is a fluorescent-penetrant inspection that ensures material integrity.
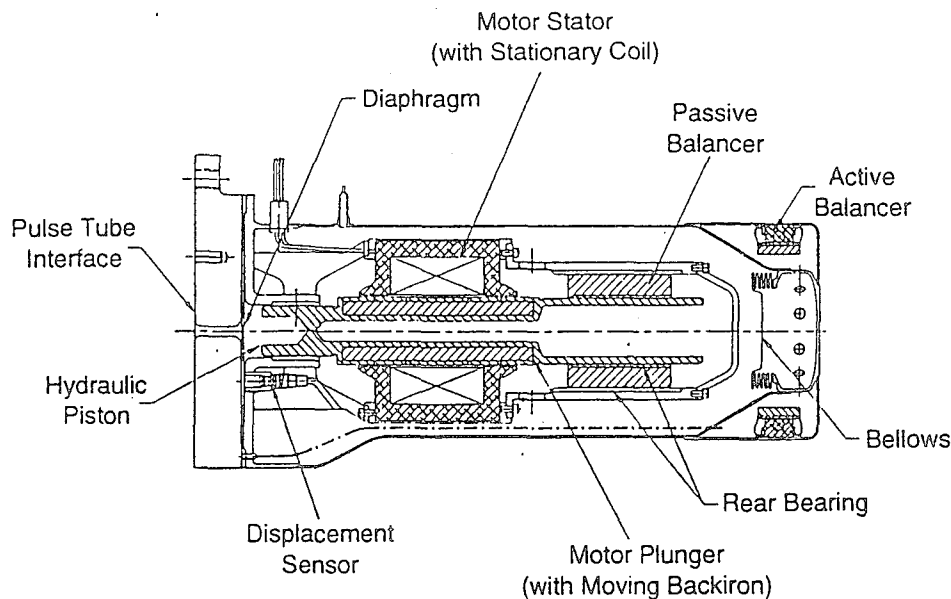
Figure 2. Cross Section of the Advanced Compressor in a Single-Module Arrangement with Hydraulically Coupled Counterbalance Mass

3.2.2 Method of Diaphragm Actuation

The diaphragms are hydraulically actuated using a highly refined synthetic oil selected for its long-term stability and compatibility. (The characteristics of the hydraulic fluid are described in Subsection 5.5.) This method of actuation results in the following advantages:

- Differential pressure loads directly imposed on the diaphragms are minimized, with maximum loading being about 0.05 MPa (7 psi). This results in minimal levels of diaphragm stress.

- The linear motors can be designed for long-stroke operation to minimize their size and weight. Whereas peak-to-peak deflection of the diaphragms will be of the order of 0.2 cm (0.079 in.), peak-to-peak stroke of the linear motors will be ~1.2 cm (0.47 in.).

Hydraulic actuation of each diaphragm is achieved by a piston directly connected to the linear motor plunger. The piston also serves as one of the motor bearings in each of the compressor drive modules.

Each of the pistons is "mid-stroke-ported" to the hydraulic fluid in the drive motor cavity. Mid-stroke-porting provides a means for compensating for any net leakage of hydraulic fluid through the piston clearance seal. The porting action is achieved with totally passive drillways. These drillways communicate the hydraulic cylinder with the drive motor cavity twice each cycle as the piston passes through its mid-stroke region. This porting action provides a very simple means for pumping hydraulic fluid into or out of the hydraulic cylinder depending on the amount and direction of offset in the dynamic mid-stroke position of the motor plunger. This pumping mechanism is utilized for closed-loop control of the mid-stroke position of the diaphragms as

8

described in Section 7.0. Mid-stroke porting has been used extensively in MTI's free-piston machines, with both gas and hydraulic fluid as the working fluid. The porting design for the cryocooler compressor is described in Subsection 5.6.

3.2.3 Compressor Drive

Each compressor drive module contains a linear motor and its associated bearings. The motor drive cavity is completely flooded with hydraulic fluid. Each reciprocating piston/plunger assembly is supported by two journal bearings lubricated by the hydraulic fluid. The bearings are lightly loaded, having to support only the plunger weight when operating in a 1-g environment, plus a small amount of motor magnetic side-pull force arising from inherent magnetic and assembly eccentricities of the motor components. Since the motor cavities are completely flooded, bearing lubrication is ensured during operation in a zero-g environment.

Design of the linear motors and the bearings is described in Subsections 5.4 and 5.7, respectively. The two linear motors will be driven 180 deg out of phase at a common (identical) frequency by a solid-state electronic drive circuit as described in Section 7.0. The concept of the MTI drive circuit is essentially the same as that used for the Oxford compressor. The prototype compressor that was built and tested in Phase II utilized a laboratory version of the drive circuit fabricated from commercially available components.

3.2.4 Pressure-Balancing/Volume-Compensating Bellows

Each of the compressor drive modules shown in Figure 1 contains a metal bellows component. This component provides three important functions.

- It maintains the average hydraulic pressure in the drive motor cavity slightly above the average gas pressure of the module's compression cycle. The gas side of each bellows is connected through a flow restrictor to the helium compression chamber. Since the bellows has very low axial stiffness, the average gas pressure will, in effect, be transmitted through the bellows to the hydraulic fluid within motor drive cavity. The average hydraulic pressure within the compressor drive cavity will thus be close to, but slightly above, the average cylinder pressure at all times.

- The bellows also compensates for volume changes in the hydraulic fluid due to compressibility and thermal expansion effects under all compressor operating and nonoperating conditions. Thermal expansion effects are significant because of the -40 to +65°C range in hydraulic fluid temperature that the compressor is being designed to accommodate.

○ Lastly, the bellows provides dynamic accommodation of the cyclic changes in motor cavity volume that occur due to the swept volume displacement of the compressor piston when compressing gas in the diaphragm compression chamber. These changes occur at compressor frequency, thus imposing a high-cycle fatigue stress on the bellows.

Design of the metallic bellows, including a discussion of life and failure modes, is described in Subsection 5.3.

3.2.5 Compressor Cooling

There are five sources of energy dissipation (losses) within each compressor module. These losses are thermally transferred, primarily by conduction, to the compressor center body from which point they are rejected to the spacecraft heatsink. The five sources of thermal energy loss are listed below and discussed in Sections 5.0 and 6.0.

Thermal Hysteresis Loss in Helium Compression Chamber. This dynamic heat-transfer loss is computed as an integral part of the cryocooler cycle analysis and is reflected in the pv cycle work that must be provided by the compressor.

Motor Electrical Losses. Motor electrical losses are about equally split between eddy current and hysteresis loss in the lamination iron and i^2R loss in the motor winding.

Bearing Friction Losses. These losses consist of both fluid-film shear losses and sliding friction losses.

Thermal Hysteresis Loss in Bellows Helium Chamber. Since the helium gas within each bellows is subjected to a small dynamic pressure wave, gas-to-wall dynamic heat transfer (hysteresis) loss also occurs in this component.

Fluid Flow Losses. Fluid flow losses will occur in the motor "air" gap due to shearing velocity of the plunger and in the motor cavity due to back-and-forth shuttle flow of the hydraulic fluid as the motor plunger reciprocates.

The major features and operating principles of the advanced cryocooler compressor concept have been described. The following sections document the Phase I engineering design of the proof-of-concept compressor that was built and tested during Phase II.

10

4.0 COMPRESSOR SPECIFICATION

Early in Phase I, Phillips Laboratory selected a two-stage orifice-pulse-tube cryocooler as the cycle for which the demonstrator compressor should be designed. Since the pulse tube is a regenerative cycle, this selection dictated that a "pressure-wave" configuration of the compressor be developed.

In keeping with the goal and objectives of this demonstration program, representative mission requirements for the compressor design were specified by Phillips Laboratory as shown in Table 1. Compressor operating requirements for driving a two-stage orifice-pulse-tube were provided (via Phillips Laboratory) by Dr. Ray Radebaugh of the NIST, and these are also shown in Table 1. Table 2 presents the significant design point conditions established for the two-module, back-to-back compressor design resulting from the Phase I effort.

The compressor pressure angle shown in Table 1 is the phase angle between the fundamental harmonics of cylinder pressure variation and cylinder volume (or piston displacement) variation. Figure 3 defines this phase angle parameter and qualitatively illustrates the relationship between compressor cylinder pressure and pressure in the pulse tube.

In addition to the compressor operating requirements, Dr. Radebaugh defined the compressor-to-pulse-tube mounting interface requirements. These requirements are reflected on the proof-of-concept compressor design layout discussed in Section 6.0.

As mentioned previously, one of the Phase I requirements was to optimize the compressor design for minimum mass consistent with good pulse tube performance. Since compressor pv power and pressure conditions were fixed, only three parameters were available for compressor design optimization: compressor (pulse tube) frequency, motor stroke, and type of linear motor (moving backiron versus stationary backiron).

It is well known that increasing frequency (speed) of any compressor is the most direct route for reducing compressor mass. However, for resonant operation of a reciprocating free-piston machine, there are limits on maximum compressor frequency based on the ability to achieve resonant operation of the compressor. Maximum resonance frequency is dependent on the maximum achievable ratio of system "spring" stiffness to reciprocating mass. Furthermore, pulse tube technology is still in the formative stage, and it is not clear yet how high in frequency this type of cryocooler can go before significant performance degradation sets in.

Table 1. Representative Mission Requirements

Phillips Laboratory Requirements
Operational Life: >100,000 hr
Reliability: 95 percent at 60 percent confidence level
Power source: 28 V dc ±20 percent
Compressor Residual Vibration: < 0.1 N rms
Compressor Design Envelope: compatible with pulse-tube installation
Compressor Ambient Temperatures Minimum nonoperating: -40° C Minimum operating: 0° C Nominal operating: 27° C Maximum operating: 50° C
Compressor Frequency: 40 Hz[a]
NIST Compressor Operating Requirements
Gas: Helium
Mean Pressure: 2.0 MPa
Pressure Ratio: 1.5 nominal
Compressor Pressure Angle: 40 deg ±5 deg
Compressor PV Power: 250 W nominal

[a]Optimized for minimum compressor mass, but not to detriment of pulse-tube performance.

Table 2. Siginificant Design Point Conditions for Two-Module, Back-to-Back Compressor

Clearance Volume Ratio: 0.10
Swept Volume: 15.45 cc
Plunger Stroke: 12 mm
Motor Electrical Efficiency: 85.4 percent
Compressor Mechanical Efficiency: 97.7 percent
Compression Space Hysterisis Loss: 20.2 W
Motor Input Power: 324 W
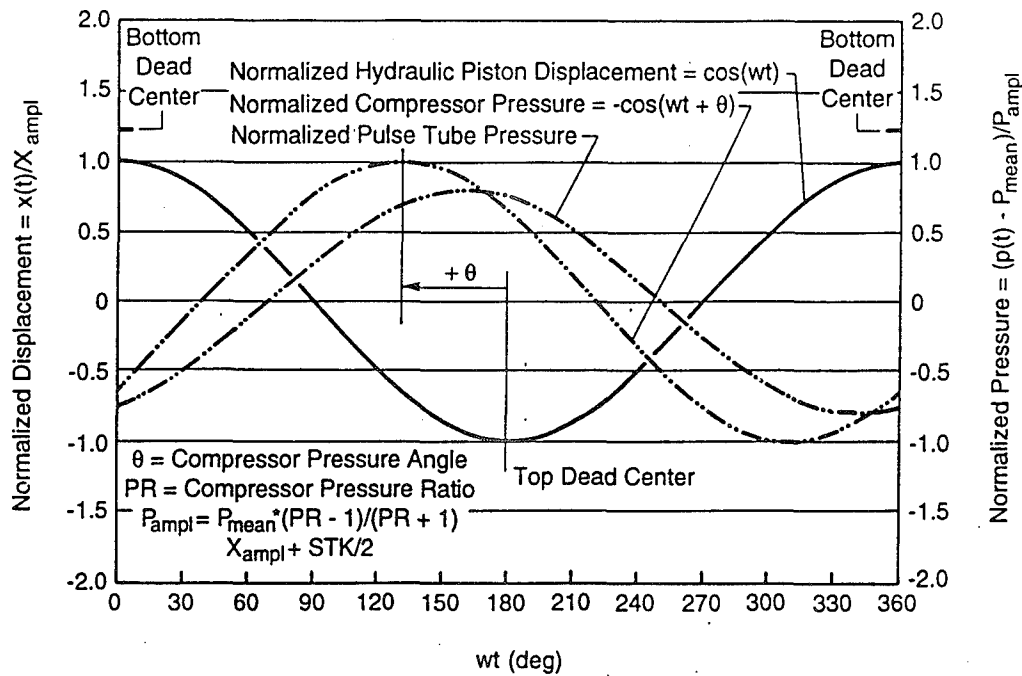
Figure 3. Nomenclature for Orifice-Pulse-Tube Compressor

Since mass of the linear motor materials typically represents 40 to 50 percent of total compressor mass, motor stroke is another parameter that has a sizable optimizing effect. It was expected from previous studies that there would probably be a value of stroke that would minimize compressor mass, all other factors being equal.

Finally, the type of linear motor has an influence on maximum achievable resonant frequency and, therefore, motor size and mass. The reciprocating mass of a stationary backiron motor will always be less than that of a moving backiron motor designed for the same power rating and stroke. However, this does not necessarily mean that the total mass of a compressor driven by a stationary backiron motor will be less.

Early in Phase I, design surveys were conducted to evaluate the effect of the three compressor optimization parameters: frequency, motor stroke, and motor type. Figure 4 shows the effect of frequency on several compressor parameters. For this plot, stationary backiron motors operating at 1.4-cm stroke were designed at four values of frequency. Several compressor layouts were then prepared to estimate overall compressor size and weight. It was found from these layouts that the weight of the motor materials was ~45 percent of the total weight of the compressor. This 45-percent ratio was then used to estimate total compressor weight for the balance of the design survey calculations.

Figure 4 shows that doubling the frequency from 30 to 60 Hz reduced estimated compressor mass from 9 to 5 kg, with the greatest percentage reduction occurring between 30 and 40 Hz. The upper dashed curve of Figure 4 shows the amount of reciprocating mass needed to

achieve resonant operation of the compressor. The lower dashed curve shows the reciprocating mass of just the motor's magnets. The difference between these two curves represents the amount of mass that can be allocated to the rest of the reciprocating plunger assembly. Typically, an allowance of twice the magnet mass for the rest of the plunger structure represents about the lightest plunger assembly obtainable. Consequently, as the curve of required resonance mass approaches twice the value of magnet mass, the feasibility of designing the compressor for higher frequency operation becomes problematic. Figure 4 indicates that 60 Hz is probably close to the upper limit of frequency at which resonant operation can be maintained.

Figure 5 is similar to Figure 4 except that the stationary backiron motors were all designed for a 2.25-cm stroke. Although the increased stroke resulted in a small increase in compressor mass at all frequencies, the most significant effect of increasing stroke was a 33-percent reduction in the upper frequency limit for resonant operation, from 60 Hz down to 40 Hz. The reasons for this reduction were (1) an increase in motor magnet mass and (2) a decrease in spring stiffness available from the compressor gas cycle. At 40 Hz, Figure 5 shows the estimated total compressor mass to be almost 7.5 kg, as compared to 5 kg from Figure 4 at 60 Hz. These two plots clearly show the significant influence of both frequency and motor stroke on compressor mass.
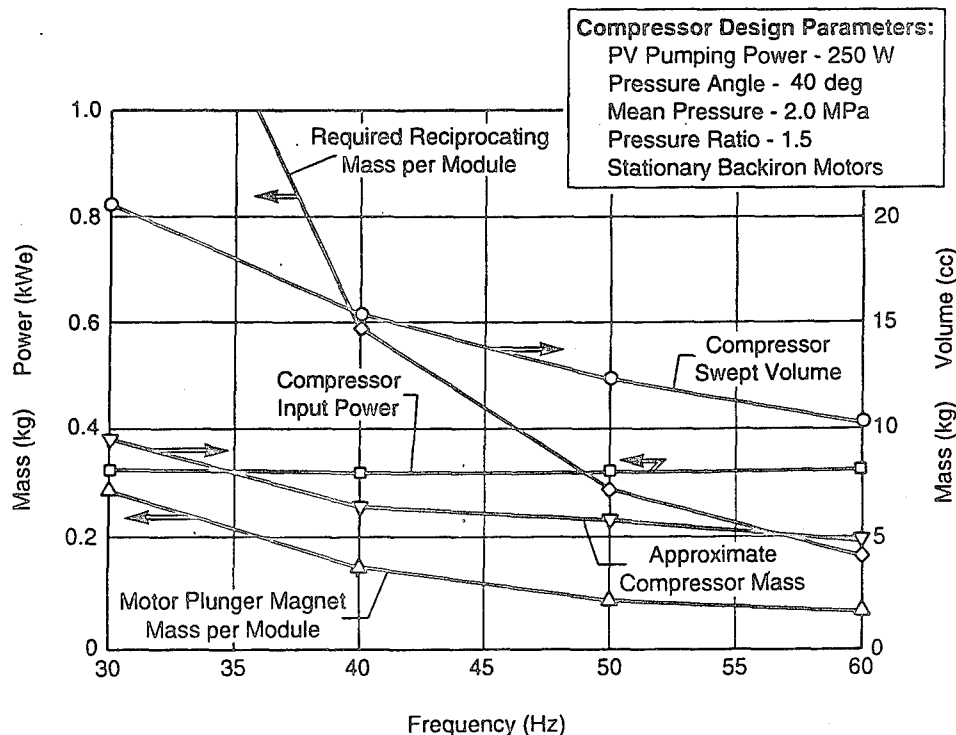
Figure 4. Effect of Frequency on Compressor Designs Using Stationary Backiron Motors Operating at 1.4-cm Stroke
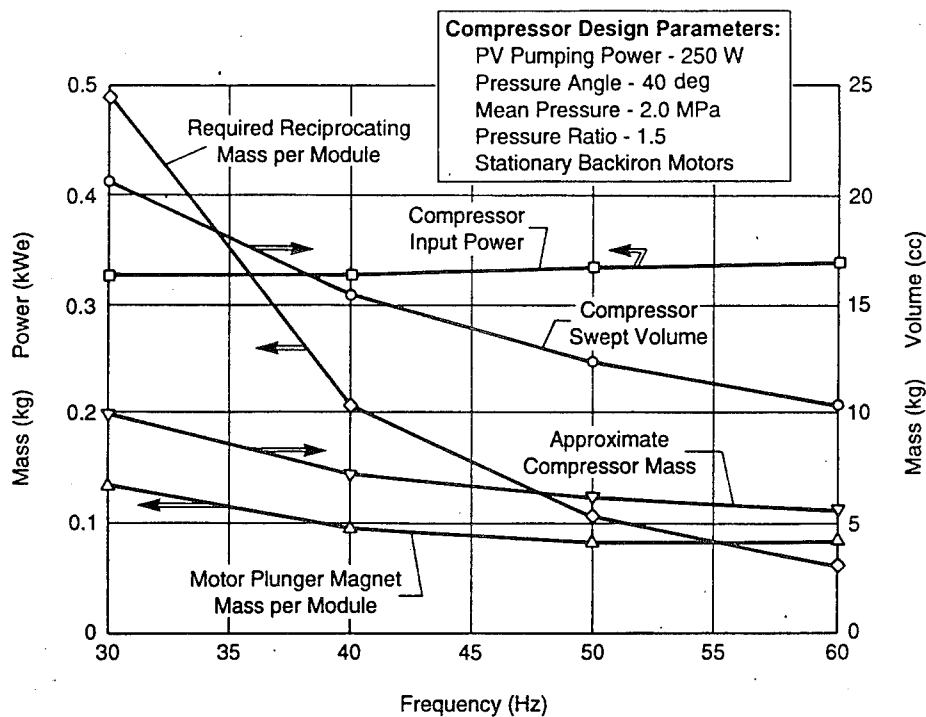
**Figure 5. Effect of Frequency on Compressor Designs Using
Stationary Backiron Motors Operating at 2.25-cm Stroke**

Although some pulse-tube testing has been reported at 40 Hz, no data has yet been published at higher frequencies. While a 60-Hz compressor design appears feasible (and many 60-Hz resonant compressors have been built by MTI), Dr. Radebaugh recommended that 40 Hz be selected for the proof-of-concept compressor because of insufficient pulse-tube performance data at higher frequencies.

At 40 Hz, Figure 4 shows the allowance for plunger structure mass to be more than two times the magnet mass. This suggested that a moving backiron motor, with its heavier plunger mass, should be feasible at 40 Hz. Since fabrication of a moving backiron plunger is simpler than a stationary backiron plunger, design surveys were next performed for moving backiron motors at different strokes while holding frequency constant at 40 Hz.

Figure 6 shows the effect of motor stroke on the various compressor parameters for moving backiron motors operating at 40 Hz with constant compressor swept volume of 15.45 cc. The plot is based on motor designs at six stroke values. It is seen that while total compressor mass is minimized at a stroke of 1.6 cm, a lesser stroke is required to have sufficient allowance for plunger structure mass while maintaining resonance at 40 Hz. Compressor layout studies indicated that a motor stroke in the range of 1.2 to 1.3 cm could satisfy a 40-Hz resonance frequency.

Also shown in Figure 6 is a curve of predicted bearing life. It is seen that bearing life increases with decreasing stroke. This results from the combined interactions of plunger velocity and bearing (i.e., piston) diameter with the net effect being a decrease in the bearings' wear pv, and hence increased life, with decreasing stroke.

In summary, the results of the compressor optimization studies showed that a 60-Hz compressor, using a stationary backiron motor, would yield a feasible, minimum-mass resonant compressor design. Estimated total compressor mass would be about 5 kg. However, in view of the still-emerging state of pulse-tube technology, a 40-Hz compressor frequency was selected with an attendant 40-percent increase in compressor weight (to ~7 kg). Because of the reduced operating frequency, a moving backiron motor could be used instead of the more complex (from a fabrication standpoint) stationary backiron motor. However, it should be emphasized that the stationary backiron motor is a feasible motor for this application. If it can be demonstrated that satisfactory pulse-tube (or Stirling) cryocooler performance can be obtained at 50 or 60 Hz, then substantial compressor weight reduction would be available by increasing compressor frequency.
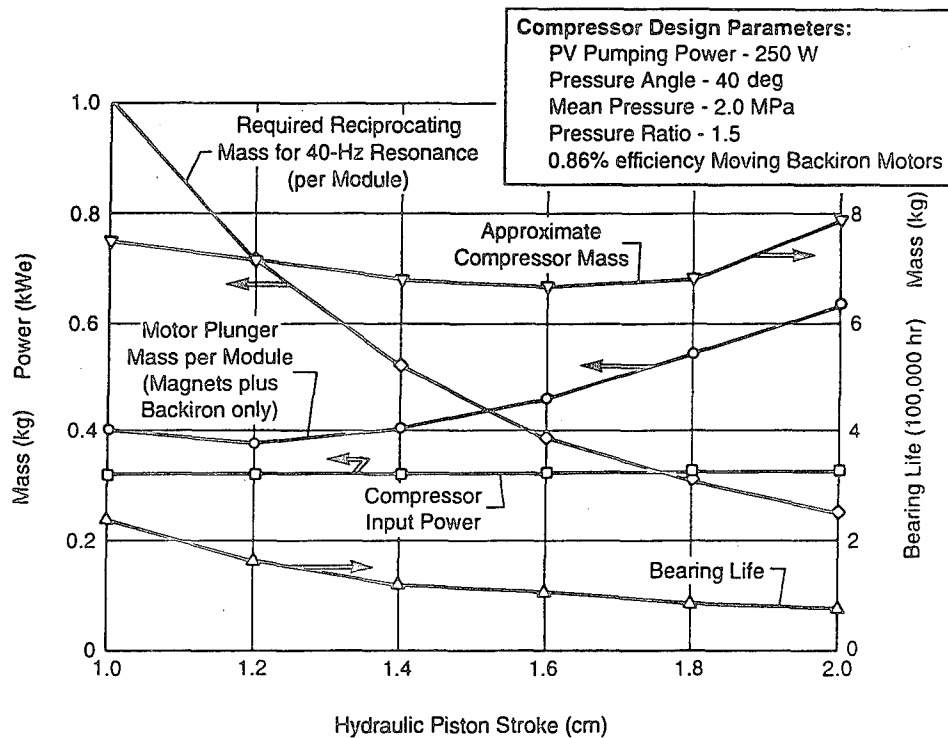
Figure 6. Effect of Motor Stroke on Compressor Designs Using Moving Backiron Motors Operating at 40 Hz

5.0 SUBSYSTEM AND COMPONENT DESIGN

The advanced cryocooler compressor, in its entirety, consists of two major subsystems:

- A mechanical subsystem (including the linear drive motors) that accomplishes helium compression when electric power is applied to the drive motors
- An electronic subsystem that drives and controls the mechanical subsystem.

Since the advanced aspects of the compressor concept reside only in the mechanical subsystem, almost all of the Phase I engineering effort was focused on design of this subsystem. A compressor of this type does not currently exist. Consequently, availability of off-the-shelf components is very limited. Most of the key components had to be custom designed using criteria and procedures applicable to the life and reliability requirements listed in Section 4.0. To a large extent, this represented "original" engineering design effort.

The electronic subsystem, on the other hand, is conceptually similar to the electronic subsystems currently being flight tested for Stirling cryocoolers. The major difference will be in power level. (The proof-of-concept compressor will deliver 6.8 times more pv power than that delivered by current generation Oxford compressors for 80-K Stirling cryocoolers.) To a very large extent, operation of the proof-of-concept compressor will be accomplished using an electronic subsystem composed of commercially available sensors and electronic components. Accordingly, aside from defining the control system in terms of functional requirements, minimal engineering effort was applied to the electronic subsystem during Phase I. This subsystem is described in Section 7.0.

Table 3 is an extensive tabulation of pertinent design data for the mechanical subsystem of the proof-of-concept compressor built and tested during Phase II. Data are presented for nominal design point operation as well as for three off-design operating conditions. The following paragraphs discuss key aspects of the mechanical subsystem design in more detail. Overall design of the proof-of-concept compressor system is provided in Sections 6.0 and 7.0.

5.1 Procedure for Setting Allowable Component Design Stresses

It is clear from the description of the advanced compressor concept in Section 3.0 that the compressor diaphragms and bellows must undergo significant dynamic (periodic) elastic deflections to perform their intended functions. Consequently, these components will be subjected to significant dynamic stresses. Based on 100,000 hr of continuous compressor operation at 40 Hz, over 14 billion stress cycles will accumulate. The diaphragms and bellows

Table 3. Design Data for Phase II Compressor for 30-K Orifice-Pulse-Tube Cryocooler (Based on mean pressure, pressure ratio, pv power, and pressure angle estimates provided by the NIST)

> Boxed values are input values for various compressor design & operating conditions.

Moving backiron motor

			Symbol	Units	Fixed Values Metric	Fixed Values English	Design Stroke	Lower Stroke	Lower Freq	Max Stroke
							Various Operating Conditions			
11	Cryocooler rating-point conditions									
12	Frequency		F	hz			40.0	40.0	35.0	40.0
13	Cooling capacity		Qr	W	0.500					
14	Temperature		Tr	K	30.0	290.0				
16	Compressor rating-point conditions									
17	Pressure ratio		PR		1.50					
18	Mean pressure		Pmean	MPa (psia)	2.000	290.0				
19	Clearance volume ratio (to point of		CVR		0.100					
20	cryocooler interface)									
21	Percentage of compressor dead volume		%UDV		30.0%					
22	which is unsweepable by diaphragm									
23	Pressure amplitude		Pampl	MPa (psi)	0.400	58.00				
24	Estimated PV pumping power (total)		PVp	W			250.00	225.00	218.70	285.00
25	Total swept volume		SV	cc			15.450	14.162	15.450	17.614
26	Total dead volume		DV	cc			1.545	1.416	1.545	1.761
27	Pressure angle (phase shift of 1st		ef	deg			40.078	39.209	40.067	40.075
28	harmonic of pressure relative to									
29	negative piston displacement based									
30	on pumping power only)									
31	Power dissipation due to compressor		PVhys	W			27.16	24.89	26.88	30.96
32	gas-to-wall cyclic heat transfer									
33	Total compressor PV power		PVt	W			277.16	249.89	245.58	315.96
34	Total pressure angle		θ	deg			45.54	44.59	46.29	45.54
35										

Table 3. Continued.

#	Description	Symbol	Units				
37	Estimated mass of motor EM materials		%	45.0%			
38	as percent of total compressor mass						
39	Estimated compr mass (flight version)	Mc	kg	7.508	7.508	7.508	7.508
41	Compressor rating-point performance						
42	Mechanical efficiency	EFFm		0.919	0.919	0.916	0.918
43	Motor shaft power (total)		kW	0.302	0.272	0.268	0.344
44	Motor electrical efficiency	EFFe		0.851	0.851	0.851	0.851
45	Motor input power (total)		kW	0.354	0.320	0.315	0.404
47	Cryocooler specific cooling power						
48	a) Referenced to piston face	1/COPp	W/W	554.32	499.79	491.16	631.92
49	b) Referenced to motor terminals	1/COPe	W/W	708.66	639.25	630.04	808.85
51	Cylinder sizing parameters						
52	Number of compressor cylinders	Ncyl		2			
53	Hydraulic Piston Stroke	STK	cm	1.20	1.08	1.20	1.37
54			(in)	0.4724	0.4252	0.4724	0.5386
55	Swept volume per cylinder	SVcyl	cc	7.725	7.081	7.725	8.807
56	Mid-stroke volume per cylinder	MSV	cc	4.635	4.635	4.635	4.635
57	Max sweepable volume per cylinder	SVmax	cc	8.807	8.807	8.807	8.807
58	Hydraulic piston area	Ap	cm2	6.4375	6.4375	6.4375	6.4375
59	Hydraulic piston diameter	Dp	cm	2.8629	2.8629	2.8629	2.8629
			(in)	1.1271	1.1271	1.1271	1.1271
61	Diaphragm Data (from PLATEAN analysis)						
62	Max equivalent Von Mises alternating stress for 0.9995 reliability for diaphragm deflecting to limit stops		MPa (psi)	273.03	39600		
65	Diaphragm uniform thickness		cm	0.0378	0.0378	0.0378	0.0378
66	Diaphragm OD	Dd	cm	10.972	10.972	10.972	10.972
67	Diaphragm deflection amplitude at limit stops	Ymax	cm	0.110	0.110	0.110	0.110
68	limit stops						
69	Diaphragm operating amplitude	Yd	cm	0.0961	0.0881	0.0961	0.1096
70	Diaphragm TDC head clearance		cm	0.0135	0.0215	0.0135	-0.0000
71			(in)	0.0053	0.0085	0.0053	-0.0000
72	Diaphragm elastic stiffness	Kd	N/cm	4001.9	4001.9	4001.9	4001.9
73	Diaphragm pressure area	Ad	cm2	94.56	94.56	94.56	94.56
74	Diaphragm equivalent piston area	Adeq	cm2	40.193	40.193	40.193	40.193

1/7/93

19

Table 3. Continued.

#	Description	Symbol	Units				
77	Bellows Data						
78	Bellows equivalent piston area	Ab	cm2	37.742	37.742	37.742	37.742
79	Bellows gas volume (undeflected)	Vb	cc	140.00	140.00	140.00	140.00
80	Bellows internal surface area	SAb	cm2	415.90	415.90	415.90	415.90
81	Bellows elastic stiffness	Kb	N/cm	78.80	78.80	78.80	78.80
82	Bellows effective mass (with end cap)	Mb	kg	0.064	0.064	0.064	0.064
83	Bellows deflection amplitude						
84	a) at piston swept volume	Yb	cm	0.102	0.094	0.102	0.117
85	b) at limit stops		cm	0.117	0.117	0.117	0.117
86	Bellows gas volume at nominal						
87	operating point (nop)	Vbnop	cc	128.06	128.06	128.06	128.06
88	Bellows pressure amplitude at						
89	piston swept volume & nop	Pbnop	MPa	0.1058	0.0966	0.1058	0.1213
90			(psi)	15.34	14.01	15.34	17.59
91	Bellows axial natural frequency		hz	87.4	87.6	87.2	87.4
93	Motor data per cylinder (from LPMMA and QUICK-D) Magnet Thickness			0.055"	0.055"	0.055"	0.055"
94	Motor type: Stationary backiron = 0			1	1	1	1
95	Moving backiron = 1						
96	Electrical efficiency	EFFe		0.851	0.851	0.851	0.851
97	Magnetic axial stiffness	Km	N/cm	67.60	67.60	67.60	67.60
98	Magnetic side-pull gradient	Ksp	N/cm	7172.0	7172.0	7172.0	7172.0
99	Stator mass (motor copper coil and	Ms	kg	1.1240	1.1240	1.1240	1.1240
100	stator lamination iron only)						
101	Plunger mass (motor magnets and	Mp	kg	0.5652	0.5652	0.5652	0.5652
102	moving backiron only)		(lbm)	1.246	1.246	1.246	1.246
103	Required shaft power	Spwr	W	150.77	136.00	134.04	172.08
104	Input power (at coil terminals)		W	177.17	159.81	157.51	202.21

1/7/93

20

Table 3. Continued.

#		Symbol	Units				
107	Stiffness data per cylinder						
108	Gas-spring stiffnesses referenced to						
109	hydraulic piston face						
110	a) Cylinder stiffness	Kgc	N/cm	300.58	339.56	296.58	263.68
111	b) Bellows stiffness	Kgb	N/cm	113.51	115.21	113.51	114.18
112	Diaphragm + bellows elastic stiffness	Ke	N/cm	20.84	20.84	20.84	20.84
113	referenced to hydraulic piston face						
114	Total effective spring rate between	Kt	N/cm	502.53	543.21	498.53	466.30
115	stator and reciprocating plunger			286.97	310.20	284.68	266.28
116	(includes motor axial stiffness)		(lbf/in)				
119	Cylinder module dynamics						
120	Mass of plunger assembly (excluding	Ma	kg	0.22	0.22	0.22	0.22
121	magnets and moving lamination iron)						
122	Effective mass of hydraulic fluid	Moil	kg	0.0371	0.0340	0.0371	0.0423
123	Total effective mass of reciprocating	Mr	kg	0.8241	0.8211	0.8241	0.8293
124	plunger assembly	Mr	(lbm)	1.8169	1.8102	1.8169	1.8284
125	Module α angle (piston velocity	α	deg	-3.10	3.78	16.45	-11.12
126	relative to motor coil force)						
127	Damping ratio			0.326	0.321	0.348	0.272
128	Undamped natural frequency		hz	39.30	40.94	39.14	37.74
129	Module Q $(2\pi W/\delta W)$			1.51	1.59	1.61	1.74
130	(stored energy/dissipated energy)						
131	Peak unbalanced dynamic force for one		N	301.52	293.33	299.12	318.95
132	uncompensated module unit		(lbf)	67.79	65.95	67.25	71.71
133	Unit-to-unit phase angle error		deg	0.1			
134	Unit-to-unit force amplitude mismatch		%	0.1			
135	RMS unbalanced force for two back-to-		N	0.429	0.417	0.425	0.453
136	back modules with phase and amplitude						
137	errors as listed above. (Spec is < 0.1 N)						

1/7/93

21

Table 3. Continued.

BEARING LIFE PREDICTION

Line	Description	Var	Units					
144	Piston frequency		(hz)	40.0	40.0	40.0	35.0	40.0
145	Piston stroke		(in)	0.4724	0.4252	0.4724	0.4724	0.5386
146	Average speed of hydraulic piston	Vavg	(ft/min)	189.0	170.1	170.1	165.4	215.4
147	Magnetic side-pull gradient of motor		(lbf/mil)	4.096	4.096	4.096	4.096	4.096
148	Bearing diameter (same as piston)	Dp	(in)	1.127	1.127	1.127	1.127	1.127
149	Bearing length/diameter ratio	L/D		1.00				
150	Bearing radial clearance ratio (new)	C/R		0.0010				
151	Surface finish of bearing sleeve	RMSs	(μ-in rms)	16				
152	Surface finish of bearing journal	RMSj	(μ-in rms)	8				
153	Radial offset of motor side-pull	ECCsp	(mils)	2.50				
154	gradient due to "as built" magnetic							
155	plus mechanical eccentricities							
156	Total length of two motor bearings	TLbrg	(in)	2.254	2.254	2.254	2.254	2.254
157	Radial clearance of motor brgs (new)	Cnew	(mils)	0.56	0.56	0.56	0.56	0.56
158	Permissible radial wear of motor	WEAR	(mils)	1.50	1.50	1.50	1.50	1.50
159	bearings at end of life							
160	Radial clearance of motor brgs at	Ceof	(mils)	2.06	2.06	.2.06	2.06	2.06
161	end of life							
162	Average bearing radial clearance	Cavg	(mils)	1.31	1.31	1.31	1.31	1.31
163	Average load on each motor bearing due	Fb	(lbf)	7.809	7.809	7.809	7.809	7.809
164	to motor side-pull gradient (zero-g)		(psi)	6.147	6.147	6.147	6.147	6.147
165	Boundary layer lubrication conditions							
166	1) Hydrodynamic pressure for load	PSIoil	(psi)	23.75	23.75	23.75	23.75	23.75
167	supported only by 30° bearing arc							
168	2) Boundary layer film thickness	h	(in)	5.2E-05	4.9E-05	4.9E-05	4.9E-05	5.5E-05
169	3) Fraction of load supported by	Lfract		56.7%	58.9%	59.5%	59.5%	53.8%
170	contact of surface asperities							
171	Average bearing wear PV value	WPV	(psi-ft/min)	1161.6	1045.4	1016.4	1016.4	1324.2
172	Bearing wear factor (See Note 1 below)	WF	(in3-min/lbf-ft-hr)	1.9E-11				
173	Predicted bearing life based on wear PV		(hr)	119876	128172	130561	130561	110890
174	adjusted for surface asperity fraction							

Note 1: The wear factor value (line 172) is for water-lubricated carbon-graphite face seals running against tungsten carbide at a PV value of 420,500 psi-ft/min. It is documented that wear factor values for water-lubricated face seals decrease with decreasing PV. This fact is taken into account by reducing average bearing PV (line 171) by factor Lfract (line 169) when computing bearing life.

1/7/93

22

Table 3. Continued.

COMPRESSOR HYDRAULIC AND FRICTION LOSSES (For one drive module)
===

#	Description	Symbol	Units				
184	Properties of hydraulic fluid						
185	Type of fluid: Royco 602 (MIL-C-87252)						
186	Fluid temperature		°C	40.0			
187	Kinematic viscosity		cst	5.19			
188	Thermal expansion coeff (0-50 C)	αoil	1/°C	8.1E-04			
189	Thermal conductivity (37.8 C)		cal/hr-cm-C	1.21			
190	Specific heat (37.8 C)		cal/g-C	0.54			
191	Density	Γoil	g/cc	0.8			
192	Kinematic viscosity		m2/s	5.19E-06			
193	Absolute viscosity (μ)	μ	N-s/m2	4.15E-03			
194	Thermal conductivity (37.8 C)	koil	W/m-K	1.41E-01			
195	Specific Heat (37.8 C)	Cp	W-h/kg-K	6.28E-01			
197	Motor Gap Fluid Friction Loss						
198	Velocity amplitude of motor plunger	Vpk	m/s	1.508	1.357	1.319	1.719
199	Length of stator air gap		cm	4.830	4.830	4.830	4.830
200	Diameter of magnet OD surface		cm	4.140	4.140	4.140	4.140
201	Motor radial oil-filled clearance		cm	0.060	0.060	0.060	0.060
202	Motor gap fluid friction loss:	Pgap	W	0.049	0.040	0.038	0.064
204	Motor Bearings Friction Loss						
205	Bearing average eccentricity ratio	ϵ		0.969	0.971	0.971	0.966
206	Bearing eccentricity "j" factor	j		4.030	4.167	4.204	3.869
207	Loss due to fluid-film shear (1 brg)		W	0.515	0.409	0.385	0.687
208	Loss due to asperity contact (assuming		W	1.512	1.415	1.389	1.635
209	0.08 coefficient of friction) (1 brg)						
210	Total power loss for 2 brgs:	Pbrg	W	4.056	3.648	3.548	4.643
212	Wall Flow Loss						
213	Ratio of Wall flow loss/Wall area		W/m2	23.23	18.82	16.64	30.19
214	Total wall area		cm2	660.0	660.0	660.0	660.0
215	Ratio of average fluid velocity to						
216	plunger velocity			0.2			
217	Laminar flow loss increased 10 times	Pwall	W	0.613	0.497	0.439	0.797
218	to account for possible turbulence						
219	effects						

1/7/93

Table 3. Continued.

STATIC DEFLECTIONS OF BELLOWS AND DIAPHRAGM
===

224	Total volume of oil in one compressor	Vfill	cc	586.0			
225	module at charging temperature of						
226	294 K (70 F)						
227	Static deflection of bellows at	Ybchrg	mm	-0.261			
228	charging temperature						
229	1) + value = bellows extension						
230	2) - value = bellows compression						
231	Ratio of static diaphragm deflection	Yd/Yb		0.0493	0.0493	0.0493	0.0493
232	to static bellows deflection						
233	static deflection of diaphragm at	Ydchrg	mm	-0.013	-0.013	-0.013	-0.013
234	charging temperature						
235	oil differential pressure at charge	Pchrg	MPa	-0.0005	-0.0005	-0.0005	-0.0005
236	(Pmean bellows - Pmean oil)		(psi)	-0.079	-0.079	-0.079	-0.079
238	Minimum compressor storage temperature	Tmin	C	-40.0			
239	Minimum oil operating temperature	Tmop	C	0.0			
240	Nominal oil operating temperature	Tnop	C	45.0			
241	Maximum oil operating temperature	Tmax	C	65.6			
243	Change in oil volume (relative to 294 K						
244	charge volume) at following temperatures:						
245	Tmin (minimum storage temp)		cc	-28.95			
246	Tmop (minimum operating temp)		cc	-9.92			
247	Tnop (nominal operating temp)		cc	11.49			
248	Tmax (max allowable temp)		cc	21.29			
250	static deflections and delta-P at Tmin of -40		C				
251	Bellows deflection		mm	7.028	6.681	6.681	6.681
252	Diaphragm deflection		mm	0.347	0.330	0.330	0.330
253	Bellows delta-P		MPa	0.0147	0.0139	0.0139	0.0139
254	(+ value = bellows extension)		(psi)	2.128	2.023	2.023	2.023

1/7/93

24

Table 3. Continued.

257	Static deflections and delta-P at Tmop of 0	C				
258	Bellows deflection	mm	2.244	2.244	2.244	2.244
259	Diaphragm deflection	mm	0.111	0.111	0.111	0.111
260	Bellows delta-P	MPa	0.0047	0.0047	0.0047	0.0047
261	(+ value = bellows extension)	(psi)	0.679	0.679	0.679	0.679
263	Static deflections and delta-P at Tnop of 45	C Ybnop				
264	Bellows deflection	mm	-3.163	-3.163	-3.163	-3.163
265	Diaphragm deflection	mm	-0.156	-0.156	-0.156	-0.156
266	Bellows delta-P	MPa	-0.0066	-0.0066	-0.0066	-0.0066
267	(+ value = bellows extension)	(psi)	-0.957	-0.957	-0.957	-0.957
269	Static deflections and delta-P at Tmax of 65.6	C				
270	Bellows deflection	mm	-5.621	-5.621	-5.621	-5.621
271	Diaphragm deflection	mm	-0.277	-0.277	-0.277	-0.277
272	Bellows delta-P	MPa	-0.0117	-0.0117	-0.0117	-0.0117
273	(+ value = bellows extension)	(psi)	-1.702	-1.702	-1.702	-1.702

AVERAGE PRESSURE FORCE ACTING ON PLUNGER
(During compressor operation)
==================================

279	Pmean of gas in bellows chamber	Pmb	MPa	2.0199		
280	Pmean bellows - Pmean cylinder		MPa	0.0199		
			(psi)	2.8856		
282	Pmean in motor drive cavity					
283	Tnop (minimum operating temp)		MPa	2.0152	2.0152	2.0152
284	Tnop (nominal operating temp)		MPa	2.0265	2.0265	2.0265
285	Tmax (max allowable temp)		MPa	2.0316	2.0316	2.0316
287	Average pressure force acting on plunger					
288	(positive force is towards diaphragm)					
289	Tmop (minimum operating temp)		N	9.795	9.795	9.795
290	Tnop (nominal operating temp)		N	17.062	17.062	17.062
291	Tmax (max allowable temp)		N	20.367	20.367	20.367

1/7/93

Table 3. Continued.

PORTING DESIGN FOR HYDRAULIC CYLINDER
=======================================

Line		Units				
296	Port Configuration					
297	Piston ports (circular)					
298	a) Number of ports		4			
299	b) Diameter of ports	mm	1.524			
301	Cylinder circumferential groove					
302	a) Width of groove	mm	1.524			
303	b) Offset of cylinder-wall groove from	mm	-0.635			
304	plane of piston ports when motor					
305	plunger is axially centered in					
306	stator (C/L groove to C/L ports).					
307	A "+" offset is groove offset					
308	towards motor cavity.					
310	Piston seal					
311	a) Diameter (= brg diameter)	mm	28.629	28.629	28.629	28.629
312	b) Length (from edge of groove to	mm	13.553	13.553	13.553	13.553
313	hydraulic cylinder)					
314	c) Radial clearance (= brg clr)					
315	1) At beginning of life	mm	0.014	0.014	0.014	0.014
316		(mils)	0.56	0.56	0.56	0.56
317	2) At end of life	mm	0.052	0.052	0.052	0.052
318		(mils)	2.06	2.06	2.06	2.06

Table 3. Continued.

The following porting/seal analysis results were computed using MTI's SP code. They are not computed in this spreadsheet.

Line	Description		Unit	Value	
326	Piston operating offset for net zero				
327	change in cylinder oil mass at start-of-life				
328	seal clearance and oil temperature of:				
329	Tmop (minimum operating temp)	mm (mils)	A "+" offset	0.423	(16.7)
330	Tnop (nominal operating temp)	mm (mils)	is towards	0.248	(9.8)
331	Tmax (max allowable temp)	mm (mils)	diaphragm	0.163	(6.4)
333	Piston operating offset for net zero				
334	change in cylinder oil mass at end-of-life				
335	seal clearance				
336	Tmop (minimum operating temp)	mm (mils)	A "+" offset	0.192	(7.6)
337	Tnop (nominal operating temp)	mm (mils)	is towards	-0.327	(-12.9)
338	Tmax (max allowable temp)	mm (mils)	diaphragm	-0.835	(-32.9)
340	Seal leakage at end-of-life clearance				
341	(positive leakage is out of cylinder)				
342	Tmop (minimum operating temp)	g/s		-0.273	
343	Tnop (nominal operating temp)	g/s		-0.753	
344	Tmax (max allowable temp)	g/s		-1.304	
346	EOF seal leakage as a fraction of				
347	cylinder design-point swept volume				
348	Tmop (minimum operating temp)	cc/cc		0.0011	
349	Tnop (nominal operating temp)	cc/cc	approx	0.0030	
350	Tmax (max allowable temp)	cc/cc	approx	0.0053	

Line	Description	Symbol	Unit		Min	Avg	Max
353	Porting loss at seal clearances of		mils	0.4	1.0	1.3	2.0
354	Tmop (minimum operating temp)	Pport	W	1.35	1.86	2.81	5.04
355	Tnop (nominal operating temp)		W	1.41	2.21	3.71	7.20
356	Tmax (max allowable temp)		W	1.45	2.53	4.59	9.39

1/7/93

27

Table 3. Concluded.

BELLOWS HYSTERESIS LOSS

361	Helium Properties						
362	Isentropic exponent	GAM		1.667			
363	Gas Constant	R	J/kg-K	2079			
364	Constant pressure heat capacity	CpHe	kJ/kg-K	5.234			
365	Thermal conductivity at Tnop	kHe	W/m-K	0.160			
366	Heat transfer enhancement factor			2.000			
367							
368	Berchowitz Equation						
369	Lambda factor		W/cm2	11.924	11.924	11.154	11.924
370	Bellows factor		cm2	0.158	0.132	0.158	0.205
371	Bellows hysteresis loss	Pbhys	W	3.760	3.159	3.517	4.887
378	Total Drive Cavity Losses per Compressor Module						
379	Values of Pbrg and Pport used to compute Pmech						
380	are based on average bearing/seal clearance						
381	Pgap + Pbrg + Pwall + Pbhys + Pport	Pmech	W	12.189	11.054	11.252	14.102
382	Compressor "Mechanical" Efficiency	EFFm		0.919	0.919	0.916	0.918
383							
387	Equivalent Viscous Damping Coefficients						
388	Equivalent viscous damping coefficient	Chyd	N-s/cm	0.074	0.086	0.089	0.062 (per module)
389	for all motor cavity hydraulic losses						
390	Equivalent viscous damping coefficient	Cpv	N-s/cm	2.438	2.713	2.821	2.138 (for 2 modules)
391	for total compressor PV power						

1/7/93

28

must be designed to survive their high-cycle fatigue stresses at a level of component reliability that will ensure attainment of the required 95-percent overall compressor system reliability.

Considerable effort was spent during Phase I to develop a methodology for setting maximum allowable design stresses for components that must meet statistical reliability requirements while operating under high-cycle fatigue conditions. Appendix A of this report is a design memorandum that documents the methodology and procedures used during Phase I. This memorandum was reviewed by reliability and stress analysis specialists at Aerospace Corporation who recommended several refinements to the analysis. The effect of these refinements (which would be incorporated in a flight version of the hardware) would be to further reduce the allowable cyclic stresses by about 10 percent relative to the values selected for the proof-of-concept compressor. The stresses selected for the demonstration hardware are still very conservatively rated, by any standards, for a proof-of-concept program.

5.2 Diaphragm Design

"Infinite-life" diaphragms for resonant machinery have been designed at MTI since 1978. Figure 7 shows several of these diaphragms. The largest is a 254-mm (10-in) diameter, chemically milled, contoured diaphragm with integrally machined rim. This diaphragm was used for transmission of 60-Hz output power from one of our free-piston Stirling engines. The diaphragm operated reliably throughout the prototype engine test program, accumulating in excess of 100 million cycles without evidence of degradation.

Also shown in Figure 7 is a 115.3-mm (4.5-in) diameter contoured diaphragm with integrally machined rim made from K-500 Monel. This diaphragm is representative of the first-stage diaphragm for a two-stage high-pressure oxygen compressor designed by MTI under NASA-JSC contract. Endurance testing of this diaphragm at 30 Hz and 1.8-mm (0.070-in) peak-to-peak deflection was initiated in April 1989 under an MTI IR&D program. Over 210 million cycles were accumulated without failure on both the K-500 Monel contoured diaphragm and on a flat diaphragm (also shown in Figure 7) manufactured from 0.381-mm (0.015-in) thick stainless steel sheet. However, as shown in Figure 8, the flat sheet steel diaphragm exhibited significant fretting damage at its outside diameter (OD) clamping perimeter, whereas the K-500 Monel diaphragm with its integrally machined mounting rim showed no signs of fretting. It is MTI's contention that highly reliable long-life diaphragms must be designed with integral rims to eliminate fretting fatigue as a potential and unpredictable failure mode. The following paragraphs describe the diaphragm design for the Phase II proof-of-concept compressor.
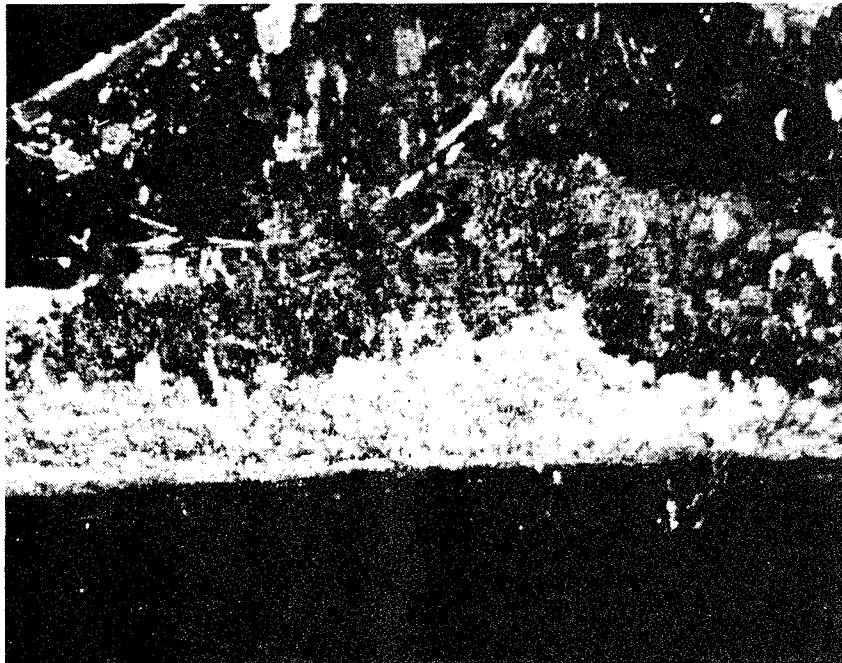
0.015-in. thick

4.5-in. dia

10-in. dia
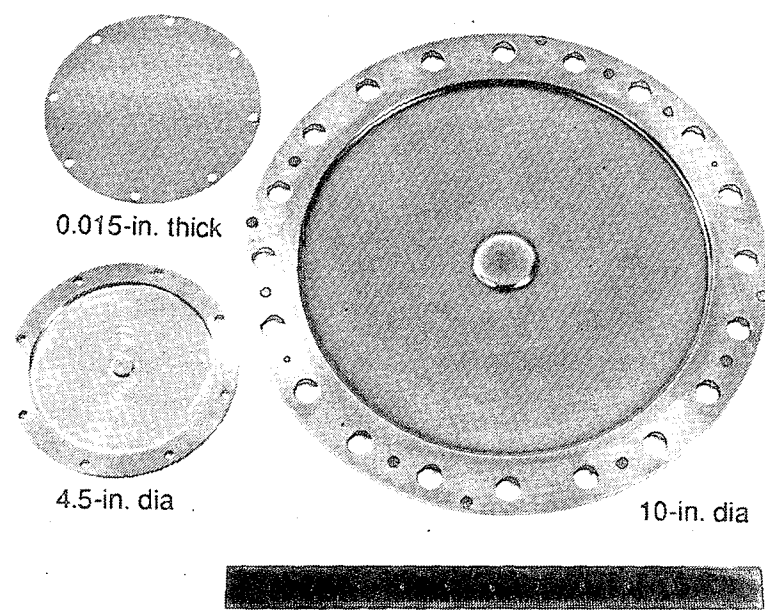
CT89245-54

Figure 7. The MTI-Designed "Infinite-Life" Diaphragms
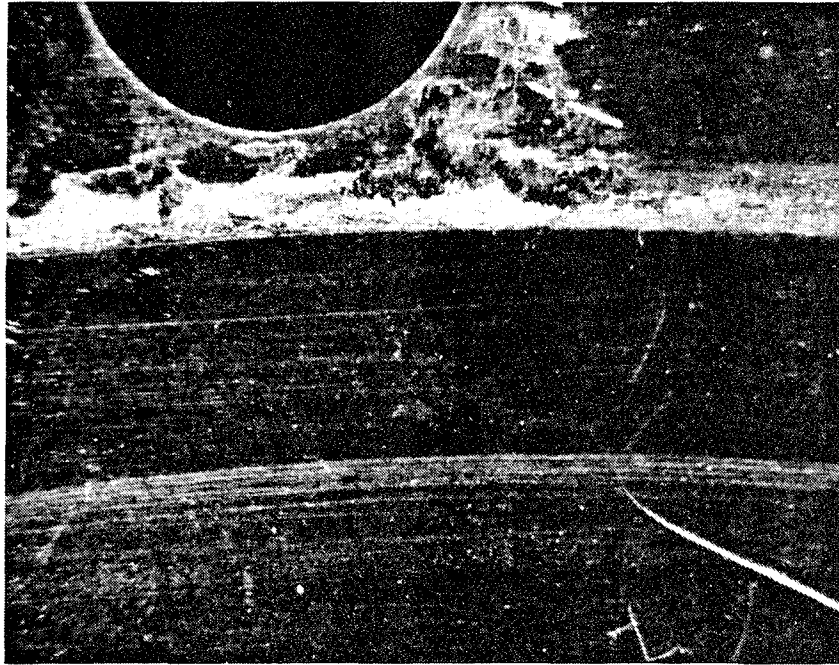
X10

X34

Figure 8. Fretting Damage on a Flat-Sheet, Clamped Diaphragm After 210 Million Deflection Cycles

5.2.1 Diaphragm Material and Maximum Allowable Design Stress

Armco PH13-8Mo precipitation-hardened stainless steel was used for the diaphragms in the proof-of-concept compressor. This is a double-vacuum-melted steel that has high metallurgical cleanliness, high chemical and stress corrosion resistance, and both high and equal endurance-limit strengths in the longitudinal and transverse directions. Appendix A gives a detailed description of the methodology used to establish the allowable design stress for the diaphragms. Available fatigue strength data for Armco PH13-8Mo is also presented. The significant assumptions and results of this statistically based methodology can be summarized as follows.

To achieve the required 95-percent overall compressor system reliability, the mechanical and electronic subsystems were each assigned subsystem reliability goals of 97.5 percent. A total of 52 possible series failure points were identified for the mechanical subsystem consisting of two compression modules. Stipulating that each of these 52 possible failure points should have the same probability of failure, the required reliability for each failure point, based on 100,000-hr life, was computed to be 0.9995. Based on this reliability requirement, and applying a 60-percent confidence level to the fatigue endurance strength data for Armco PH13-8Mo (in addition to several other strength derating factors), the maximum allowable design stress for the diaphragms was established to be 273.5 MPa (39.6 ksi). This value of maximum allowable stress is 49.6 percent of the tested endurance strength of Armco PH13-8Mo.

5.2.2 Diaphragm Stress Analysis

The radial and circumferential bending and membrane stresses in the diaphragm were computed using several computer programs, all of which treat the nonlinear biaxial combined membrane-bending stress conditions. The ANSYS finite-element program was used to evaluate stress-concentration effects that could not be handled by either the Battelle NONLIN or the MTI PLATEAN codes. The NONLIN or PLATEAN codes (which give comparable results) are used for rapid sizing and volume-displacement analysis of diaphragms. Both of these codes allow contoured (variable thickness) or flat (uniform thickness) diaphragms to be analyzed. (A contoured diaphragm minimizes diaphragm diameter for a given diaphragm swept volume and a given maximum allowable stress. However, the degree of diameter reduction usually does not justify the considerable increase in diaphragm fabrication expense.)

The biaxial diaphragm bending and membrane stresses are reduced to equivalent uniaxial alternating and mean stresses using the von Mises criterion. The von Mises equivalent alternating and mean stresses can then be plotted on a modified Goodman diagram as shown in Figure 9 to obtain a visual overview of the stress situation. However, probabilistic techniques, as discussed in Appendix A, must be used to quantitatively establish diaphragm reliability.

Armco PH13-8MO Stainless Steel
H1000 Heat Treat Condition; Rc 43 (min)
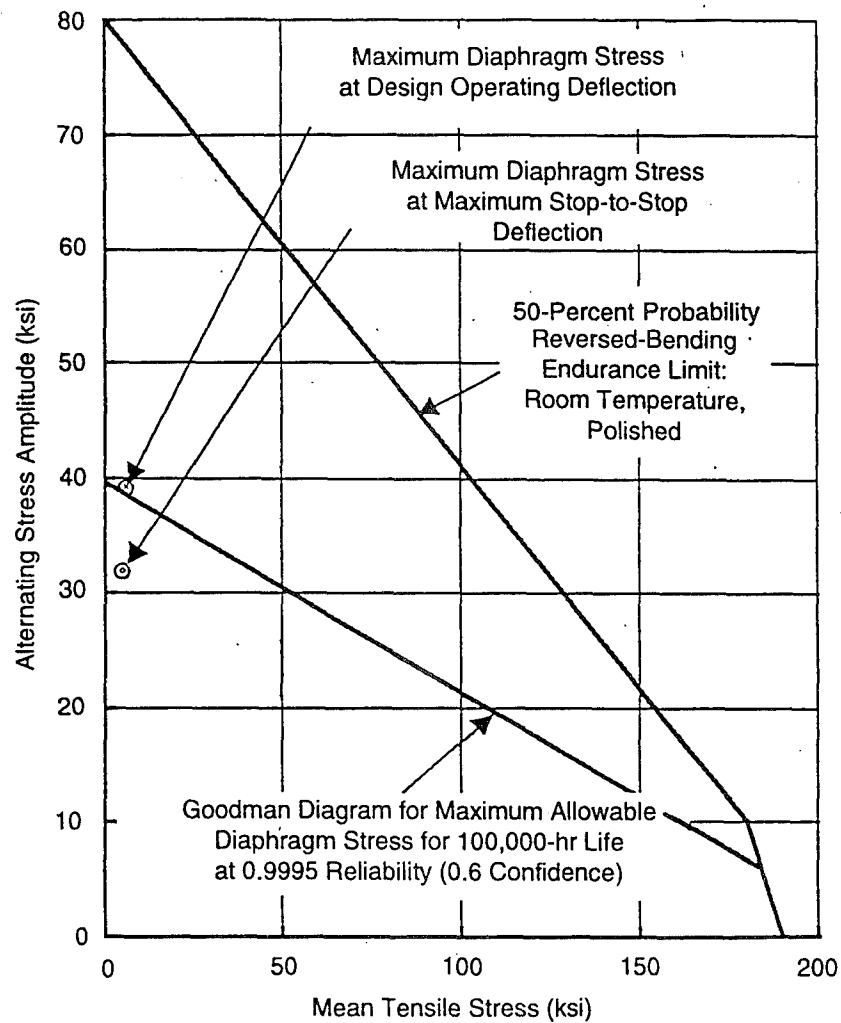UTS = 205 ksi (min); TY = 190 ksi (min)

Maximum Diaphragm Stress
at Design Operating Deflection

Maximum Diaphragm Stress
at Maximum Stop-to-Stop
Deflection

50-Percent Probability
Reversed-Bending
Endurance Limit:
Room Temperature,
Polished

Goodman Diagram for Maximum Allowable
Diaphragm Stress for 100,000-hr Life
at 0.9995 Reliability (0.6 Confidence)

Figure 9. Maximum Diaphragm Stresses Plotted on Goodman Diagram

A prime criterion in MTI's approach to diaphragm application is that the diaphragms must never operate in a bottoming (stop-to-stop contacting) mode. Nevertheless, maximum diaphragm deflection for design purposes is conservatively taken as the deflection at which bottoming against the contoured surfaces of the cylinder heads would occur. Although the diaphragms should never reach these limit stops during actual compressor operation, the stresses at this maximum deflection must still satisfy the required 0.9995 component reliability goal. When this is done, the predicted diaphragm reliability at the nominal design deflection condition will normally exceed 0.99999.

Figure 10 shows the selected diaphragm cross section for the Phase II compressor design. The nominal 0.368-mm (0.0145-in) uniform diaphragm thickness is blended into the integrally machined rim via a 6-mm transition radius. The 6-mm transition radius was selected on the basis of ANSYS finite-element analyses which showed that a radius of this size would eliminate any stress concentration effects due to changing diaphragm thickness at the rim. The effective OD of the diaphragm (with respect to PLATEAN stress calculations) is 10.97 cm (4.32 in).

The highest stress in the diaphragm will occur at the start of the transition radius. At maximum possible (stop-to-stop) diaphragm deflection, the maximum computed von Mises equivalent alternating stress is 270.3 MPa (39.2 ksi), slightly less than the maximum allowable design stress as determined from the Appendix A reliability analysis. At the nominal design-point swept volume condition, the maximum computed von Mises diaphragm stress is 219.7 MPa (31.9 ksi). The computed diaphragm reliability at this normal operating condition is >0.99999.

5.3 Bellows Design

Several functions of the bellows component in the cryocooler compressor are described in Subsection 3.2. The following paragraphs describe the bellows design for the Phase II proof-of-concept compressor.

5.3.1 Bellows Operational Requirements

Instantaneous axial deflection of the bellows can be analyzed in terms of "static" plus "dynamic" components of deflection. As a consequence of the compressibility and thermal expansion properties of the hydraulic fluid, changes in both temperature and mean pressure of the fluid will cause changes in the static deflection component. (Thermal expansion changes will be significant; compressibility changes in this application are negligible.) Based on a total hydraulic fluid volume of 586 cc, static deflections of the bellows will range from 7 mm of extension at -40°C oil temperature to 5.6 mm of compression at +65°C. It should be noted that the -40°C condition is a nonoperating environmental storage temperature condition; there would not be any dynamic bellows operation at this temperature.

Material: PH13-8Mo, Precipitation Hardened to H1000 Condition

Surface Finish within this Region to be
0.20 to 0.40 µm on both Sides of Diaphragm.
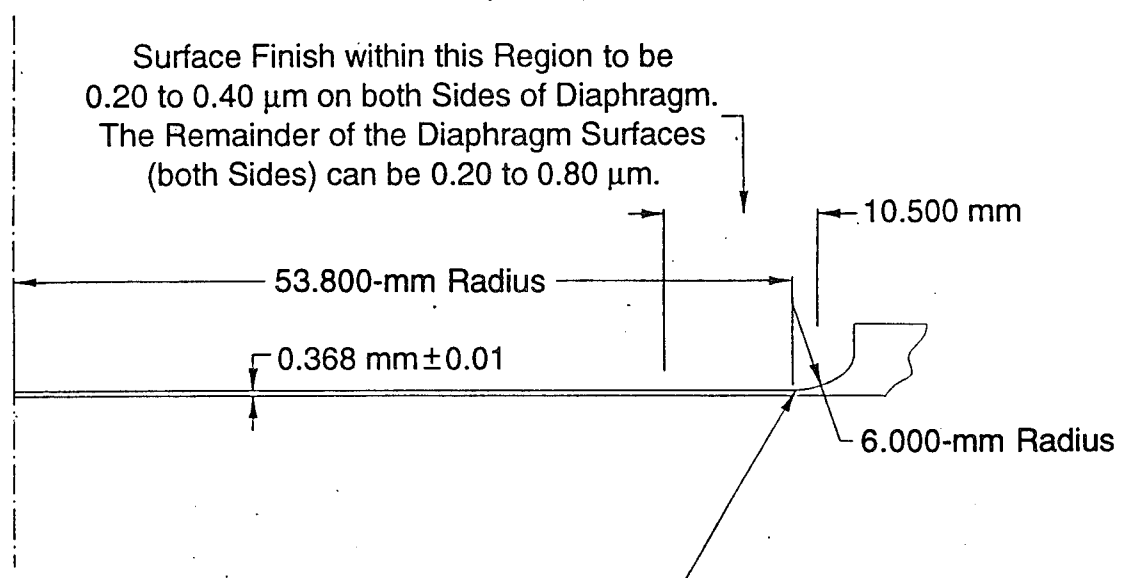The Remainder of the Diaphragm Surfaces
(both Sides) can be 0.20 to 0.80 µm.

10.500 mm

53.800-mm Radius

0.368 mm ± 0.01

6.000-mm Radius

6.0-mm Radius must Blend into 0.368-mm Thickness without Steps

Figure 10. Diaphragm Design for Phase II Compressor

The dynamic component of bellows deflection arises from the requirement that the bellows must compensate for the swept volume displacement of the compressor's hydraulic piston that occurs at compressor reciprocating frequency (40 Hz). The dynamic bellows stroke will be smaller than piston stroke by the ratio of hydraulic piston area to effective bellows area. Table 3 (line 83) shows that nominal dynamic amplitude (one-half stroke) of the bellows will be ~1 mm (0.039 in). It is clear that static deflection stresses in the bellows due to changes in oil temperature will be significantly greater than dynamic stresses, suggesting that a bellows material with high yield strength will be required.

Line 89 of Table 3 shows that the bellows is subjected to a dynamic differential pressure amplitude of about 0.10 MPa (15 psi), while the mean value of differential pressure across the bellows will range from 0.017 MPa (2.4 psi) at -40°C to -0.014 MPa (-1.9 psi) at +65°C. (A positive differential pressure produces bellows extension; a negative value produces bellows compression.) As a consequence of the pressure-induced mean and dynamic components of bellows deflection, the bellows is subjected to mean and alternating components of stress. Achievement of long-term bellows reliability in the presence of these stresses is the principal goal of bellows design.

5.3.2 Bellows Selection

There are five types of metal bellows: mechanically rolled, hydroformed, welded, chemically deposited, and electrodeposited. Each type has its advantages and disadvantages. Electrodeposited bellows have been used in previous space applications with excellent long-term success. However, this type of bellows is normally made of pure nickel, which does not have a well-defined endurance limit strength. Welded bellows take up the least amount of space for a given volume compensation requirement, but because of the large amount of welded seam length, it is very difficult to quantify long-term reliability. Rolled and hydroformed bellows are the most prevalent types and are typically fabricated from austenitic (300 series) stainless steel, Inconel 625 and 718, or beryllium copper. When both high-yield and high-fatigue strength are required, Inconel 718 is usually the material of choice.

As shown by the stress analysis results in Subsection 5.3.4, high-yield strength is a requirement of the bellows material because of the wide range of static deflection the bellows will encounter due to differential expansion of the hydraulic fluid. Additionally, since the bellows will be subjected to 14 billion dynamic stress cycles in 100,000 hr of operation, the Appendix A reliability approach to setting maximum allowable design stress must be used. This means that a large derating factor will be applied to the fatigue strength of the bellows material. Therefore, a material with high-fatigue strength is desirable. Finally, cost and time constraints for executing Phase II of this program provided strong motivation to use an existing off-the-shelf bellows for the Phase II compressor.

An extensive survey of bellows manufacturers was made, resulting in identification of several potential bellows suppliers and two candidate bellows materials: Inconel 718 and beryllium copper. Two sources of an acceptable off-the-shelf bellows were found, namely Parker Metal Bellows and the Calflex Corporation. Both companies can supply a wide selection of hydroformed bellows fabricated from either stainless steel or Inconel 718. Several samples of Calflex bellows were provided to MTI and, based on visual and cross-sectional examination, were judged to be of high quality. Accordingly, the Phase II proof-of-concept compressor has been designed to use the Calflex Code 580-103 single-ply bellows made from Inconel 718. Table 4 lists pertinent design parameters of this bellows.

5.3.3 Bellows Maximum Allowable Stress

The procedure described in Appendix A was followed to establish a maximum allowable design stress for the bellows component. Fatigue strength data for cold-rolled Inconel 718 sheet were obtained from Inco Alloys International Brochure (4M 9-86 IAI-19), from Aerospace Structural Metals Handbook (Code 4103), and from MIL-HDBK-5C. Based on these sources, a 50-percent probability fatigue strength of 262 MPa (38 ksi) at 100 million cycles was established. Although Inconel 718 is not an iron-based alloy, it does contain 18.5 percent (nominal) iron. Fatigue strength data strongly suggest that an endurance limit strength is reached between 10^7 and 10^8 cycles. However, in the interest of conservatism, the 10^{10} fatigue strength of Inconel 718 was further derated by 5 percent to 249 MPa (36.2 ksi).

The minimum required reliability for the bellows component (established in Appendix A) is 0.9995. For establishing the maximum allowable bellows design stress, the following factors for the Shigley equation (Equation 1 of Appendix A) were used:

- k_a = 0.80 (surface finish for cold drawn tube)
- k_b = 1.0 (size factor)
- k_c = 0.66 (reliability factor for 0.9995 reliability)
- k_d = 1.0 (temperature factor)
- k_e = 0.95 (stress concentration factor to cover small imperfections in finished bellows)
- k_f = 0.95 (allowance for miscellaneous effects, believed to be conservative)
- k_g = 0.981 (confidence factor for 60 percent confidence on endurance limit assuming two endurance strength tests)

Maximum allowable bellows design stress is thus 116.3 MPa (16.7 ksi), which is 46.7 percent of the 50-percent probability fatigue strength of Inconel 718.

Table 4. Properties of Seven-Convolution Bellows for Phillips Laboratory Compressor

Vendor Designation	Calflex, Code 580-103
Number of Convolutions	7 (i.e., 14 free plates)
Convolution OD	8.001 cm (3.150 in)
Convolution ID	5.799 cm (2.283 in)
Material Thickness	0.020 cm (0.008 in)
Material Description	Iconel 718; annealed, formed, and age hardened
Bellows Effective Area	37.74 cm^2 (5.85 in^2)
Free Length per Convolution	0.620 cm (0.244 in)
Flexibility per Convolution	5.969 cm/MPa (0.0162 in/psi)
Bellows Spring Rate	91.0 N/cm (52.0 lb/in)
Bellows Static Deflection Desired After Oil Fill at 21.1°C (70°F); Δp must be <0.1 psi	-0.0261 cm (-0.01013 in) compression

5.3.4 Bellows Stress Analysis

From 1965 to 1968, Battelle Memorial Institute conducted a program under USAF Contract 04 (611)-10532 to analytically develop and experimentally verify stress analysis methods for metallic bellows and diaphragms. This work is reported in Reference 1. As part of this program, Battelle developed and validated computer code NONLIN for calculating stresses in bellows and diaphragms. Battelle has maintained the NONLIN code and recently converted it for PC usage. This code was purchased from Battelle by MTI several years ago for use in designing diaphragms. Under this program, it has been used to analyze the bellows stresses.

The NONLIN code can accurately model bellows geometry, including variable wall thickness such as occurs in rolled and hydroformed bellows. One of the sample bellows provided by Calflex was sectioned and the variation in wall thickness measured. Figure 11 is a photograph of the sectioned bellows. Although the sample bellows was a two-ply bellows and not the specific size selected for the proof-of-concept compressor, it was felt that its geometry variations would be representative. Based on the measured variations, stress calculations were made for the Calflex Code 580-103 bellows geometry. Since a sample of this specific bellows was not available, a worst-case assumption of bellows geometry was made. All stress calculations were made for maximum stop-to-stop compressor displacement, even though this magnitude of operational displacement should never exist. Mean and dynamic stresses were computed for the 0, 45, and 65°C oil temperatures. Mean stress was also computed for the -40°C nonoperating storage condition.
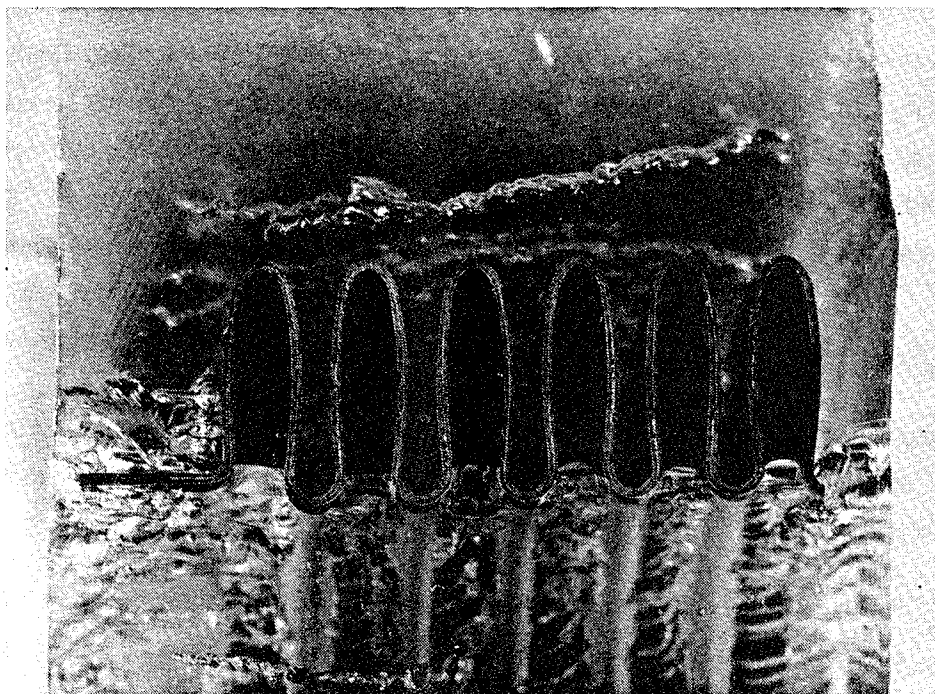
Figure 11. Sectioned Calflex Two-Ply Bellows Used to Estimate
Wall Thickness Variations for Stress Calculations

Table 5 lists the von Mises equivalent mean and alternating stresses as a function of oil temperature. The stresses at the root of the bellows convolution are significantly greater than stresses at the convolution crown. Figure 12 shows these four stress conditions plotted on a Goodman diagram. All four stress points fall below the maximum allowable Goodman line, indicating that reliability of the bellows should exceed the required minimum value of 0.9995.

5.4 Linear Motor Design

Linear electric motors and alternators have been developed at MTI since the late 1960s, and the company has obtained a number of patents related to this electromechanical conversion technology. Our experience ranges from shaft powers of 1.0 to 12,000 W. Current generation motors and alternators are achieving design point efficiencies from 85 to 90 percent. The following paragraphs describe the linear motor design used in the Phase II compressor.

5.4.1 Description of MTI Linear Motor

The electromagnetic principles of the linear motor are basically the same as those of the more common "moving-coil" type of motor. However, MTI prefers not to use moving-coil motors for the following reasons:

- A moving-coil motor must operate with a relatively large magnetic air gap in order to accommodate the moving coil. This requires a large amount of iron and copper (or permanent magnet material) to drive dc flux across the gap and increases motor size and weight for a given power and efficiency requirement.

- The moving coil motor requires flexing electrical conductors to energize the coil with ac current. Fatigue stresses and dynamic resonances of these flexing conductors tend to restrict the maximum stroke that can be attained with these motors and constitute additional potential failure mechanisms.

The MTI linear motors utilize ac windings mounted in the stator (stationary) assembly of the motor. There are no mechanical or electrical connections to the reciprocating plunger. The motor air gap is small, and the amount of iron and copper (or permanent magnet material) required to drive dc flux across the gap is minimized, resulting in reduced motor weight for the same power and efficiency levels.

Figures 1, 2 (shown earlier in Section 3.0), and 13 (shown in Section 6.0) illustrate the cross-section arrangement of the linear motor selected for the Phase II compressor design. These motors are referred to as "moving backiron" motors. Three circumferential rows of radially magnetized permanent magnets are mounted on the OD of a laminated magnetic cylinder

Table 5. Outer Surface von Mises Stresses for Displacement at 40 Hz; Four Conditions of Oil Temperature

Bellows Deflection	Root - Part 1	Crown - Part 6
δ = -0.7031 cm to δ = -0.4697 cm (oil temperature = 65.6°C)	σ_{alt} = 74.54 MPa (10,814 psi) σ_{mean} ≈ 388.6 MPa (56,377 psi compression)	σ_{alt} = 53.73 MPa (7,795 psi) σ_{mean} = 289.1 MPa (41,941 psi tension)
δ = +0.3563 cm to δ = +0.1229 cm (oil temperature = 0°C)	σ_{alt} = 89.84 MPa (13,033 psi) σ_{mean} = 180.1 MPa (26,133 tension)	σ_{alt} = 66.42 MPa (9,636 psi) σ_{mean} = 133.07 MPa (19,301 psi compression)
δ = -0.4438 cm to δ = -0.2104 cm (oil temperature = 45°C)	σ_{alt} = 77.29 MPa (11,213 psi) σ_{mean} = 225.2 MPa (32,675 psi compression)	σ_{alt} = 57.15 MPa (8,290 psi) σ_{mean} = 166.1 MPa (24,098 psi tension)
δ = +0.7439 cm (oil temperature = -40°C)	σ_e = 592.6 MPa (85,966 psi tension)	σ_e = 440.5 MPa (63,898 psi compression)
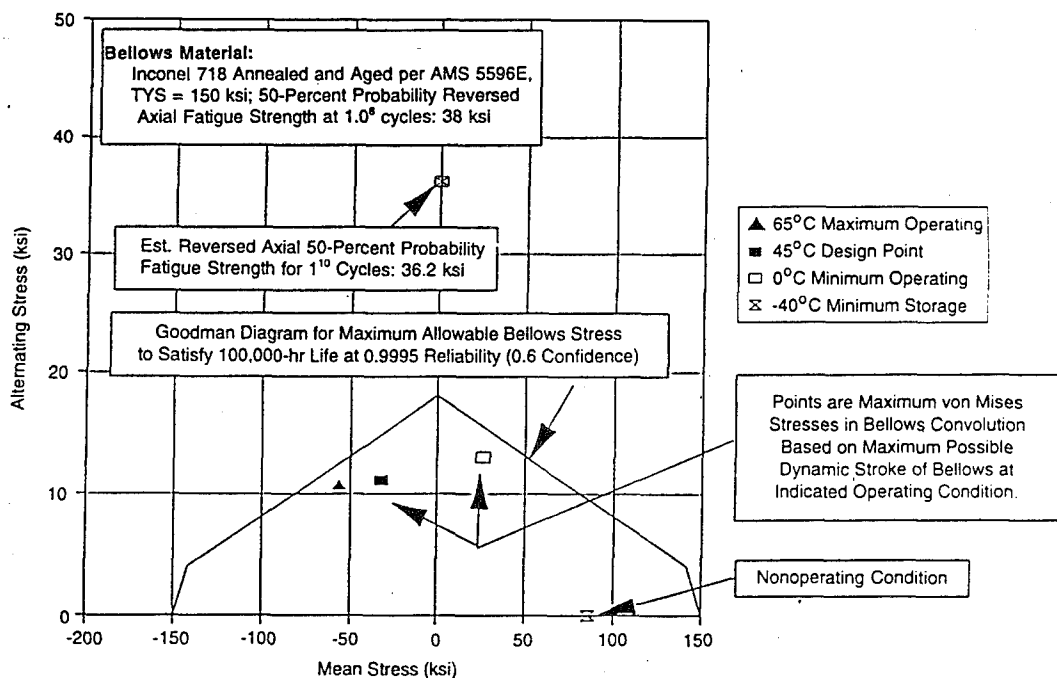
Figure 12. Bellows Stress at Four Oil Temperatures

41

formed from Hyperco-50 laminations. (Because of the length of the center magnet row, this row actually consists of two circumferential sections.) The laminations, which function as "backiron" for the magnets, are radially stacked around the axial centerline of the plunger and assembled as an integral part of the reciprocating assembly. The magnets and backiron thus move with the plunger in the motor air gap.

The three circumferential rows of radially magnetized magnets are alternately magnetized N-S, S-N, N-S. Either samarium cobalt or neodymium-iron-boron magnets can be used. For commercial applications where cost is the driving factor, MTI is using Nd-Fe-B magnets. For the Stirling Space Power Converter being developed by MTI for NASA, Sm_2Co_{17} magnets are being used in the linear alternators since these magnets must operate at 500 K. Samarium cobalt magnets are also the preferred choice for the Phillips Laboratory advanced cryocooler compressor since the long-term characteristics of these magnets are well established.

The motor stator assembly consists of a single prewound and potted ac coil. Square cross-section wire is used to obtain maximum coil packing factor and thus motor efficiency. Axially oriented Hyperco-50 laminations are stacked around the coil to form a rigid, cylindrical stator assembly. Hyperco-50 lamination material is selected for this application because of its higher flux saturation level, thus resulting in a minimum weight motor.

5.4.2 Motor Requirements

Nominal design-point operating requirements for the linear motor in each compression module of the Phase II compressor are as follows:
- Plunger Output Power: 145 W at α = 0 deg
- Plunger Stroke: 1.2 cm
- Frequency: 40 Hz
- Electrical Efficiency: 85 percent
- Electrical Power Source: 28 V dc.

Angle α referenced above is a key design parameter for linear motors. It is the phase angle between the fundamental harmonic of motor ac current in the stator coil and the fundamental harmonic of motor-generated voltage (back-emf). The product of instantaneous ac current times instantaneous generated voltage is the instantaneous shaft output power of the motor. Angle α may also be defined in mechanical terms as the phase angle between the fundamental harmonic of air-gap force produced by the ac coil current and the fundamental harmonic of plunger velocity. If angle α is 0 during compressor operation, the compressor, by definition, is said to be operating at its resonant frequency.

Maximum motor efficiency is usually obtained when angle α is about +10 deg (when generated voltage leads current). However, maximum motor output power (or alternatively, minimum motor weight) is usually obtained when α is about -20 deg. Thus, optimization of motor design is always a trade-off between efficiency and weight. Fortunately, motor efficiency is relatively flat for α from +30 to -10 deg, and a reasonable compromise is to define the nominal motor design condition to correspond to system resonance (α = 0 deg). This has been done for the Phase II compressor motors.

5.4.3 Motor Design Codes

Considerable MTI resources have been invested into developing and validating computer codes for design of linear motors and alternators. Three levels of codes are used depending on design objectives. Fast, design-oriented codes are used to perform initial design surveys and motor sizing. Once an initial motor design is established, a time-stepping code is used to obtain more detailed information on motor performance. The final step in a new motor design is to check the design using a finite-element electromagnetic code. Force generation, local flux densities, and leakage flux characteristics are checked as a function of plunger position and motor operating condition. This three-level process was used to design the motors for the Phase II compressor. Dynamometer test experience has demonstrated that motor performance is usually within 5 percent of predicted performance when this three-step design process is followed.

Table 6 lists a number of the linear motor design and performance parameters for the Phase II compressor. Some of these parameters are included in Table 3 where they are used for computing overall performance and resonance characteristics of the compressor's mechanical subsystem. In addition to providing 145 W of 40-Hz shaft power, Table 3 shows that the motor is designed to also provide 31 N (7 lbf) of air-gap dc force. This dc force capability is required to counteract the average pressure force acting on the plunger motor as listed in lines 287 to 291 of Table 3. During compressor operation, the motor's dc force level will be established by closed-loop control of dc current in the motor coil. This control loop will actually be controlling the mid-stroke position of the compression module's diaphragm via adjustment of the amount of mid-stroke offset of the motor plunger. This control function is further described in Section 7.0.

43

Table 6. Motor Design and Performance Parameters

Moving backiron motor for Phillips Laboratory				Rectangular coil slot	
0.5-W, 30-K Compressor at 12 mm, 40 Hz				HYPERCO LAMS	
				SQUARE WIRE	

OPERATING CONDITIONS:

ALPHA ANGLE =	0.0	DEG	ELECT POWER =	170.60	W
SHAFT POWER =	145.181	W	EFFICIENCY =	85.12	%
STROKE =	0.472	IN	BAC/BR =	0.400	
FREQUENCY =	40.000	HZ	FRINGING COEFF =	0.975	

GEOMETRY: (BR IRON = 2.000 T; IRON SIZING ALPHA = 10.00 DEG)

MAGNET O.D. =	1.630	IN	BMAX INNER =	2.009	T
PLUNGER DIA. =	1.575	IN	OUTER DIAM =	3.652	IN
STATOR GAP =	0.079	IN	MOTOR LENGTH =	2.446	IN
COIL WIDTH =	0.816	IN	CASING THICK =	0.000	IN
COIL HEIGHT =	0.719	IN	MAGNET THICK =	0.055	IN
PLUNG. CLEAR =	0.0237	IN	BORE DIAM =	0.684	IN
POLE WIDTH =	0.543	IN	ARM WIDTH =	0.268	IN
TOOTH GAP =	0.816	IN	TOOTH ANGLE =	0.000	DEG
MAGNET/GAP =	0.700		POLE ANGLE =	50.000	DEG

MAGNET ASSUMPTIONS: (MAGNET MATERIAL = Sm2Co17)

BASE Br =	1.08	T	NON-RAD LOSS =	0.989	
WIR WAY LOSS =	0.950		T-STRUT LOSS =	1.000	
SIDE-PULL =	3.843	LBF/MIL	FINAL Br =	1.014	T

MASSES: (MOTOR IRON, COPPER, AND MAGNET MATERIALS ONLY)

PLUNGER =	1.246	LBM	MAGNET =	0.196	LBM
OUTER STATOR =	1.400	LBM	INNER STATOR =	1.047	LBM
COIL =	1.017	LBM	PLUNGER WRAP =	0.004	LBM
POTTING =	0.061	LBM	TOTAL =	3.724	LBM

LOSSES: (MARGIN = 2.000 PTS; STATOR IRON LOSS = 8.600 W/KG)

COIL =	7.192	PTS	COIL TEMP =	50.000	DEG C
MAGNET =	0.089	PTS	STATOR =	5.600	PTS
CASING =	0.000	PTS	STRUCTURE =	0.000	PTS
			MOTOR EFF =	85.119	%

ELECTRICAL:

AC LINE VOLTS =	14.416	V RMS	MTR TERM VOLTS =	14.416	V RMS
COIL TURNS =	55.000		PACKING FACTOR =	0.739	
WIRE GAGE =	11	SQUARE	SLOT LINER THK =	0.020	IN
WIRE WIDTH =	0.097	IN.	COIL RES. =	0.042	OHMS
INDUCTANCE =	2.443	MILLI-H	COIL REACT. =	0.614	OHMS
SER. CAP. =	0.000	MICRO-F	CAP. REACT. =	0.000	OHMS
AC CURRENT =	16.656	A RMS	DC CURRENT =	3.810	AMPS
LINE PF =	0.705		LINE ANG(V-I) =	45.181	DEG
MOTOR PF =	0.705		MTR ANG(V-I) =	45.181	DEG
EGEN =	8.714	V RMS	BETA =	1.174	

MOTOR AIR-GAP FORCES DUE TO COIL CURRENT:

AC FORCE COMPONENTS			DC FORCE =	7.000	LBF
VELOCITY =	43.289	LBF-AMPL			
DISPLACE =	0.000	LBF-AMPL			
TOTAL =	43.289	LBF-AMPL			

16-Apr-92

44

Table 3 shows the total weight of the motor's iron, copper, and magnet materials to be 1.69 kg (3.72 lbm) per motor. Specific motor power is thus 85.8 W/kg at a motor efficiency of 85.1 percent. The somewhat low motor efficiency is due to the fact that computed eddy current and hysteresis losses in both the lamination iron and the magnets (including loss margin) represent 52 percent of the motor's electrical losses. The i^2R loss in the ac coil accounts for the remainder of the losses. About 5 percent of the i^2R loss (or 0.37 points of motor efficiency) is due to the dc coil current.

5.5 Hydraulic Fluid

Each compressor drive module and its associated diaphragm hydraulic cylinder will be completely filled (i.e., vacuum filled) with hydraulic fluid. The key requirements for this fluid are long-term stability and chemical inertness with the internal parts of the compressor at temperatures up to 65°C. Additional important characteristics are

- Low viscosity
- Freeze or pour point well below -40°C
- Low specific gravity (low density)
- Low coefficient of thermal expansion
- High electrical resistivity
- Lubrication properties at least equivalent to water.

Preliminary investigation indicated that silicone oils used as damping fluids in aerospace guidance equipment would be a good choice for the hydraulic fluid. These oils have been used in a number of long-life space applications with excellent results. The oils are chemically benign and electrically insulating and can, therefore, be used in direct contact with the linear motor materials. Kearfott oil C101180004 has a minimum flash point of 102°C (215°F), a maximum pour point of -54°C (-66°F), a density of 0.90 g/cc, and a viscosity of 3.0 centistokes at 24°C (76°F). The flash point can be increased by using oil C101180005 which has a minimum flash point of 135°C (275°F), a maximum pour point of -54°C (-66°F), a density of 0.92 g/cc, and a viscosity of 5.0 centistokes at 24°C (76°F).

Further investigation has identified a synthetic polyalpha-olefin (PAO) product available from either Bray Oil Company (a division of Castrol) or Royal Lubricants Company (part of the Royal Dutch/Shell Group). The properties of Royco 602 are listed in Table 7. These are MIL-certified oils used to cool aircraft avionics by direct oil flooding of the electronics boards.

Both the silicone and PAO oils appear to be excellent hydraulic fluid candidates for the cryocooler compressor. Because of its lower density and lower thermal expansion coefficient, the PAO oil has been selected for the Phase II compressor. While the manufacturers of these oils express high confidence about the long-term stability of these oils, MTI has not yet found actual 10- to 20-year experience data to substantiate these opinions.

Table 7. Royal Lubricants Product Bulletin

Royal Lubricants

Product Bulletin

ROYCO 602
COOLANT FOR AIRCRAFT AVIONIC SYSTEMS

MIL-C-87252

DESCRIPTION:

ROYCO 602 synthetic base fluid is composed of highly branched, compact and very stable molecules known as polyalphaolephins (PAO), blended with additives to provide long term storage stability.
ROYCO 602 fluid offers exceptional performance over a wide temperature range and does not react with water, resulting in clean systems and long fluid and component life.

APPLICATIONS:

ROYCO 602 is most widely used as a cooling fluid for aircraft avionic systems, whose benefits include lower initial cost, longer fluid life, lower weight and lower toxicity when compared with other types of avionic systems coolants. Since ROYCO 602 does not react with water, no reclamation equipment is required, adding further to the cost advantage. ROYCO 602 is qualified against Mil-C-87252 (USAF).

TYPICAL PROPERTIES:

Gravity, API	45.3
Specific Gravity, ASTM D-1298	.7999
Viscosity, cSt, ASTM D-445	
@212 F	1.72
@104 F	5.19
@-40 F	277
@-65 F	1296
Viscosity Index	145
Pour Point, F, ASTM D-97	-100
Flash Point, F, ASTM D-92	350
Fire Point, F, ASTM D-92	380
Evaporation Loss, %. ASTM D-972 @ 400 F, 6.5 hrs.	17
Total Acid Number, ASTM D-974	<.01
Water Content, ppm, KARL FISCHER	<56

(Continued on back)

Table 7. Concluded.

TYPICAL PROPERTIES:
  Density, g/cc, Dialatometer
    @ 0 deg C   0.8058
    @ 100 deg C   0.7392
    @ 190 deg C   0.6768

  Specific Heat, cal/g-deg C, ASTM D 2766
    @ -17.8 C   0.49 (e)
    @ 37.8 C   0.54
    @ 149 C   0.63
    @ 260 C   0.72
    (e) extrapolated

  Thermal Conductivity, Heat Probe Method
  cal/hr sq cm(deg C/cm)
    @ -17.8 C   1.26
    @ 37.8 C   1.21
    @ 149 C   1.12
    @ 260 C   1.02

  Coefficient of Thermal Expansion, Dialatometer
    1/deg C
    0-50 deg C   0.00083
    50-100 deg C   0.00092
    100-150 deg C   0.00103
    150-190 deg C   0.00117

  Dielectric Constant, 400 Hz   2.10

  Power Factor, 400 Hz   < 0.0001

  Dielectric Breakdown Voltage, Kv, ASTM D-877   43.2

  Volume Resistivity, ohm-cm, ASTM D-1169 2.9×10^{15}

  Particle Count, automated   typical
                         5-15 mu   1500
                         16-25 mu   150
                         26-50 mu   50
                         51-100mu   0
                         > 100 mu   0

  Elastomer Compatibility
    Recommended   Marginal   Not Recommended
    (Swell <5%)   (< 15%)   (Swell > 15%)

    Nitrile*   Nitrile**   Ethylene Propylene
    Fluorosilicone   Buna N
    Fluorocarbon   SBR
    Polyacrylate

    * N 674-70
    **N 497-70

5.6 Mid-Stroke-Porting Analysis

The purpose of mid-stroke-porting is described in Subsection 3.2.2. Design and analysis of the porting function is done using MTI computer code SP (Seals and Ports). The objective of porting analysis is to determine the number, size, and location (relative to supply groove) of ports needed to compensate for piston seal leakage without excessive amounts of piston offset.

Design parameters for the ports and results of the porting analysis are listed in lines 296 through 356 of Table 3. Two 0.75-mm (0.030-in) diameter holes are drilled through the piston seal skirt (wall). A 0.75-mm wide circumferential supply groove is machined into the cylinder wall (i.e., into the bearing sleeve). This groove is connected by holes through the cylinder wall to the motor drive cavity. The groove is therefore always filled with hydraulic fluid at drive cavity pressure. The plane of the piston ports is offset 0.45 mm (towards the motor) from the centerline of the supply groove when the plunger is axially centered in the motor stator.

Operational offset of plunger position was computed for three oil temperatures, 0°C, 45°C, and 65°C, and for two values of piston radial clearance, 0.013 mm (0.0005 in) and 0.076 mm (0.003 in). The small value of clearance is the beginning-of-life clearance, while the large clearance is the predicted end-of-life clearance increased by 50 percent to ensure design margin in porting functionality. The results show that piston offset will range from 0.23 mm (0.009 in) at 0°C and minimum clearance to -0.13 mm (-0.0051 in) at 65°C and maximum clearance. (A positive offset is plunger shifted towards the diaphragm.) This range of plunger offset is easily accommodated by the motor design.

5.7 Bearing Design

Each compressor drive module will contain two journal bearings, one on each side of the motor. (One of these bearings also serves as the hydraulic piston that actuates the compressor diaphragm.) Since the bearings operate in the compressor drive compartment, they are completely immersed in oil. As discussed in the following paragraphs, these bearings will have a wear life in excess of 100,000 hr, will have low friction loss, and because of their completely passive, simple, and rugged nature, will have very high reliability.

The stationary part of each bearing consists of a bronze-filled carbon-graphite sleeve pressed (captured) into the bearing housing. The reciprocating journal of each bearing is an integral part of the linear motor's plunger assembly. The surface of each journal will have a flame-sprayed tungsten carbide coating ground to a final thickness of 0.051 to 0.102 mm (0.002 to 0.004 in). This combination of bearing surface materials (tungsten carbide against bronze-filled carbon graphite) is well known from face-seal applications to be an excellent combination with respect to long wear life

under boundary-lubricated conditions. Flamed-sprayed coatings and carbon-graphite sleeves for liquid- and gas-lubricated bearing applications are two areas where MTI has extensive experience.

Wear factor data for various grades of carbon-graphite sliding against various counterface materials can be found in the Wear Control Handbook published by the American Society of Mechanical Engineers (Ref. 2), as well as from other sources. In particular, wear factors ranging from 4.83E-13 to 3.83E-12 mm^2/N (2.4E-12 to 1.9E-11 in^3-min/lbf-ft-hr) have been measured for tungsten carbide sliding against bronze-filled carbon graphite in water (Ref. 2). For the calculation of bearing life shown in line 171 of Table 3, a conservative value of 2.0E-11 has been used.

In a zero-g environment, the only load imposed on the bearings will be a magnetic "side-pull" load from the magnets of the linear motor. The magnitude of this loading depends on the total mechanical-plus-magnetic eccentricity of the motor plunger relative to the bore of the motor stator. At zero eccentricity, the side-pull load is zero. The computed side-pull gradient of the linear motors for the Phase II compressor is 7172 N/cm (4095 lb_f/in). Measurements of side-pull gradient have agreed well with computed values on previous motor developments.

Mechanical eccentricity of the motor plunger relative to the stator bore depends on the sum of (1) assembly eccentricity due to machining tolerances, (2) radial clearance of the bearings, and (3) total bearing wear at any instant of time. For a maximum possible assembly eccentricity of 0.025 mm (0.001 in), a maximum radial bearing clearance (new) of 0.013 mm (0.0005 in), and a permissible bearing wear of 0.038 mm (0.0015 in), the end-of-life total mechanical eccentricity of the plunger would be 0.076 mm (0.003 in). However, in addition to strictly mechanical eccentricity, there will be magnetic eccentricity due primarily to variability in magnetization and thickness of the plunger's magnet segments. Experience shows that 0.025 mm (0.001 in) of magnetic eccentricity should be allowed for in a motor of this size. Assuming the worst-case stack-up of magnetic and mechanical eccentricities gives 0.102 mm (0.004 in) of end-of-life side-pull eccentricity. The corresponding end-of-life bearing load for the Phase II compressor would be 36.4 N (8.2 lbf) per bearing.

Lines 144 through 174 of Table 3 document the design and life computations for the Phase II compressor. The average speed of the plunger at 1.2-cm stroke and 40 Hz is 57.6 m/s (189 ft/min). Average bearing load, corresponding to 0.019 mm (0.00075 in) of wear, is 34.2 N (7.7 lbf). Average bearing pressure loading is 0.042 MPa (6.06 psi). Because of this very light loading, significant hydrodynamic fluid-film load capacity will be generated. Line 167 of Table 3 shows that only 56.4 percent of the bearing load will be carried by boundary layer asperity (wearing) contacts. The remaining 43.6 percent of bearing load will be carried hydrodynamically. For a wear factor of 2.0E-11 and a permissible wear of 0.038 mm (0.0015 in), bearing life of 116,254 hr is predicted.

The face seal wear-factor data of Reference 2 was obtained at pv values 360 times higher than will exist in the Phase II compressor. It is well established that wear factor decreases with decreasing pv conditions. Additionally, these face seal data were obtained with water. The increased lubricity of the hydraulic fluid for the Phase II compressor would be expected to further decrease wear factor. For these reasons, the bearing life predictions of Table 3 should be quite conservative.

The measured friction coefficient of tungsten carbide sliding against carbon graphite in water is given in Reference 2 to be 0.07. Using a value of 0.08, line 208 of Table 3 shows the friction loss due to asperity contacts to be 1.5 W per bearing. Friction loss due to fluid film shear is shown in line 207 to be 0.5 W per bearing. Total loss for two bearings is 4.0 W, which represents 85 percent of the total predicted drive cavity hydraulic and friction losses. These losses, when added to the bellows hysteresis loss, result in an effective compressor "mechanical" efficiency of 94 percent.

Since the bearings are immersed in oil, the oil film in the bearing clearance will act as a damping fluid during space vehicle launch. This damping action, in combination with the large surface area of the bearings and the completely passive nature of the bearing design, means that caging of the plunger assembly in the bearings should not be necessary to survive launch-imposed shock and vibration loads.

6.0 PROOF-OF-CONCEPT COMPRESSOR DESIGN

6.1 Overall Description

The proof-of-concept compressor layout developed under Phase I is shown in Figure 13. It is identical in concept and arrangement to the one previously shown in Figure 1. The primary difference between the two is that the one shown in Figure 1 was designed for minimum weight and is hermetically sealed. The design shown in Figure 13 is a laboratory demonstrator version designed for ease of manufacture and disassembly and incorporates laboratory instrumentation that would not be required for actual space applications.

The critical compression process, diaphragm, motor, and bearing design details are identical for the two units and are consistent with the values previously given in Table 3. Furthermore, the diaphragm; motor lamination, magnet, and coil; bearing surface combination; and bellows materials are identical to those described in Section 5.0. The bellows design parameters given in Table 3 were based on a final oil volume of 586 cc.

The compressor assembly shown in Figure 13, being a proof-of-concept design, is a bolted and flanged construction that uses standard O-rings for sealing. Except for the "O" ring that separates the helium in the volume compensation bellows from the oil-filled motor cavity, all "O" rings seal high-pressure helium or oil to atmosphere. The bellows-motor cavity seal, on the other hand, seals only the small pressure amplitude within the helium side of the bellows. This fluctuating pressure will cause micromotion of the "O" ring and, over long periods of time, may result in some leakage. If this should occur, the bellows assembly can be welded to the motor end cap if the end cap material is changed from aluminum to stainless steel.

All structural components, except those mentioned in the preceding paragraphs, are made from 6061-T6 aluminum. The electrical connectors are commercially available semi-hermetic types that employ "O" ring seals between their bodies and the compressor structure.

The compressor is mounted to a rigid structure through four force transducers that will be used to characterize the compressor vibrational characteristics (both at the fundamental and at higher harmonics). The other principal mechanical interface is the compressor output flow connection. This has been designed specifically to interface with the NIST pulse-tube unit, and adequate space has been provided to accommodate its precooler and vacuum bonnet.
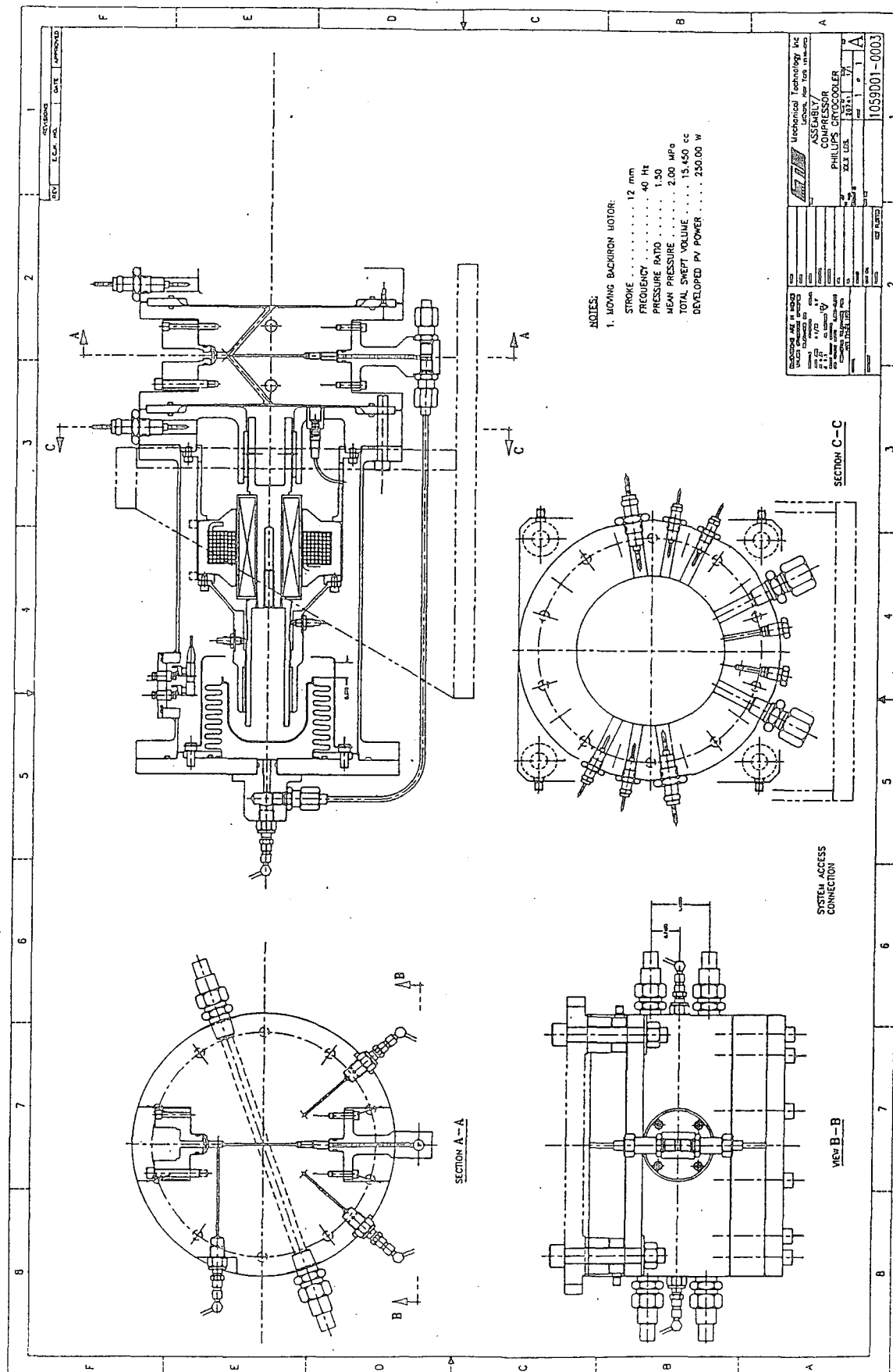
Figure 13. Proof-of-Concept Compressor Layout

6.2 Estimated Temperature Distribution

Conservative estimates of the temperatures within the compressor module were made based upon the assumption that all internally generated heat was transferred by conduction to a cooled central channel (hole) in the center body. This water-cooled channel is intended to simulate a heat-pipe-type heatsink (one possible cooling means in a spacecraft application). The node structure for the thermal analysis is shown in Figure 14, with the model is shown in Figure 15.
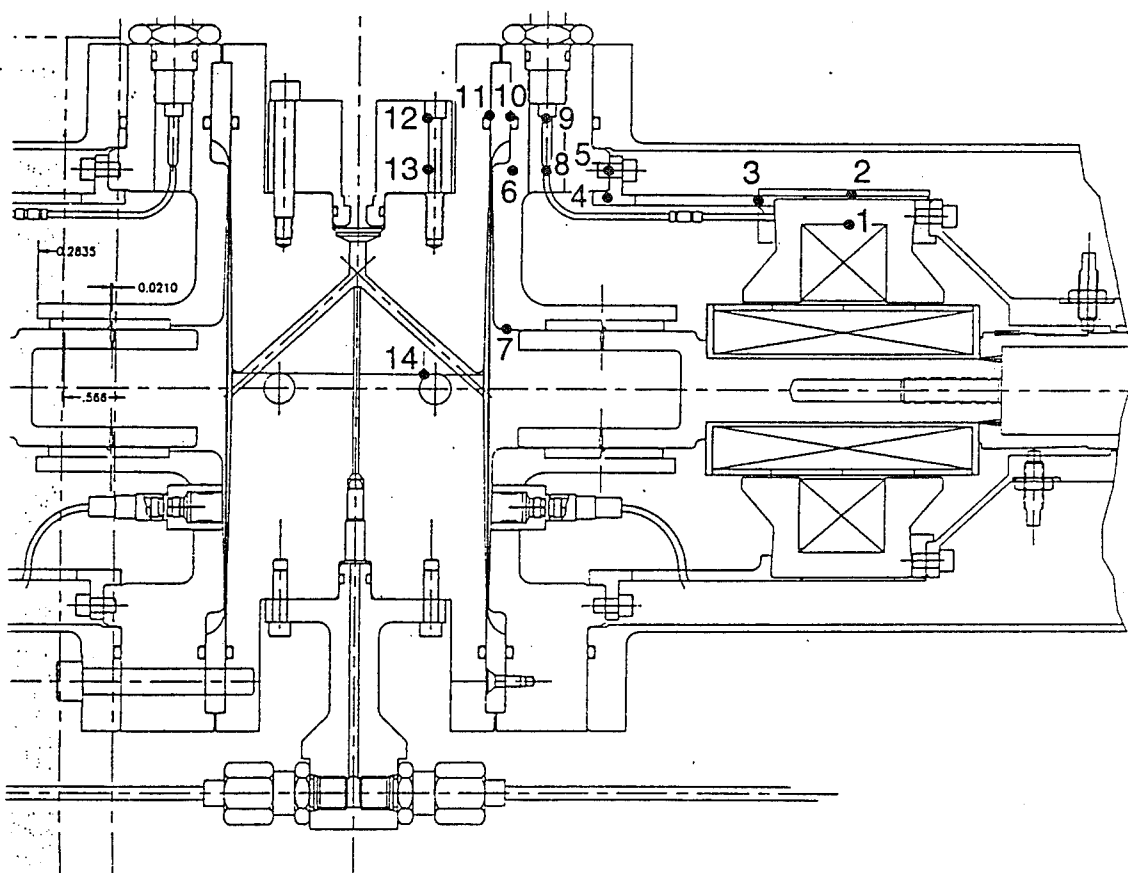
Figure 14. Thermal Analysis Node Structure

13-8 Mo Diaphragm

T_{12} ⌇∿∿∿— T_{11} —∿∿∿— T_{10} —∿∿∿— T_9 ←— 3.8 W Bellows Hysteresis

T_{13} ←— 5 W Hysteresis

T_6 —∿∿∿— T_8 —∿∿∿— T_5

$T_{14} = 70°F$

T_3 —∿∿∿— T_2 ←— 2.3 W (Pump and Bearings)

T_4

←— Hyperco 27 Laminations

43.4 W to Sink

T_7

T_1

7.3 W
(5 W Hysteresis
and 2.3 W for
Pump and Bearings)

25 W (Motor Loss)
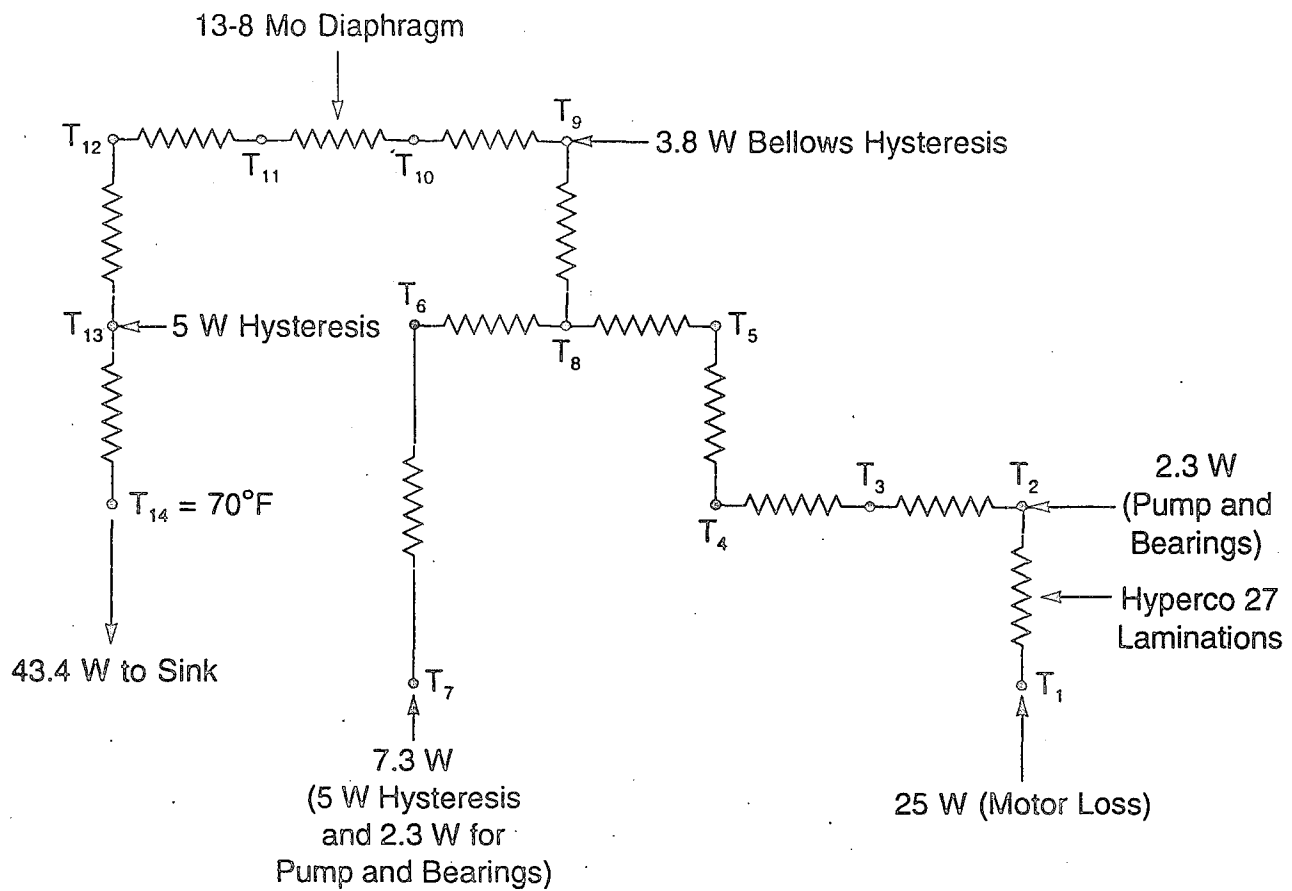
Nodes	Materials
1-2	Hyperco 27, K = 31.7 Btu - ft/hr - ft^2 - °F
2-10 & 11-14	6061 - T6 Aluminum, K = 104
10-11	13-8 Mu, K = 8.0

Figure 15. Thermal Model

54

The losses considered (and shown in Figure 15) are summarized below:

- Hysteresis Loss: 10 W to the structure divided between nodes 7 and 13 (approximately 75% of line 31 of Table 3, the other 25% assumed to be removed by the aftercooler).

- Total motor loss: 25 W (one-half the difference between lines 45 and 43 of Table 3), applied to node 1.

- Bearing and pumping losses: 2.3 W (one-half the sum of lines 208 and 217 of Table 3), applied to nodes 2 and 7.

- Bellows hysteresis loss: 3.75 W (line 371 of Table 3), applied to node 9.

Table 8 summarizes the significant calculated temperatures, assuming that 18°C (65°F) water is flowing at 12.6 cc/s (0.2 gpm) through the center body coolant channels. This table also indicates that the motor coil temperature is well controlled if the only heatsink is the small cooling channel within the center body. Furthermore, the largest temperature gradient is within the center body itself. Thus, the best place to cool the compressor module is in the flange area (generally in the area of nodes 9-12). This area lends itself nicely to the use of heat shunting straps (for the final spacecraft application).

Table 8. Summary of Significant Temperatures

Node	Temperature (°C/°F)
14	21/70
11	25/77
10	27/81
7	29/84
5	28/83
1	58/136

As was indicated above, water cooling was used as a laboratory expedient to simulate heat pipe technology cooling. Temperatures resulting from other types of cooling can be estimated from the information given in Table 8 and Figure 15.

If a heat pipe were used instead of water and the heat pipe/center body interface temperature was 70°F, all temperatures shown in Table 8 would be unchanged. If the interface temperature was different from 70°F, all temperatures would change by the value of the difference.

If cooling were achieved by using a thermal strap attached to a cooling plate (or other heatsink) and, for example, to node 11 (approximately the center body OD) and the strap/center body interface temperature was 77°F, all temperatures shown in Table 8 would be essentially unchanged. If the interface temperature was different from 77°F, all temperatures would change by approximately the value of the difference.

6.3 Instrumentation

In addition to the four force transducers mentioned above, the unit incorporates the following sensors mounted internally to each module:

- ○ One capacitance-type displacement probe that senses diaphragm position and motion. This is the primary sensor used to control the compressor (see Section 7.0).

- ○ Three eddy-current-type displacement probes. Two of these probes sense plunger axial motion (wired in "push-pull" so as to subtract any radial plunger motion). The other probe senses plunger position relative to the centering port. These probes are for development purposes and will be utilized to correlate plunger/diaphragm motions, determine accuracy of the placement of the centering port, and provide general diagnostic information.

- ○ Two resistance temperature detectors (RTDs). One is mounted and potted into the motor coil to determine motor "hot spot" temperature and the other is mounted on the diaphragm end bearing support structure ~180 deg from the capacitance probe.

- ○ Pressure transducers. One is used to sense compression space pressure and the other to sense the compensating bellows pressure. Another pressure transducer is provided to sense the compressor pressure at the juncture of the two module discharge ports in the center body.

6.4 Compressor Hardware

Figure 16 presents the motor hardware, showing the outer stator mounted in its frame and the motor plunger on which the bearing and moving magnet surfaces are evident. The motor assembled onto the support structure is also shown in this figure. Figure 17 shows the volume compensation bellows assembly. The front (flat) and back (recessed) faces of the integral rim diaphragms are shown in Figure 18.

Figure 19 shows the diaphragm end of the assembled compressor module and the contoured face of the center body. The completely assembled back-to-back compressor on its mounting stand with the "pulse-tube simulator" installed is shown in Figure 20.
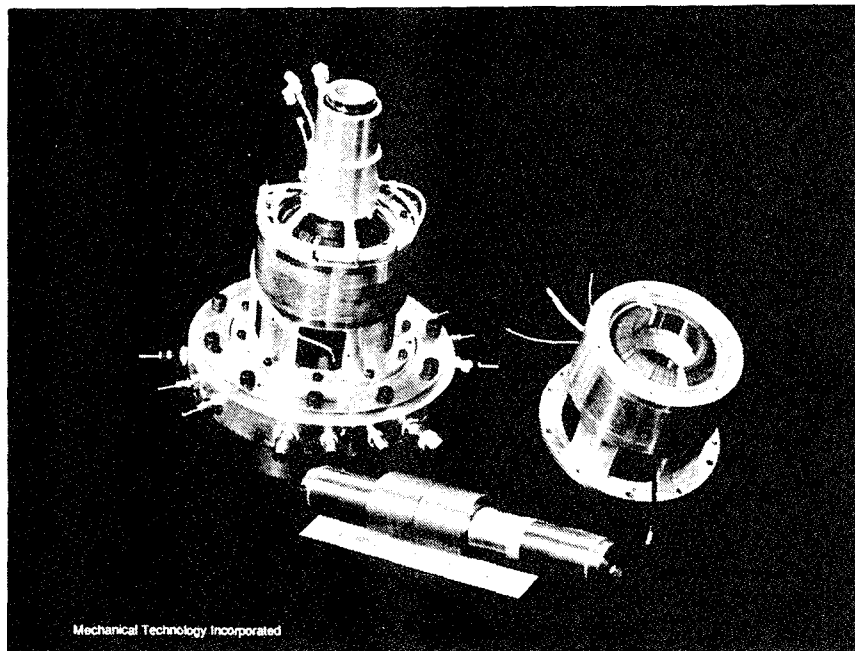
Figure 16. Motor Hardware
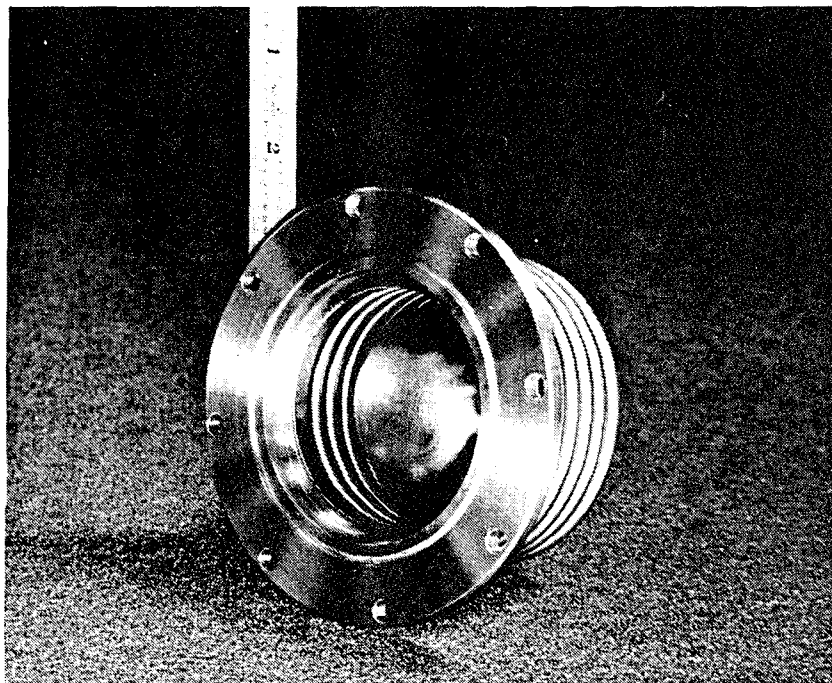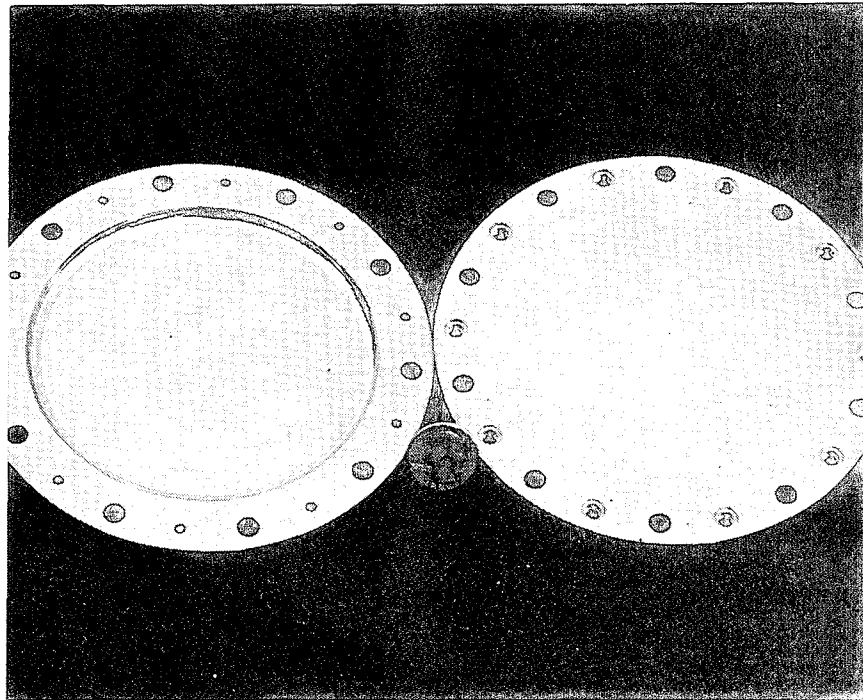

Figure 17. Volume Compensation Bellows Assembly

Figure 18. Integral Rim Diaphragm

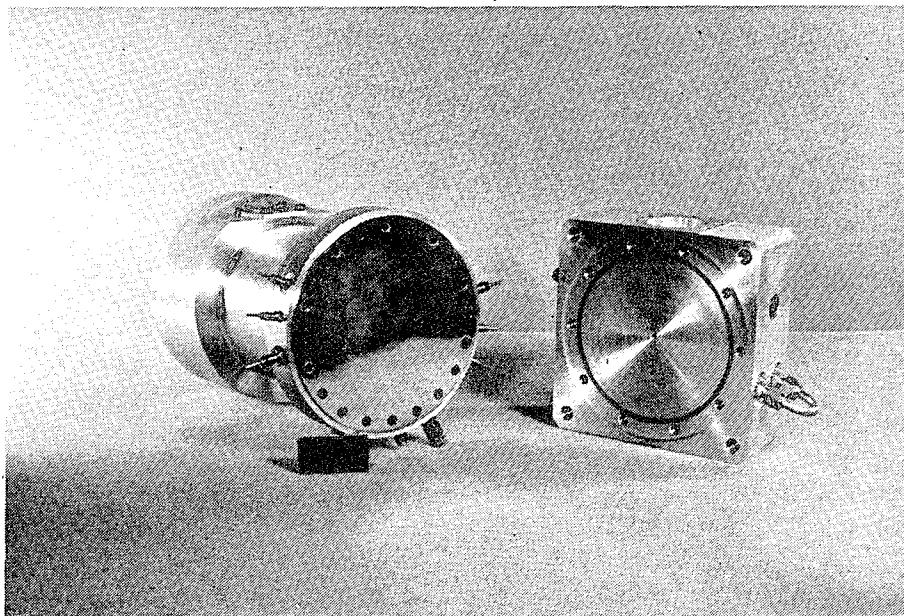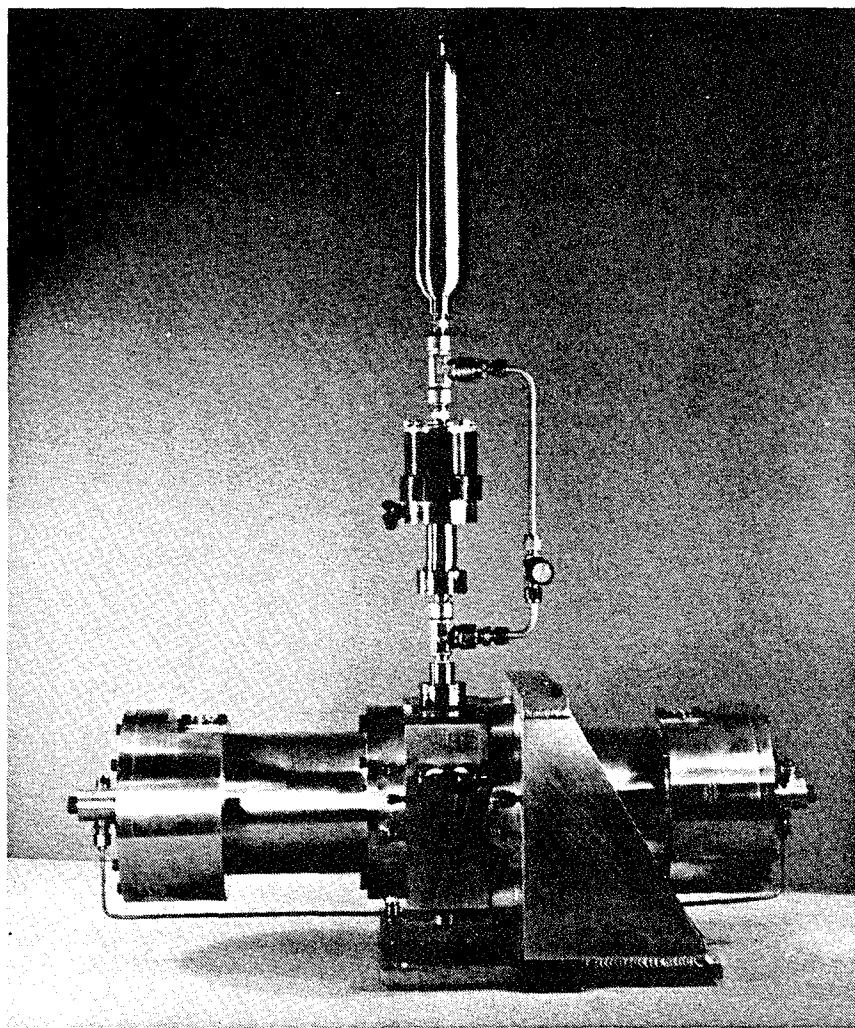Figure 19. Assembled Module and Center Body

Figure 20. Compressor Assembly with Pulse-Tube Simulator Installed

7.0 COMPRESSOR CONTROL AND POWER ELECTRONICS

7.1 System Requirements

The functions of the proof-of-concept compressor control system are to

- Provide a nominal 14-V rms, 40-Hz power to each compressor motor
- Provide ac power to each motor that is nominally 180 deg out of phase with each other
- Control ac voltage to each motor to maintain the desired diaphragm setpoint amplitude
- Control dc voltage to each motor to maintain the desired diaphragm offset position (nominally zero offset)
- Provide a manual means of trimming phase and amplitude between each compressor to vary the first harmonic of residual vibratory forces transmitted to the mounting structure.

7.2 System Description

The control system consists of two subsystems: one controlling each of the two modules (master and slave). Each subsystem uses a capacitance probe (one monitoring each diaphragm) to control the stroke amplitude and dc offset of the two diaphragms. The two halves (subsystems) operate in a master/slave configuration. Figure 21 details the electronic circuitry needed to accomplish this and shows the master (upper half)/slave (lower half) relationship.

The diaphragm capacitance probe is the sensor used for all (ac and dc) waveform measurements. Its output is basically a capacitive charge proportional to the distance between the probe and the target (the hydraulic fluid side of the diaphragm). The probe amplifier is excited by a 16-kHz oscillator and converts and amplifies the charge signal. The signal is then demodulated and filtered to remove the 16-kHz oscillator carrier component. At this point, the signal will resemble the waveform shown on the block diagram.

The signal is then routed to a low-pass filter and a peak detector. The low-pass filter (0.1 Hz) extracts the dc offset, while the peak detector measures the maximum excursion of the diaphragm. The peak amplitude signal (from the peak detector) and the dc offset signal are connected to a microcomputer within the controller.
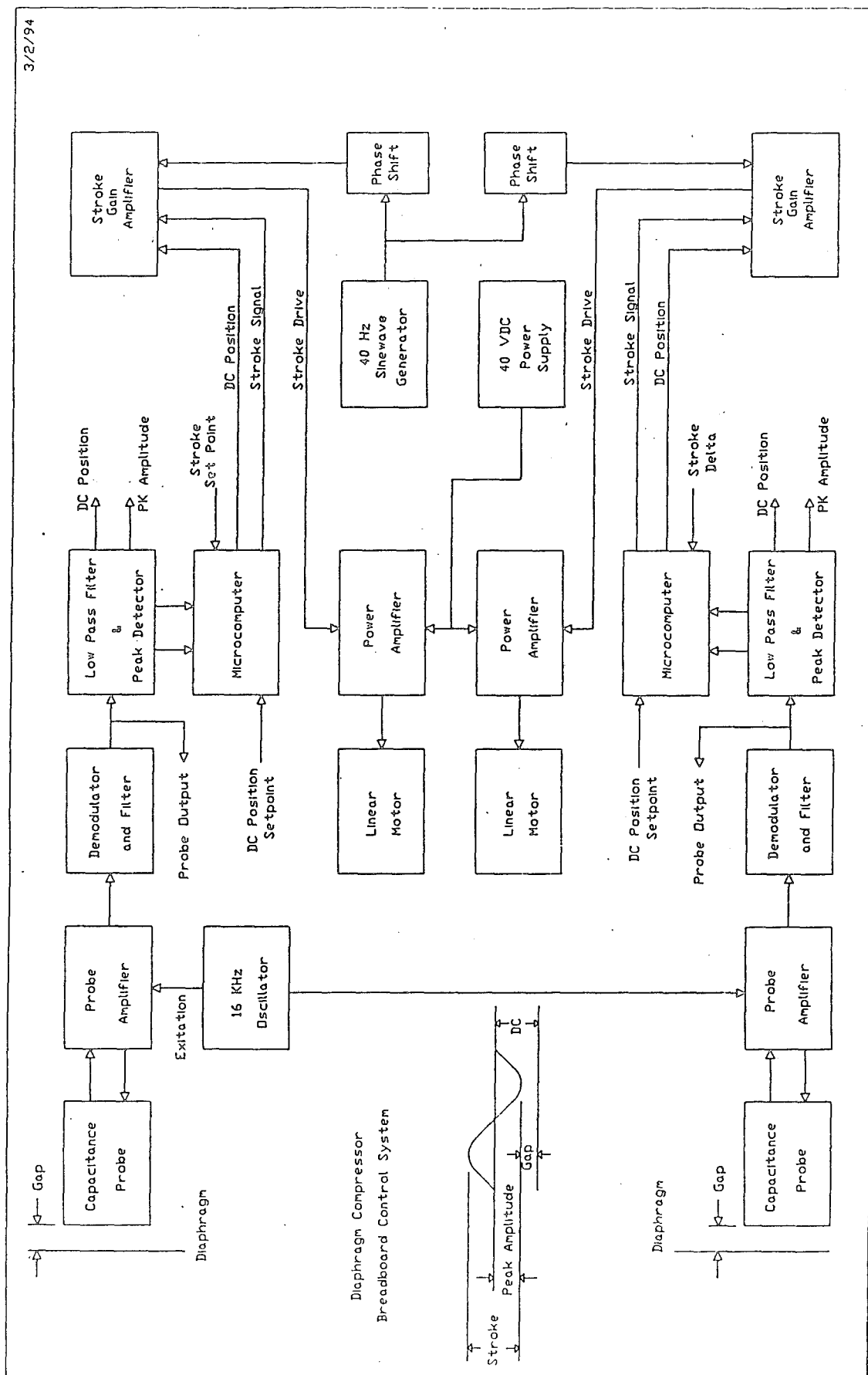
Figure 21. Control System Electronic Circuitry

The microcomputer, shown in two places in the figure, accepts seven dc inputs and generates four dc outputs as given below:

dc inputs: overall stroke setpoint, master peak amplitude, slave peak amplitude, master dc offset setpoint, slave dc offset setpoint, master dc position, and slave dc position.

dc outputs: master stroke error, slave stroke error, master dc drive, and slave dc drive.

The dc position is read by a 10-bit analog-to-digital (A/D) converter and compared to a scaled reading from the dc offset setpoint control potentiometer. The resultant dc error value is processed by a proportional integral (PI) control block before being output via an 8-bit digital-to-analog (D/A) converter to the pulse-width-modulated (PWM) servo amplifiers feedback input connections.

The dc position is also compared to the peak amplitude signal to produce the gap value. This measurement is then tested to see if the gap setpoint (software adjustable) is violated. If so, the stroke drive output signal is limited to prevent the diaphragm from being driven into the head.

The above-mentioned peak amplitude signal is also multiplied by two to develop a peak-to-peak stroke value that is then compared to the overall stroke setpoint input. The resultant stroke error is processed by another PI control and output to the stroke gain amplifier block. This process is repeated for both the master and slave halves of the control system.

The stroke gain amplifier is basically a multiplier circuit with the stroke drive output being the product of the driving waveform from the phase shift and bypass circuit and the stroke error signal from the microcomputer. The stroke error signal is adjustable, allowing for small differences in the stroke drive requirements of the two halves of the control system.

The stroke drive output and the dc error signal are both connected to the PWM servo amplifier that keeps the diaphragm centered and at the proper stroke amplitude by controlling the action of the linear motor. The ac power component controls motor plunger amplitude and the dc power component controls motor plunger position. The relative piston port location controls the diaphragm position. The basic driving frequency and amplitude for the power amplifier are provided by the 40-Hz sine wave generator via a phase-shifting circuit.

Figure 22 is a photograph of the front panel of the control system showing the diaphragm position and amplitude meters, control switches and knobs, and various output jacks. The computer equipment shown to the right of the controller is a portion of the MTI data acquisition system. Figure 23 shows a close-up of the front panel with the circuit board cover panel removed. Figure 24 shows a close-up of the rear of the control system showing the input and output terminals, and Figure 25 shows the compressor power supply cabinet.
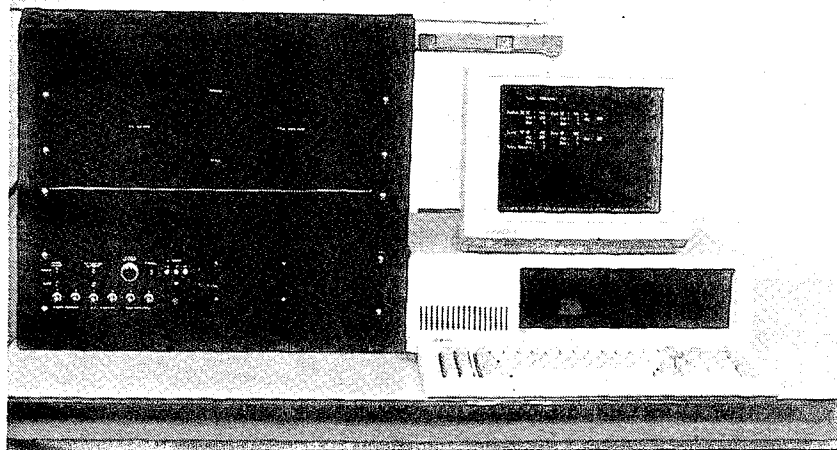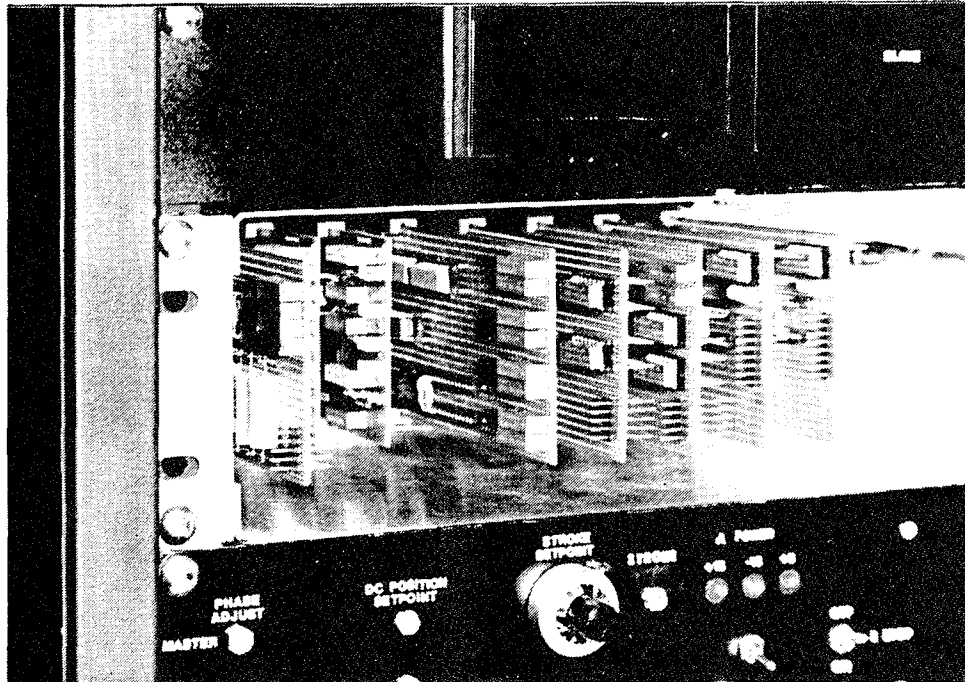
Figure 22. Control System Front Panel

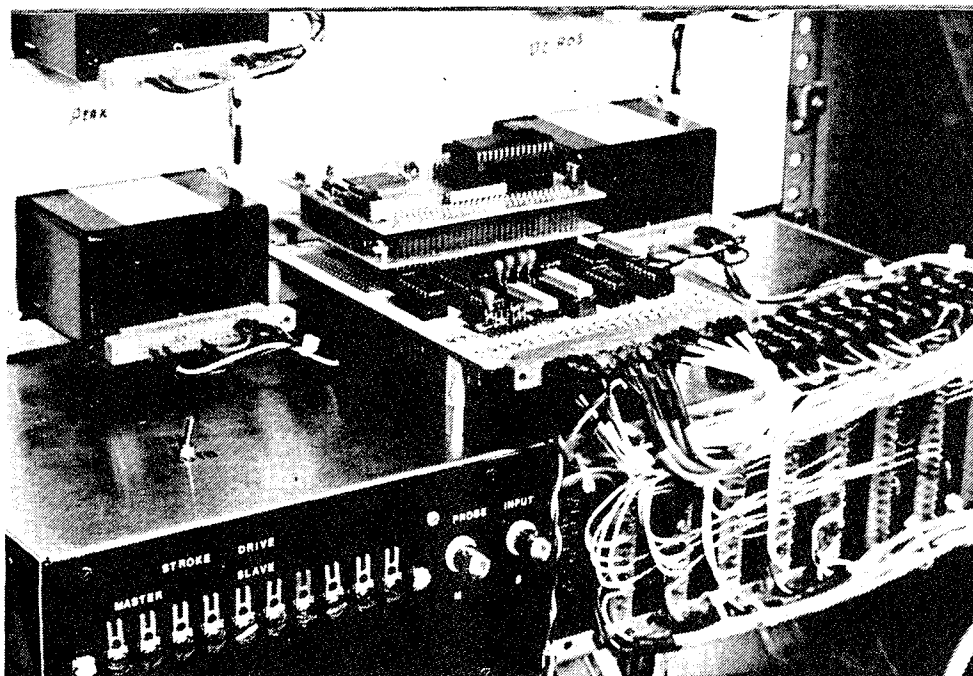**Figure 23. Front Panel Close-up**

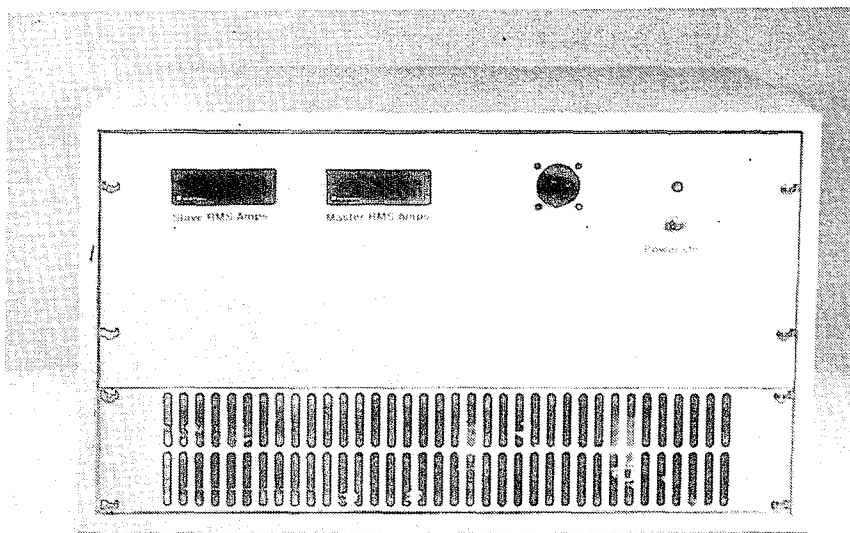**Figure 24. Input and Output Terminals on Rear Panel of Control System**

Figure 25. Compressor Power Supply Cabinet

7.3 Control System Software Description

The control system software is written in Forth and resides entirely in the file called PHILLIPS.TDS. The program listing (the Forth source code) is included in this report as Appendix B. When a Forth program is compiled, it is done on a target system, and there is no linking to other subroutines or generation of object code as in other languages. The control program consists of Forth words defined by the programmer. These words start with a ":" and end with a ";".

The controller is designed as a state machine with five different states defined: inactive, ramp, stabilize, run, and calibrate. The control system is always operating in one (and only one) of these states. Figure 26 shows the states along with the definitions and requirements for state transition. The first line on the PC CRT displays the present state.

The beginning of the program defines all system constants, variables, and names. There are also several words here that set up the A/D and D/A subsystems on the pulse processor card and should not be changed. The program starts at the word "GO," which initializes all variables, clears the screen, and begins the foreground program loop CONTROL. CONTROL is the main loop and executes the words ANALOG, SCALE, CALCS, SUPER, LOOP-SWITCH, and DA. Figure 27 shows the flow of the data through the software as described below.

ANALOG acquires raw data from all 10 channels of the A/D converter. Any ground offset voltage measured is then subtracted, and the data are stored with a descriptor ending in -IN. The word SCALE then acts on the raw data using the input*m/n+p format and stores it by descriptor.
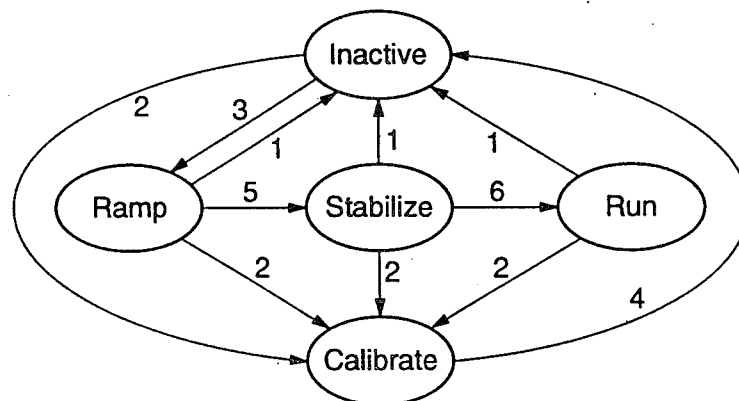
1 E-Stop In or Trip = 1
2 Cal In = 1
3 E-Stop In and Trip = 0
4 Cal In = 0
5 Ramp Timer Ends
6 Stabilize Timer Ends

Figure 26. Control System State Diagram

67

Figure 27. Flow of Data Through Software

The word CALCS first calls the word FILTER, which adds a specified percentage (K-FILTER/100) of the new reading for both dc and peak values to the old reading. Then all gap dc errors and peak errors are calculated. The slave peak setpoint is determined by subtracting the peak delta value from the master peak setpoint setting. The word SUPER is called next. Here, the variable CSTATE is evaluated to see what state is set, and the appropriate action is taken.

The word LOOP-SWITCH determines which side of the compressor is active, master or slave. The time that each side is active is determined by counting up to LOOP-TAR.

The last task executed by CONTROL is DA. This word sends the four calculated demand values (two dc and two peak) to the pulse processor direction registers to be sent to the output ports.

This loop is interrupted once a second by the word INTWORK. INTWORK disables the interrupts, calls SHOW, enables the interrupts, then goes away for a second. SHOW writes the data display to the PC CRT.

When entering any of the five states (except Calibrate), a test is made to see if the E-stop switch is turned on or if the trip flag is set. A second test is made to see if the Calibrate switch is set to CAL.

The action taken in each of the five states is

- INACTIVE-ACTION: All D/A outputs are set to zero. All integrator terms and status flags are set to zero. The E-stop LED is turned on.

- RAMPUP-ACTION: The dc and peak D/A outputs are ramped up to a predetermined value, and the ramp timer is incremented. When the timer counts down, the stabilize mode is called.

- STABILIZE-ACTION: The two dc PI loops are activated with control constants set to about one-half the final values. The system remains at this point for ~2 min. The peak D/A outputs are then slowly ramped to 50 bits below setpoint. The system again remains stable at this point for about 2 min. After this, all four PI loops are released. They are slowly ramped to their final constant and front panel stroke setpoint targets. The run mode is then called. Total time from inactive to run is about 10 min.

- RUN-ACTION: Protection is invoked to shut down if the diaphragm gets too close to the head or the total motor current exceeds the maximum allowed. All four PI control loops are called.

- CALIBRATE-ACTION: Sends a preset value out to all four D/As until the Calibrate switch is turned off.

All four PI control loops are essentially the same. Each begins with a test to see if the integrator saturated flag is set for that particular loop. If it is, the integrator is skipped and only the proportional control is used. If not, a new integrator value is calculated (the -X term). The proportional contribution is then determined, the two are added together, and the result is the demand value for the D/A. Before it leaves, the output value is tested to see if it is saturated. If so, the appropriate flag is set. The output value is also passed through a limiter to prevent math problems in the pulse processor.

To edit and recompile the control program, the following steps must be executed in the order shown:

1. Refer to Figure 28. Move the X-W jumper on the TDS9090 processor card from "X" to "W". This enables the NV-RAM write enable input line.

2. Cycle the ±15 V dc power switch, hit F1 on the PC, and enter "I".

3. At the "ok" prompt, enter "cold" to clear the application program and restart the processor.

4. Press "enter" to get the next "ok" prompt, hit F1, and then enter "E". The file to edit should be <PHILLIPS>. The Forth source code in Kedit should appear.

5. After editing and filing, the "ok"' prompt will reappear. Hit F1 and select "C". The program will compile into the controller line by line.

6. After the program has successfully compiled, place the X-W jumper on the TDS9090 card back to the "X" position to disable the write enable line and again cycle power. The PC should display an operating screen.
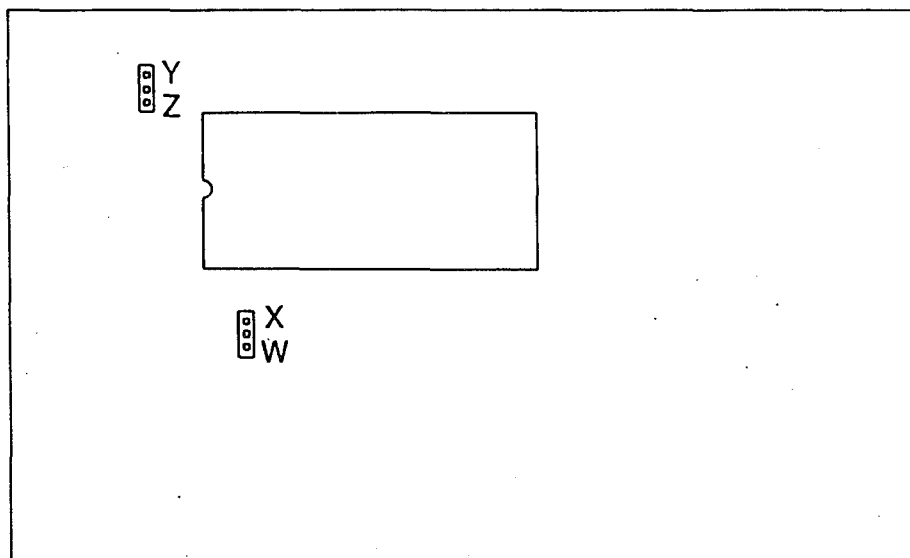
X RAM Write Disabled
W RAM Write Enabled
Z 8K x 8 RAM
Y 16K x 8 RAM

Figure 28. X-W Jumper on TDS9090 Processor Card

8.0 TEST PROGRAM

The proof-of-concept compressor test program was initiated in February 1993. Initial testing involved characterization of the linear motors to compare predicted versus measured air-gap force. Dynamic tests were next conducted on each individual compressor module to measure and optimize module performance and to check operation of the PWM amplifiers. Finally, the complete back-to-back compressor configuration was tested at its design-point conditions using a pulse-tube simulator to produce the required pneumatic loading of the compressor (i.e., the required pressure amplitude, pressure angle, and pv power). The following paragraphs describe the compressor instrumentation and these various tests.[1]

8.1 Instrumentation

The proof-of-concept compressor was instrumented with dynamic stroke, pressure, voltage, and current transducers. A PC-based data acquisition system (DAS) utilizing high-speed A/D converters was used to record and calculate compressor performance.

8.1.1 Plunger Displacement

Eddy-current displacement transducers were used to measure dynamic stroke (amplitude and dc offset) of the two motor plungers (or equivalently, stroke of the two hydraulic pistons). These transducers were used only for data analysis and monitoring purposes. They were not used for compressor control.

8.1.2 Diaphragm Displacement

One capacitance displacement transducer was used in each module to measure dynamic diaphragm displacements (amplitude and dc offset). The capacitance transducer was radially offset 28.83 mm from the center of the diaphragm. The effective radius of the diaphragm was 54.86 mm. Accordingly, the transducer was located at a radius ratio of 28.83 mm/54.86 mm, or 52.5 percent of the diaphragm radius. At this radius ratio, the calculated ratio of diaphragm center deflection to deflection at the transducer was 1.103 mm/0.731 mm = 1.509.

---

[1] Two sets of compressor hardware were built (a total of four modules), one with Air Force contract funding and one with MTI IR&D funding. Some of the testing was done with the Air Force hardware and some with the MTI hardware. All four modules performed essentially the same, so no effort is made herein to distinguish between the two compressors.

In addition to using these transducers for data analysis, the diaphragm amplitude and dc offset signals from each module were used as the inputs to the closed-loop compressor controller. Accordingly, these transducers required accurate calibration. A special fixture was used to allow in-situ calibration of the capacitance transducers. The fixture held three dial indicators for mechanical (reference) measurement of diaphragm deflection. One indicator was located at the transducer location (on the opposite side of the diaphragm). A second indicator was mounted diametrically opposite the transducer location at the same radial distance from the center of the diaphragm. The third indicator measured center deflection of the diaphragm. Figure 29 is a photograph of the calibration setup.

The diaphragm was statically deflected by applying positive and negative pressure (relative to atmospheric pressure) to the oil side of the diaphragm. In this manner, a complete calibration curve was obtained for the transducer and associated electronics of each module. Figure 30 shows the calibration curve for the final assembly of the master module prior to shipment to Phillips Laboratory. The measured ratio of diaphragm center deflection to deflection at the transducer is also plotted in Figure 30 and is seen to be in close agreement with the calculated ratio of 1.509.
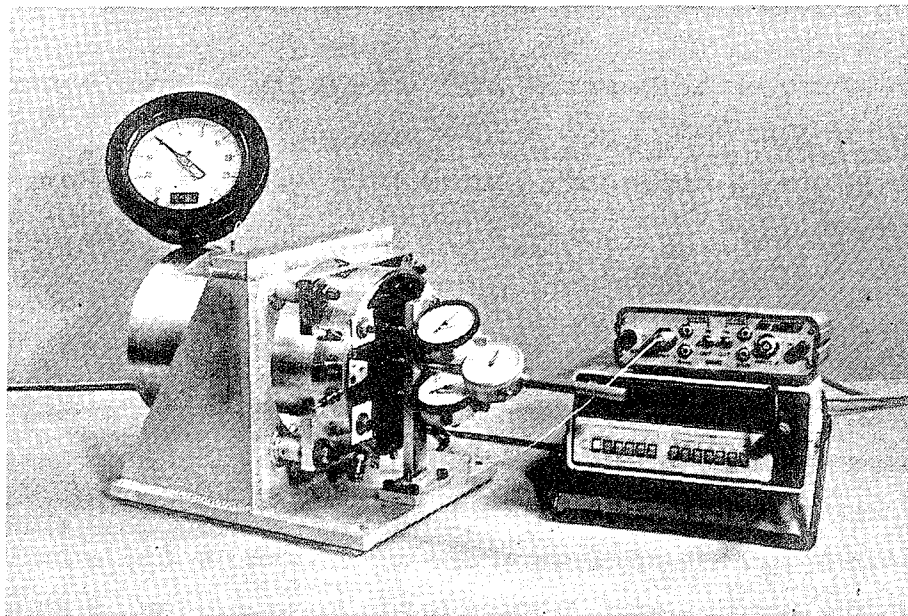

Figure 29. Setup for Calibrating Diaphragm Deflection Transducers
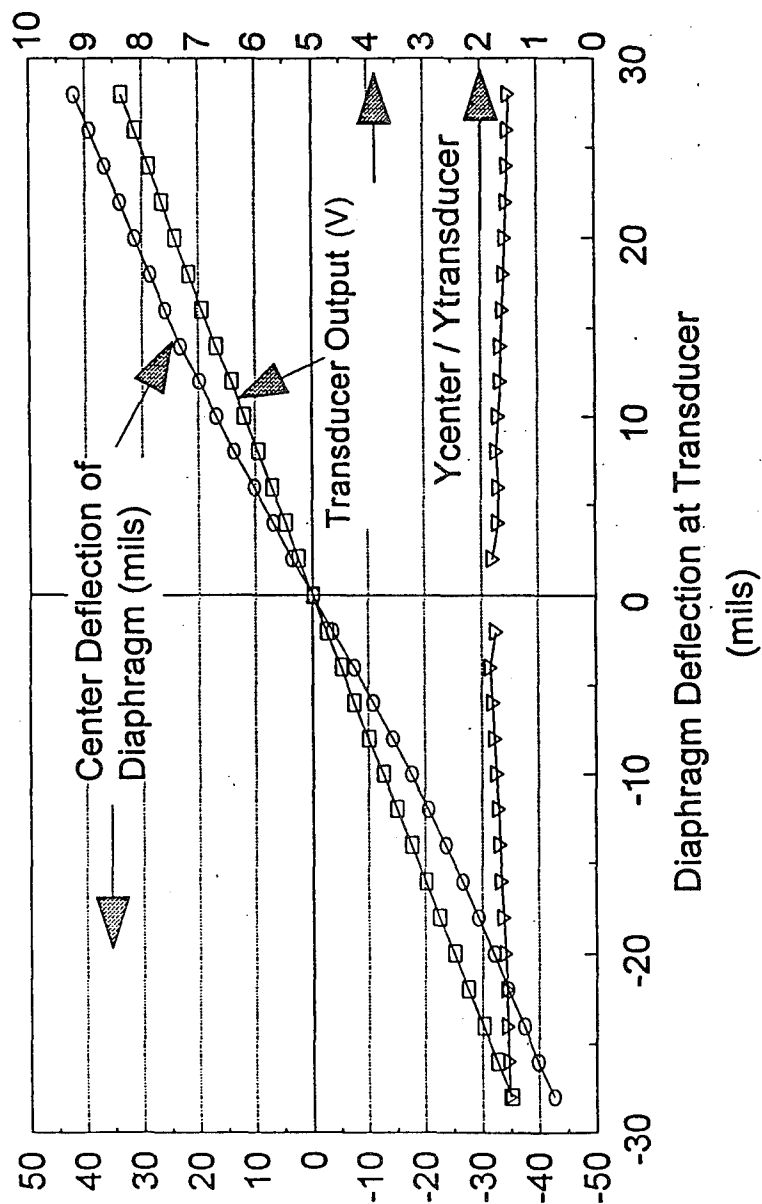
Figure 30. Calibration Curve for Diaphragm Capacitance Transducer

8.1.3 Pressures

Strain-gage pressure transducers were used to measure helium dynamic and average pressure at (1) the compressor discharge port, (2) in each of the diaphragm compression chambers, and (3) inside each of the volume-compensation bellows. Although these transducers were subject to small amounts of dc drift, their change in output voltage per unit change in pressure (dv/dp) was both constant and linear, thus allowing accurate measurement of pressure amplitude and phase angle as required for calculation of pneumatic pv powers.

8.1.4 Motor Current and Voltage

Both motor current and terminal voltage were also transduced for each compressor module so that current and voltage dynamic amplitudes and dc offsets could be measured. Unfortunately, the electronic filter circuit used to transduce the 35-kHz switched PWM voltage waveform did not yield accurate voltage amplitude measurements. Consequently, accurate calculation of motor input power was not possible.

8.2 Motor Air-Gap Force Measurements

Static tests were performed on each linear motor to measure force production capability. In these tests, a force transducer was used to measure air-gap force acting on the plunger as the plunger was slowly displaced through one stop-to-stop (and return) displacement cycle. The plunger displacement cycles were repeated for different constant values of dc current in the motor's ac coil. Current values ranged from zero to ±29 A. The zero-A data gave the axial "spring" force gradient of the motor due to the plunger's magnets.

Figure 31 shows the measured air-gap force curves for motor SN-2 as a function of plunger displacement and coil current. (The curves for motor SN-1 were almost identical.) Each force curve exhibits a hysteresis loop characteristic. Part of this hysteresis force represents bearing friction as the plunger was moved through its displacement cycle. However, it is believed that most of the hysteresis effect was introduced by the piezoelectric force transducer.

At the plunger's mid-stroke position, predicted motor force gradient was 8.17 N/A. Measured force gradient was 8.45 N/A and -8.27 N/A for currents of +25 and -25 A, respectively. This excellent agreement between predicted and measured "coil" forces indicated that the motor would be capable of producing its design shaft power of 145 W.
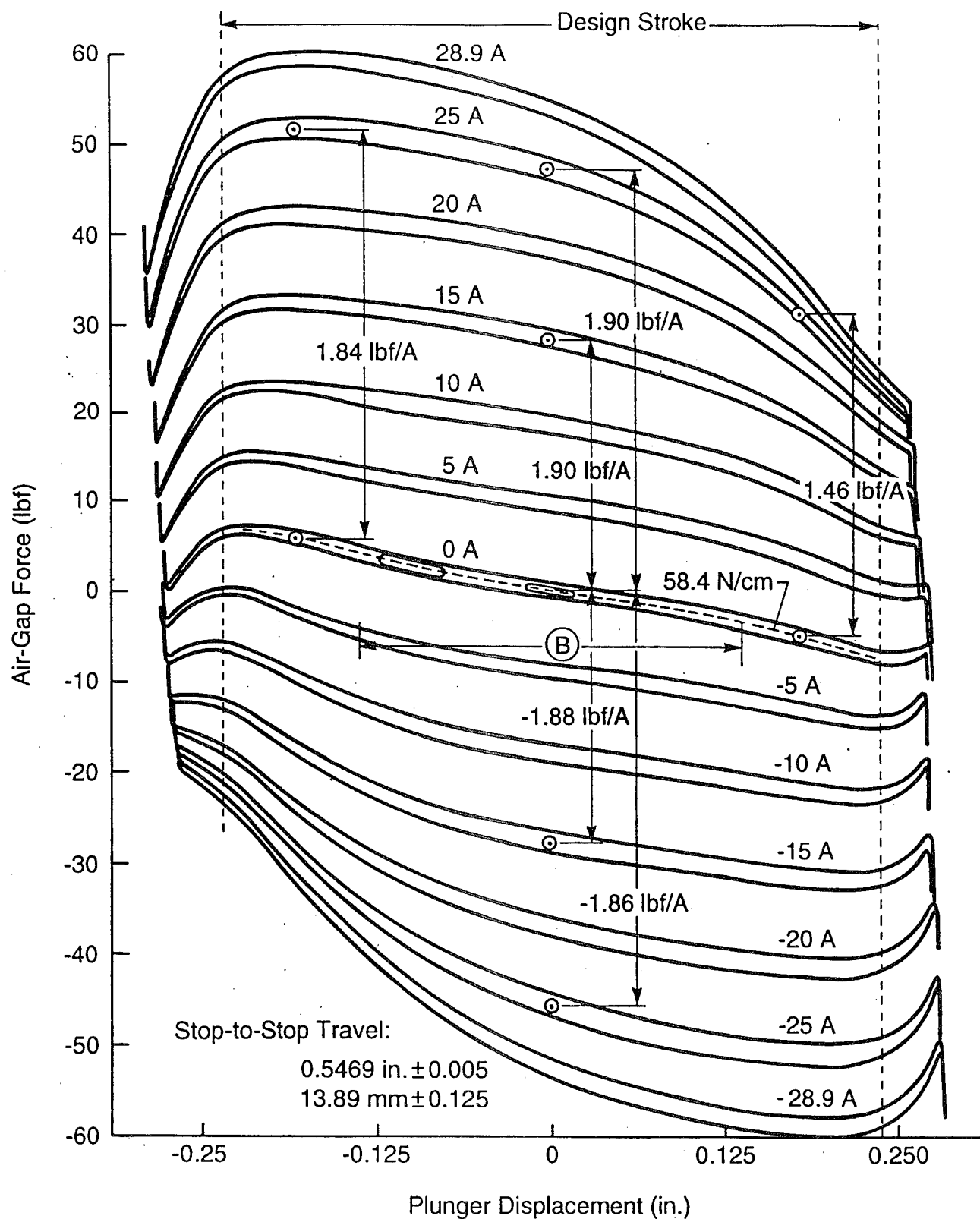
Figure 31. Measured Air-Gap Force as a Function of Coil Current

The predicted magnet spring-force gradient was 67 N/cm as compared to measured values that ranged from 44.5 N/cm for small plunger displacements to 58.4 N/cm for large displacements. The reason for these somewhat low and nonlinear gradient values was not identified from the testing. The lower measured value of magnet axial stiffness was not judged a problem (confirmed by subsequent testing) since compressor dynamics would be dominated by the compression cylinder plus bellows gas-spring stiffnesses.

8.3 Individual Module Test Results

In order to test the individual compressor modules, as well as the complete back-to-back compressor assembly, a means of pneumatically loading the modules and compressor assembly had to be provided. Accordingly, a pulse-tube simulator was designed and built consisting of a water-cooled aftercooler to remove the compressor pv work, a variable orifice throttling valve, and a variable-volume ballast chamber. This simulator, as designed, was sufficient to load the individual modules very close to their design-point conditions. However, as discussed in Subsection 8.4, the simulator hardware had to be modified to achieve total design-point loading conditions when the complete compressor assembly was tested.

Testing of the individual "master" and "slave" modules was conducted from April 1993 through June 1993. During these tests, diaphragms manufactured from 0.30-mm (0.012-in) thick sheet valve steel were used in place of the integral-rim diaphragms (the integral-rim diaphragms were not available until May 1994)..

The master module, tested first, exhibited minimal start-up problems. Essentially design-point performance was demonstrated on May 5, 1993. The slave module was tested next, achieving essentially design-point performance on June 2, 1993.

Throughout the May-June period, several small modifications were made to the master and slave modules, such as grooving the cylinder head to reduce possible diaphragm-induced blockage of cylinder discharge flow in the vicinity of top-dead-center deflection. Only one of these modifications was deemed significant, that being an 80-percent increase in the flow area of the cylinder's discharge drillways to reduce discharge pressure drop. The drillways were increased from 2.946 to 3.962 mm. Table 9 shows the result of this increase. Drillway pressure drop was reduced from about 13 kPa (1.9 psi) to about 3.4 kPa (0.5 psi). The pv power available at the compressor discharge port increased by about 11 W (10.4 percent). The increase in drillway diameter was the only performance-related modification made to the compressor drawing package.

Table 9. Effect of Enlarged Discharge Drillways in Slave Module
(80-Percent Increase in Discharge Flow Area)

	Design Point Value	Slave Module with Plain Head		Percent Difference Enlarged Relative to Original Drillways
		Original Drillways[a]	Enlarged Drillways[b]	
Dynamic Data				
Piston Stroke, mm	12	11.248	11.503	2.27
Piston Offset, mm	0.248	0.5062	0.4065	-19.70
Piston Phase, deg	0	0	0	--
Diaphragm Stroke, mm	1.92	1.8748	1.932	3.05
Diaphragm Offset, mm	-0.095	-0.0523	-0.0773	47.80
Diaphragm Phase, deg	0	0.5707	0.5144	-9.87
Cylinder Mean Pressure, psig	275	288.9	289.77	0.30
Cylinder Pressure Amplitude, psi	58	55.19	55.398	0.38
Cylinder Pressure Angle				
Relative to Piston, deg	--	40.16	39.14	-2.54
Relative to Diaphragm, deg	40	39.59	38.63	-2.43
Compressor Discharge Pressure				
Mean, psig	--	286.1	290.3	1.47
Amplitude, psi	--	53.29	54.91	3.04
Phase Relative to Piston, deg	--	37.21	38.89	4.51
Phase Relative to Cylinder Pressure, deg	--	-2.95	-0.25	-91.53
Phase Relative to Diaphragm, deg	--	36.64	38.38	4.74
Static Data and Calculated Results				
Motor Coil Temperature, °F	113	87.3	88.3	1.15
Piston Frequency, Hz	40	40.44	40.44	0.00
Cylinder Pressure Ratio	1.5	1.454	1.445	-0.62
Diaphragm Effective Area, m²	0.004019	--	--	--
Piston Area, m²	0.000644	--	--	--
Cylinder Gas-Spring Stiffness, N/cm	300.6	332.84	331.54	-0.39
Piston Swept Volume (SV_p), cc	7.725	7.238	7.402	2.27
Diaphragm Swept Volume (SV_d), cc	7.725	7.535	7.765	3.05
(SV_d) (SV_p)	--	1.041	1.049	0.77
Compression Cylinder PV Power, W	124.8	116.1	117.6	1.32
PV Power Available at Discharge Port, W	124.8	104.9	115.9	10.46
		Computed from measured amplitudes and phases		

[a]DAS Data File/Scan Number: 06029315/8
[b]DAS Data File/Scan Number: 06049313/4

Two problems were identified during the individual module testing. As mentioned previously, the PWM amplifiers used to drive the motors had a 35-kHz switching frequency. The resulting high-frequency electromagnetic radiation introduced significant noise levels on various transducer signals. Accordingly, inductive filters were purchased and inserted in the output power leads. This eliminated most of the transducer noise problems. However, the electronic filter circuit used to transduce PWM output voltage still did not give accurate measurement of the voltage harmonics as evidenced by (1) voltage readings well below predicted values and (2) computed motor input powers less than motor output shaft power. This problem was not corrected and prevented measurement of overall compressor efficiency throughout the test program.

The second problem was saturation of the negative peak of the PWM output current as design-point operation was approached. This problem was apparently due to the amplifier being slightly undersized, since the saturation was eliminated when a larger (MTI-owned) PWM amplifier was used. However, there was no evidence that this saturation caused any compressor operational problems.

8.4 Dual-Module Compressor Testing

Initial performance testing and automatic operation of the complete dual-module compressor assembly was conducted during July and August of 1993. The temporary flat-sheet diaphragms continued to be used during this period.

In order to achieve full design-point loading of the two-module assembly, additional volume had to be incorporated into the pulse-tube simulator circuit, and the variable-orifice throttling valve was moved to a bypass line around the aftercooler. With these changes, it was possible to produce the exact design-point loading conditions on the compressor. Figure 32 shows the compressor assembly with the modified pulse-tube simulator installed.
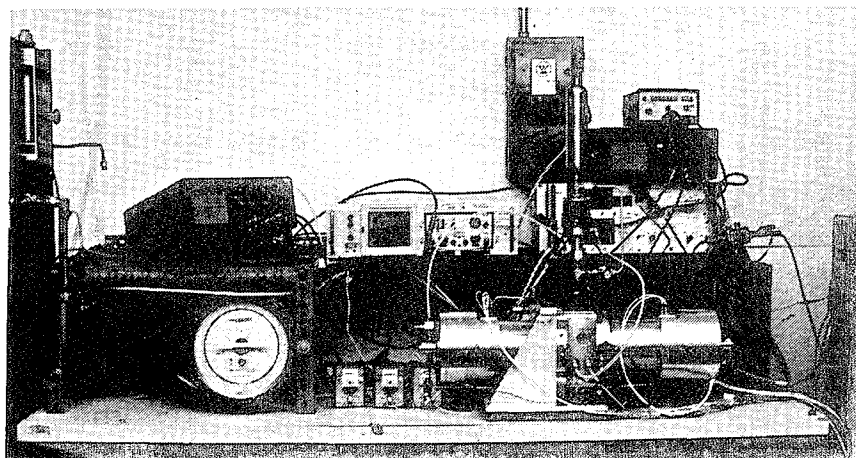

Figure 32. Compressor Assembly with Pulse-Tube Simulator

8.4.1 Modes of Compressor Operation

The dual-module (back-to-back) compressor assembly was successfully operated both manually (open loop) and automatically (with closed-loop controller). For manual operation, a variable-frequency electronic oscillator with adjustable ±dc and ac voltage outputs was used to provide a common input drive signal to the PWM amplifier of each module. Since a common drive signal was provided to both amplifiers, independent adjustment of PWM output currents to each drive motor was not possible. Consequently, diaphragm dc offset could be reduced to zero by oscillator dc adjustment only in one (or the other) of the modules. The second module then operated with a small amount of diaphragm offset due to manufacturing tolerance differences between the two modules. While this limited the maximum over-stroke range of the compressor, open-loop design-point operation was achieved. The dual-module assembly was dynamically very stable during open-loop operation.

Under closed-loop operation, independent control of PWM ac and dc output currents to each drive motor is provided by the controller so that diaphragm offset can be zeroed in both modules. However, difficulty was initially encountered in maintaining stable closed-loop operation during compressor start-up. The instability problem may have been due to the fact that a finite amount of piston stroke is required before the piston ports begin to function, and/or possibly due to motor magnetic dissimilarities at very low power levels. In any case, the start-up instability problems were overcome by modifying the software control algorithms. Stable start-up and ramp-up to steady-state design-point conditions under fully automatic control was achieved. At the present time, the ramp-up interval takes about 10 min to reach design-point conditions. Further development of the control algorithms could probably reduce this time.

8.4.2 Compressor Performance

A design-point performance validation test was performed on August 9, 1993. The overall measured performance of the compressor is compared to design-point conditions in Table 10. Because the test values of swept volume, pressure amplitude, and frequency slightly exceeded the design-point values, compressor output power exceeded the 250-W design value by 4.2 percent. The estimated accuracy of the measured data is ±2.0 percent.

As noted in Table 10, the test value of overall compressor efficiency had to be estimated since an accurate measurement of motor input power was not available. The estimated value of test efficiency is based on measured cylinder pv values for each module and calculated values of module drive losses. The drive losses consist of bearing and hydraulic pumping losses, bellows dynamic heat transfer, and motor losses (i^2R coil loss plus eddy-current and hysteresis losses in the magnetic iron and plunger magnets). Calculated design-point values of motor

Table 10. Compressor Design Point Performance: Design versus Test

Compressor Performance	Design	Test[a]
Frequency, Hz	40	40.2
Piston Swept Volume, cc	15.5	15.7
Diaphragm Swept Volume, cc	15.5	15.9
Mean Pressure, psig[b]	275	276.8
Pressure Ratio	1.5	1.5
Pressure Amplitude, psi[b]	58	58.3
Pressure Angle (relative diaphragm), deg[b]	40	40.2
PV Power to Cryocooler, W[b]	250	260.6
Compressor Efficiency	0.71	0.74

[a]Test point number: 08099312-5.
[b]At compressor discharge port.

efficiency and the other drive losses are listed in Table 3 (shown earlier in Section 5.0). The fact that estimated compressor efficiency is three points higher than the predicted efficiency may be due to lower-than-predicted dynamic heat transfer losses in the compression cylinders. Line 31 of Table 3 shows that 27.2 W of dynamic heat transfer loss were included in the compressor design calculations based on correlations from previous work (this loss is inherently included in the measured cylinder pv powers). However, the true value of overall compressor efficiency can only be determined from an accurate measurement of motor input power, which should be a primary objective of future compressor testing.

Table 11 compares single module design versus test performance for the validation test point given in Table 10. Since the measured data for each module were very close to being identical, the average of the two modules is tabulated.

Comparison of Tables 10 and 11 (discharge pressure amplitude minus cylinder pressure amplitude) shows the compressor discharge pressure drop to be about 4.8 kPa (0.7 psi), consistent with the individual module test data of Table 9. The fact that measured cylinder pressure angle is 2.6 deg smaller than the design pressure angle further suggests that the actual dynamic heat transfer loss in the cylinders was less than allowed for in the design calculation of Table 3. Table 11 also clearly shows the inaccuracy of the PWM voltage measurement, resulting in the measured motor input power being less than the cylinder's pv power (which, of course, is not possible).

Table 11. Module Design Point Performance: Design versus Test

Module Performance[a]	Design	Test[b]
Piston Amplitude, mm	6.0	6.07
Diaphragm Amplitude, mm	0.96	0.99
Bellows Amplitude, mm	1.04	N/A
Cylinder Pressure Amplitude, psi	58.0	59.0
Cylinder Pressure Angle, deg	45.5	42.9
Cylinder PV Power, W	138.5	135.2
Motor Shaft Power, W	150.8	N/A
ac Current Amplitude, A	23.5	23.6
ac Voltage Amplitude, V	20.5	12.0[c]
Motor Alpha Angle, deg	-3.1	-11.7
Motor Efficiency, percent	85.1	N/A
Motor Input Power, W	177.2	112.0[c]

[a]Average of two modules.
[b]Test point number: 08099312-5.
[c]Inaccurate measurement of PWM drive voltage.

Finally, Table 11 shows measured motor alpha angle to be -11.7 deg, 8.6 deg more negative than the -3.1-deg design value. Whereas the design alpha angle represents compressor operation almost exactly at resonance, the -11.7-deg angle means the natural frequency of the compressor was slightly below the 40.2-Hz operating frequency. This may have been the combined result of lower-than-predicted motor magnet stiffness (discussed in Subsection 8.2), and larger-than-design test stroke and test frequency, all of which would tend to make alpha more negative. Opposing this negative shift would be the higher cylinder pressure amplitude and reduced pressure angle. Since so many factors affect alpha angle, the degree of agreement between design and measured values is, in fact, quite good. Although motor efficiency is maximized for alpha angle in the range of +10 to 0 deg, the reduction in efficiency at -11.7 deg is small, and operation at this condition is otherwise totally satisfactory. If all other parameters remain fixed, alpha angle can be readily reduced to the vicinity of zero by increasing compressor mean pressure or slightly reducing operating frequency.

Figure 33 shows typical piston and diaphragm waveforms, which are reasonably good sine waves. Figure 34 shows a Fast Fourier Transform (FFT) plot of compressor frame acceleration in the direction of piston reciprocation taken during design-point operation. The first-harmonic acceleration amplitude of 0.0085 g represents a residual unbalanced first-harmonic force amplitude of 3.02 N acting on the frame. This is 0.97 percent of the 311-N unbalanced frame force that would be imposed by a single, uncompensated module. With active vibration suppression, further significant reduction in residual frame force should be realized.

Diaphragm Displacement
(1.95-mm Stroke)

Piston Displacement
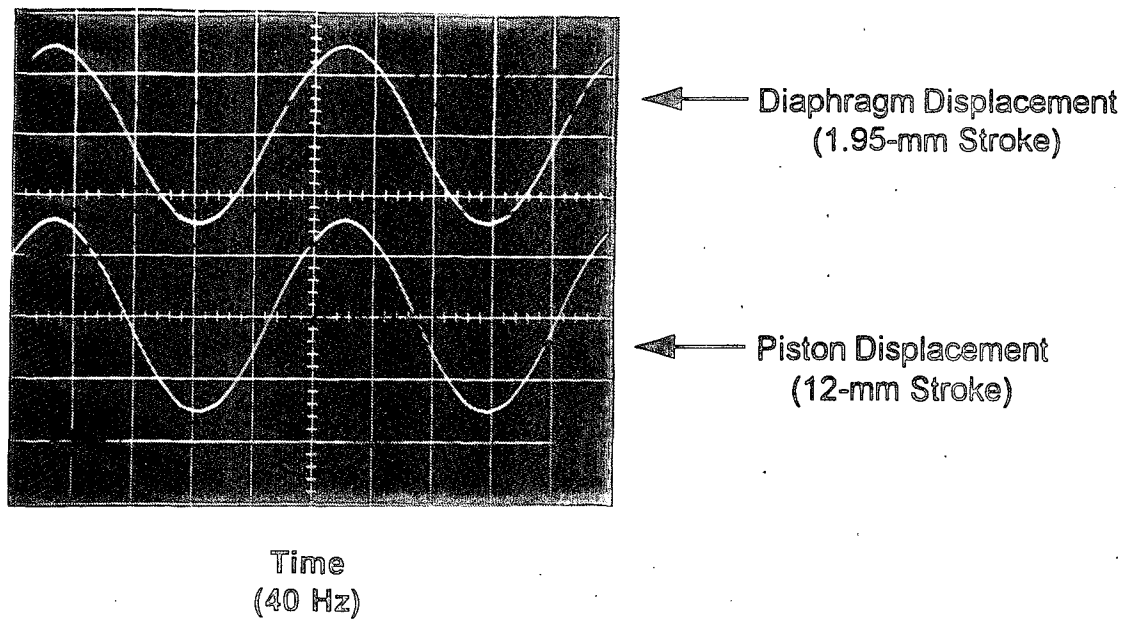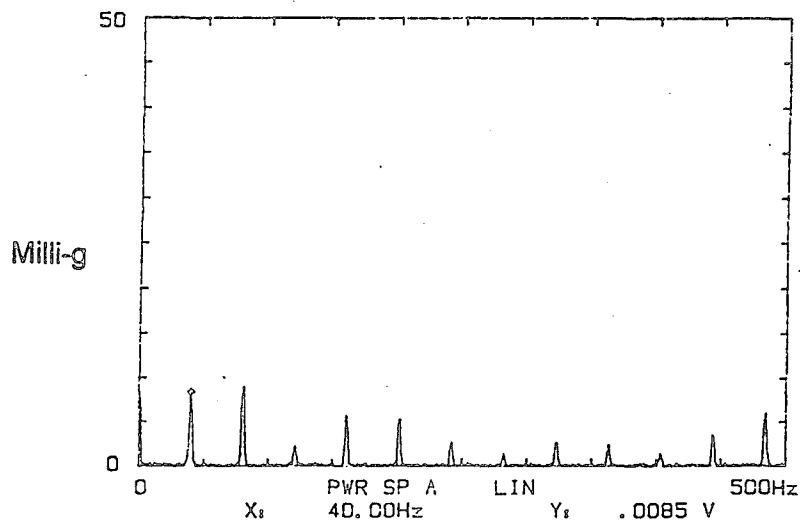(12-mm Stroke)

Time
(40 Hz)

Figure 33. Diaphragm and Piston Displacement Waveforms at Design Point Operation

Mass of one plunger assembly:	0.82 kg
Uncompensated plunger inertia force amplitude at 40 Hz:	311 N
Amplitude of fundamental vibration force acting on compressor frame:	3.02 N

Figure 34. The FFT of Compressor Frame Acceleration
(Without Active Vibration Suppression)

All testing was accomplished using cooling water ~65°F at 0.25 gpm). The first-order effect of changing cooling temperature is a change in mean system pressure. This is because the helium system is a small volume-closed system, and any change in helium temperature directly impacts system pressure. System pressure, in turn, directly affects gas spring stiffness and resonant frequency. Changes in resonance have a second-order effect on motor power and stroke. Thus, performance is affected by changes in system temperature. However, if the initial charge of helium is adjusted to accommodate a different operating temperature, the compressor performance is essentially unchanged.

For the cooling water conditions that were used in the MTI laboratory, the initial room temperature helium charge was set at 260 psig. This charge resulted in a mean pressure of 275 psig at operating temperature conditions.

8.5 Bellows Failure

During extended testing of one of the MTI compressor modules at almost its stop-to-stop stroke limit, a crack developed in the longitudinal seam weld of the bellows component. The crack occurred at a sharp corner leading into the root of the first bellows convolution (a similar corner also exists at the exit from the last bellows convolution). These sharp corners were standard manufacturing practice of the bellows manufacturer, a fact that MTI was not aware of, and did not properly protect against in our detailed bellows drawing. We assumed that the lead-in radius to the first (and last) convolution would be the same as the nominal root radius of the bellows.

Scanning electron microscope examination of the failed bellows definitely established that the crack originated in the weld at the sharp corner. It was also found that the weld contained slag inclusions, indicative of poor welding practice. We believe the sharp lead-in corner resulted in significant stress concentration, which in combination with the weld inclusions, resulted in initiation of the fatigue crack.

Two remedies are required to preclude this type of failure. First, rigorous nondestructive testing of the weld quality must be done prior to forming the bellows (i.e., while the bellows material is still in the form of a simple tube). Second, the bellows must be formed with a lead-in radius at both ends that is the same as the nominal root radius of the bellows convolutions. The bellows manufacturer has confirmed that this can readily be done. Since the design operating levels of bellows stresses are below the statistically set allowable levels for 100,000-hr reliability, MTI continues to believe that bellows can be used for this application. However, if our belief is not confirmed by subsequent endurance testing of properly manufactured bellows, an alternative, albeit somewhat heavier, compressor design approach can be used that eliminates subjecting the bellows to high-cycle stresses. This approach would use a second, identical diaphragm, to

accommodate the dynamic oil displacements, while using a bellows to accommodate the "static" thermal expansions of the oil.

The compressor being supplied to Phillips Laboratory contains two bellows having the sharp corners (a total of four possible crack initiation sites). Accordingly, reliability of these bellows is statistically much lower than the 100,000-hr design criteria to which they were designed.

9.0 CONCLUSIONS

The objective of the overall program was to demonstrate the advantages (high reliability, low weight, long life) of hermetically sealed diaphragm-type compressors intended for space cryocooler applications. Although a bellows failure was experienced, it was attributed to manufacturing flaws. To this end, a proof-of-concept compressor was designed, built, and tested. The compressor was a two-module assembly with the modules assembled back to back and operating 180 deg out of phase with one another for vibration cancellation. Each module was a diaphragm-type compressor that employs a moving-magnet-type motor contained in an oil-filled cavity. The compressor was designed and optimized to mate with a 30-K, 0.5-W orifice-pulse-tube cryocooler that was designed by the NIST.

Results of the design point tests were excellent. With the compressor operating within between 0.5 and 1.2 percent of its design frequency, stroke, mean pressure, pressure amplitude, and phase angle, the pv power and estimated compressor efficiency exceeded design values by ~4 percent. Given these results, the program demonstrated the performance advantages of hermetically sealed diaphragm-type compressors intended for space cryocooler applications. The low weight characteristic of these machines (compared with conventional Oxford-type compressors) was also demonstrated during the early design analysis phase of the program.

Long life and reliability were demonstrated by means of appropriate industry-accepted design, analysis, and reliability prediction techniques. Although a bellows failure was experienced, it was attributed to manufacturing flaws. Actual endurance and other proof-type testing will be required to fully document the compressor's life and reliability potential.

REFERENCES

1. Trainer, T.M., L.E. Hulbert, J.F. Lestingi, and R. E. Keith. "Final Report on the Development of Analytical Techniques for Bellows and Diaphragm Design." Technical Report No. AFRPL-TR-68-22, Battelle Memorial Institute, Columbus Laboratories, Columbus, Ohio, March 1968.

2. Peterson, M.B. and W.O Winer, eds. *Wear Control Handbook.* American Society of Mechanical Engineers, New York, New York, 1980.

Appendix A

Determination of
Allowable Design Stresses Under
High-Cycle Fatigue Conditions

DESIGN MEMORANDUM

Determination of Allowable Design Stresses for Components Which Must Meet Statistical Life and Reliability Requirements While Operating Under High-Cycle Fatigue Conditions

1.0   Introduction

Under Air Force Contract F29601-91-C-0112, MTI is developing an advanced compressor for possible use in SDI cryocooler applications. Attachment 1 defines the requirements for the proof-of-principle compressor. This Design Memorandum addresses the life and reliability aspects of Attachment 1 with respect to design stress criteria for the components of the compressor which are subjected to high-cycle fatigue stresses.

This memorandum represents the first step by MTI's Power Systems Division towards formalizing design procedures for meeting aerospace life and reliability requirements. It is intended primarily to document interpretations and methodology. It is not a bona fide reliability analysis for the cryocooler compressor. Numerous assumptions and simplifications have been made which may have to be replaced by more refined techniques for a final space design. It is expected that this Design Memorandum will be periodically revised and up-dated to reflect the necessary refinements. A much more detailed reliability effort will be needed during final design of a space-qualifiable machine.

High-cycle fatigue stresses are expected to be highest in the diaphragm and bellows components of the cryocooler compressor. In the following sections, the diaphragm requirements are used to illustrate the procedures for determining allowable design stresses. In addition to the diaphragms and bellows, the methodology can and should be used for all other components which are subjected to high-cycle fatigue (e.g., the compressor housing, and all assembly joints which experience high-cycle fatigue stresses).

2.0 Life and Reliability Requirements

As stated in Attachment 1, the life and reliability requirements for the cryocooler compressor are as follows:

Operational Lifetime: 100,000 hours

Reliability: 95% (at a 0.60 confidence level).

Attachment 1 does not specifically state whether the term "compressor" includes the compressor's drive and control electronics. However, assuming that the SDI application is an unmanned application (i.e., no maintenance or replacement of electronic modules is possible), it would seem logical that the life and reliability requirement would apply to the complete compressor system.

Attachment 1 does not state the duty cycle of the compressor. It is assumed that once the compressor system is "on station", the system will be turned on and the compressor will run continuously.

The operating frequency of the proof-of-principle compressor will be 40 hz. The diaphragms and bellows components of the compressor will be cyclically deflected at this frequency, thus imposing a cyclic stress condition on the materials from which these components are fabricated. The diaphragms and bellows are single-point failure components, meaning that the entire cryocooler will fail if any one of these components fail. Since the concept of redundancy does not appear to be practically feasible for these components, the reliability of these components is critical.

Compressor operation for 100,000 hours at 40 hz represents 14.4 billion stress cycles on the diaphragms and bellows. The failure mechanism of concern is high-cycle fatigue of the bellows and diaphragm materials. Closely related to the fatigue issue is the issue of long-term corrosion or erosion of the diaphragm and bellows materials. Corrosion or erosion in the form of surface pitting or intergranular attack will give rise to stress concentration effects which will degrade fatigue life.

MTI is not aware of any product experience or laboratory test data where bellows or diaphragms have been designed or tested for 14-billion cycles. Indeed, basic material fatigue strength testing is normally conducted for only 10 million cycles, and occasionally for 100 million cycles. In the absence of test data, it becomes essential to apply probabilistic (statistically-based) procedures which analytically address diaphragm/bellows

life and reliability requirements at the design stage of these
components.

3.0   Useful Life of Components

Attached Figure 1 taken from [1] shows the nature of component
failure rate versus time. The initial part of this plot, from
T=0 to Tb, is the early failure or burn-in period during which
some proportion of a population of similiar components will
exhibit a high failure rate due to substandard material,
fabrication errors, or poor quality control. The period from Tb
to Tw is called the useful life of the component. During this
period the component reaches its lowest (and relatively constant)
failure rate. Failures during this period are called chance
failures and occur randomly. When component life reaches Tw,
wearout becomes noticeable, and from this point on wearout
increases rather rapidly.

To minimize the probability of early diaphragm or bellows
failures for the SDI type of application, it will be necessary to
ground test the actual flight hardware for some specified number
of hours, perhaps of the order of several thousand hours. It may
be acceptable to do this burn-in testing at the component level,
rather than at the complete system level (although complete
system level burn-in testing will probably also be required).

The statistical variability of many wearout phenomena can be
quite well approximated by the normal, or Gaussian, failure
distribution. With respect to the diaphragm and bellows
components of the compressor, the wearout mode would in fact be
the fatigue failure mode. While the fatigue strength of metals
is most accurately described by the Weibull and lognormal
distributions, the assumption of a normal distribution will
usually result in more conservative designs [2]. A normal
distribution of fatigue strength is assumed for the procedures
described herein.

4.0   Maximum Allowable Nominal Design Operating Stress

Maximum alternating stress levels in both the diaphragm and
bellows components will occur when the compressor is operating at
its maximum possible displacement (i.e., maximum swept volume).
Deflection limiting stops must be designed into the compressor to
limit maximum diaphragm deflection in either direction to a fixed
value (the same value in both directions). Maximum possible
compressor displacement will then correspond to the maximum

deflection limits of the diaphragms, and these deflection limits will establish the maximum possible alternating stresses in the diaphragms and bellows. It is intended (in fact, required) that the compressor will always be operated at slightly less than its maximum displacement condition. However, there will always be some measurement uncertainty as to exactly what displacement the compressor is operating at. Accordingly, design of the diaphragm and bellows components with repect to life and reliability requirements should be based on the maximum stop-to-stop displacement condition.

Fatigue strength test data for engineering metals is almost universally obtained using highly-polished test specimens which are subjected to simple (unidirectional) alternating axial or bending stress. A maximum allowable nominal design operating stress for both the diaphragm and bellows materials must be derived from these test data according to a methodology based on the statistical nature of the reliability requirements. The methodology used herein is that described by Shigley [3], modified to account for the specified reliability confidence level. Once the maximum allowable nominal design operating stresses have been established, appropriate stress analysis procedures must be used for the diaphragms and bellows which relate the computed maximum operating stresses to the maximum allowable stresses.

The modified Shigley methodology for establishing the maximum allowable nominal design operating stress is expressed by the following equation:

$$S_{ed} = (k_a)(k_b)(k_c)(k_d)(k_e)(k_f)(k_g)(S_{et}) \qquad (1)$$

where

S_{ed} = maximum allowable nominal design operating stress for the diaphragm or bellows component

S_{et} = 50% probability fatigue strength for the diaphragm or bellows material as determined from fatigue test data. It is essential that the value of S_{et} be based on the number of stress cycles to which the diaphragm or bellows will be subjected over the required liftime of these components.

k_a = surface finish factor

k_b = component size factor (compared to the size of the fatigue strength test samples)

k_c = component reliability factor

k_d = operating temperature factor

k_e = stress-concentration factor

k_f = miscellaneous-effects factor

k_g = material strength confidence factor.

Factors b, c, and g above may be thought of as modifiers to the basic test value of material fatigue strength, S_{et}. Factors e and f are related to the specific design of the component. Factor c recognizes that both the material and the component are subject to unavoidable statistical variations in properties, fabrication tolerances, and operating conditions. Procedures for evaluating the above k factors (except for K_g) are given in Shigley and other references. Factors k_c and k_g are both based on statiscal probability theory and because of their importance to SDI applications are discussed in the following paragraphs.

5.0 Reliability and Confidence Factors (k_c and k_g)

The product of the reliability and confidence factors ($k_c * k_g$) is a function of the following items:

1. The number of fatigue tests which have been conducted on the particular materials from which the diaphragms and bellows will be made. These tests must be conducted in a manner appropriate to the stress conditions which will exist in the diaphragms and bellows (i.e., reversed bending or reversed axial stress) and must pertain to the final heat treatment condition which will exist in the finished part.

2. The statistical distribution characteristics (mean value and standard deviation) of the fatigue strength test data.

3. The confidence level assigned to the mean values of material fatigue strengths.

4. The statistical distribution characteristics (mean value and standard deviation) of the maximum operating stress to which the diaphragms and bellows will be sujected.

5. The required component reliability needed to
   satisfy the overall compressor life and reliability
   specification.

With respect to Items 1 and 2 above, the mean value of a
material's fatigue strength is commonly accepted to be the mean
stress value at which 50% of the fatigue test specimens will have
failed after a specific number of stress cycles. For high-cycle
fatigue applications where the number of stress cycles exceeds 10
million, most iron-based materials exhibit an "endurance limit
strength" which implies that the material has a specific fatigue
strength value below which failure will not occur regardless of
the number of additional stress cycles imposed. Non-ferrous
metals on the other hand generally do not exhibit an endurance
limit strength; their fatigue strengths continue to decrease,
usually at a decreasing rate, with increasing numbers of stress
cycles.

Item 3 arises from the fact that fatigue testing is usually done
on a very limited number of test samples. The question thus
arises as to what level of confidence do we have (or do we want
to have) that all subsequent parts made from the same type of
material, and having the same type of heat treatment, will have
fatigue strength characteristics equal to or better than the test
samples. The answer to this question is derived from probability
theory and manifests itself in the form of the k_g confidence
factor.

With respect to Item 4, the mean value of the maximum operating
stress distribution for the component is related to the
previously mentioned maximum allowable nominal design operating
stress for the part. During the design stage, the nominal value
of maximum operating stress will be a computed value based on
maximum diaphragm or bellows deflection, nomimal dimensions, and
nominal material properties for the part. The true value of
maximum nominal operating stress will depend on the accuracy of
the stress analysis procedures used during the design process.
Furthermore, the actual distribution of maximum operating stress
will vary from part to part depending on actual deflections,
dimensions, and material properties, all of which will have a
statistical variation.

With respect to Item 5, the required component reliability will
be dependent on both the total number of parts which affect
overall compressor reliability, and the individual reliabilities
of these other parts. For the compressor system under
consideration here, the individual component reliabilities must
be much higher than the required overall compressor reliability.

5.1 Confidence Factor k_g

The next three paragraphs are paraphrased from Chapter 22 of Reference 1.

Fatigue testing of a finite number of material test specimens to determine fatigue strength of a material gives us, in statistical terms, a **point estimate** of the true fatigue strength of the material. Only if we tested an infinite number of test specimens could we have 100% confidence that the measured mean and standard deviation of fatigue strength coincides with the true values of these parameters. Accordingly, it is more meaningful to express statistical point estimates in terms of a range or interval with an associated probability or **confidence** that the true value lies within the range or interval.

Confidence intervals around point estimates can be interpreted as either **two-sided** or **one-sided** confidence intervals. If a two-sided interval is implied, there will be a finite lower confidence limit L, and a finite upper confidence limit U, associated with a specific confidence level for a particular parameter. For example, if the confidence level for a point estimate of mean fatigue strength is stated to be 60%, and a two-sided confidence interval is implied, then there would be a 60% probability that the true mean value of fatigue strength would lie between the upper and lower confidence limits, L and U, associated with the point estimate of mean strength.

In specifications we often find the requirement that the mean wearout life must exceed a specified minimum value with a stated confidence level. In this case, only the lower confidence limit is of interest. We consider the specified minimum life requirement to be the lower confidence limit, L, and assume that the upper confidence limit extends to infinity. We use the procedure of so-called "one-sided" confidence limits to determine the lower confidence limit. In this case, a 60% confidence level applied to a point estimate of mean fatigue strength would mean there is a 60% probability that the true value of mean strength is equal to or greater than the lower confidence limit L.

For a given confidence level, there is a significant difference in the value of L depending on whether a one-sided interpretation or a two-sided interpretation of confidence level is used. A one-sided interpretation yields a higher value of L than does a two-sided interpretation. Reference 1 states that the one-sided interpretation is often used in the context of wearout life. Since wearout is the failure mode of the bellows and diaphragms, we will use the one-sided interpretation for the cryocooler compressor development.

With respect to a material's fatigue strength, the lower confidence limit of fatigue strength, L_{et}, can be computed from the following equation:

$$L_{et} = S_{et} - t_{(\alpha;n-1)}\sigma_{et}/n^{\frac{1}{2}} \qquad (2)$$

where

S_{et} = point-estimate mean value of material fatigue strength as determined from fatigue testing

$t_{(\alpha;n-1)}$ = number of standard deviations of the mean fatigue strength corresponding to the desired confidence level; determined from Student's t distribution

σ_{et} = standard deviation of material fatigue strength

n = number of tests used to determine S_{et}.

We define a coefficient of variation for the fatigue strength distribution, C_{et}, as

$$C_{et} = \sigma_{et}/S_{et} . \qquad (3)$$

From Equations 2 and 3 we can solve for k_g:

$$k_g = L_{et}/S_{et} = 1 - t_{(\alpha;n-1)}C_{et}/n^{\frac{1}{2}} \qquad (4)$$

The values of $t_{(\alpha;n-1)}$ for different confidence levels and three values of n are tabulated below (from table of Student's t distribution):

Confidence Level	$t_{(\alpha;n-1)}$ (one-sided)		
	n≥26	n=4	n=2
60%	0.256	0.277	0.325
80%	0.856	0.978	1.376
90%	1.316	1.638	3.078
95%	1.708	2.353	6.314
99%	2.485	4.541	12.706

5.2 Reliability Factor k_c

In addition to the statistical variability of fatigue strength data, there will also be statistical variability in the maximum stress occuring in the diaphragms and bellows. This variability will occur due to variations in (1) operating deflections, (2) actual component dimensions, and (3) material parameters (such as modulus and Poisson's ratio).

Figure 2 illustrates the relationship between the distributions of material fatigue strength and component maximum operating stress for a typical component, assuming that both the strength and stress can be represented by normal distributions. Also shown is the distribution of strength minus stress. The area under the strength minus stress distribution which lies to the left of the origin represents the probability that the operating stress will exceed the fatigue strength, that is, the probability of failure (P_f). The area which lies to the right of the origin represents the reliability (R) of the component (R = 1- P_f).

We now assume that the distribution of material fatigue strength is normal (Gaussian) about the lower confidence limit L_{et}, and retains the same standard deviation σ_{et} and coefficient of variation C_{et} as obtained for the S_{et} distribution. The standardized variable for the strength minus stress distribution curve, assuming a normal (Gaussian) operating stress distribution, is [2]:

$$u = \frac{L_{et} - S_{ed}}{[(\sigma_{et})^2 + (\sigma_{ed})^2]^{\frac{1}{2}}} \qquad (5)$$

where

   u = standardized variable

   σ_{ed} = standard deviation of operating stress

We define a coefficient of variation for maximum operating stress, C_{ed}, as

$$C_{ed} = \sigma_{ed}/S_{ed} \qquad (6)$$

and the reliability factor, k_c, as

$$k_c = S_{ed}/L_{et} \qquad (7)$$

Rev. 2; March 26, 1992

Manipulating Equations 5, 6, and 7 gives

$$k_c = 1 - u[(C_{et})^2 + (k_c * C_{ed})^2]^{\frac{1}{2}} \qquad (8)$$

According to [2], the standardized variable u is a relatively complex function of P_f. For the purposes of engineering design the following values of u can be used for a required reliability.

P_f	R	u
1E-2	0.99	2.326
1E-3	0.999	3.090
1E-4	0.999 9	3.719
1E-5	0.999 99	4.265
1E-6	0.999 999	4.753
1E-7	0.999 999 9	5.199
1E-8	0.999 999 99	5.610
1E-9	0.999 999 999	5.997
1E-10	0.999 999 999 9	6.361
1E-11	0.999 999 999 99	6.700

To solve for k_c, values for the coefficients of variation, C_{et} and C_{ed}, must be specified. As mentioned previously, $C_{et} = 0.08$ has been established as being a good value for the fatigue of steels. We will assume for now that $C_{ed} = 0.10$ is a reasonable estimate for the maximum operating stress distribution. Using these values, together with the above values of u, we can solve Equation 8 for k_c:

R (Reliability)	k_c
0.99	0.7456
0.999	0.6763
0.999 9	0.6229
0.999 99	0.5788
0.999 999	0.5410
0.999 999 9	0.5075
0.999 999 99	0.4774
0.999 999 999	0.4496
0.999 999 999 9	0.4240
0.999 999 999 99	0.4006

Figure 3 is a plot of k_c versus probability of failure.

To select the appropriate value of k_c, we need to determine the required reliability for the particular component being designed. If we assume that the component will have a constant failure rate

during its useful life, then its reliability can be expressed by a simple exponential function as follows [1]:

$$R_x = \exp(-t/m_x) \tag{9}$$

where

R_x = reliability of component x

t = time

m_x = mean time between failures for component x
($1/m_x$ = component failure rate)

exp = e raised to the exponent.

For the purpose of this discussion, we separate the cryocooler compressor system into two subsystems; the electronic subsystem which drives and controls the compressor, and the mechanical subsystem (which includes the linear drive motor parts) which accomplishes helium compression when electric power is applied to the drive motors. The mechanical subsystem is an example of a **series** subsystem. This means that if any component of this subsystem fails, the entire cryocooler will fail. The electronic subsystem, on the other hand, could have some degree of redundancy designed into it. Thus the electronic subsystem could consist of a combination of **series** and **parallel** connected components. To design the overall compressor system to a specified level of reliability (95% in this case) requires three things:

1. A detailed knowledge of the total system design down to the individual component level;

2. Failure rate (mean time to failure) data for each component;

3. A rigorous reliability analysis which takes into account the combined series/parallel (redundant) aspects of the overall compressor design.

The current Phillips Laboratory contract is a proof-of-principle contract. As such, standard off-the-shelf laboratory electronics and instrumentation will be used to demonstrate compressor operation. It is clearly beyond the scope of the current contract to perform a complete compressor system reliability analysis. Accordingly, for the purposes of designing the demonstrator compressor's mechanical subsystem, we will assume that the individual reliabilities of both the mechanical and

electronic subsystems must be 97.5% to yield an overall system
reliability of 95%. Although the electronic subsystem will have
many more parts than the mechanical subsystem, it is assumed that
its 97.5% reliability level can be achieved via the use of
redundancy.

Since the compressor's mechanical subsystem is a series system,
the overall subsystem reliability is given by the following
equation:

$$R_{ms} = \exp\{-t\Sigma(1/m_x)\} \tag{10}$$

where

R_{ms} = overall mechanical subsystem reliability

$\Sigma(1/m_x)$ = summation of failure rates for all the
series components of the mechanical
subsystem.

Since we have assumed that R_{ms} must be 97.5% for 100,000 hours of
compressor operation, we can solve Equation 10 for the overall
failure rate of the mechanical subsystem:

$$\Sigma(1/m_x) = -\ln(R_{ms})/t = -\ln(0.975)/100000$$

$$= 2.5318E-07 \text{ failures/hr}$$

We next identify the number of potential series failure points in
one compression module of the mechanical subsystem which are
subjected to failure-inducing stresses:

     2 max stress planes per diaphragm
     7 max stress planes per bellows
       (based on 7 convolutions per bellows;
        maximum stress occurs at the convolution
        root; stress at the convolution crown is
        significantly less than at the root)
     1 plunger assembly
     1 one motor winding
     2 bearings
     2 electric conductor seals for motor winding
     2 electric conductor seals for position sensor
     1 pressure shell
     2 capillary line terminations
     6 assembly weld joints
     ──
    26 total failure points per module

Thus, for a two module mechanical subsystem there would be a total of 52 series elements which could be subject to failure. If we now assume that each of these 52 potential failure points has the same failure rate, the required failure rate per failure point will be:

$$1/m_x = 2.5318E-07/52 = 4.869E-09 \text{ failures/hr}$$

or a mean time between component failures of 205 million hours.

The required component reliability for 100,000-hour life can now be computed from Equation 9:

$$R_x = exp(-100000*4.869E-09) = 0.9995$$

which corresponds to a 0.0005 component probability of failure. From the Figure 8 plot of failure probability versus k_c we obtain the required reliability factor for Equation 1:

$$k_c = 0.660$$

6.0 Fatigue Strength, S_{et}, for Diaphragm Material

A candidate material for the diaphragms is Armco PH13-8Mo stainless steel (XM-13, UNS S13800), precipitation hardened to the H1000 condition. The attractive characteristics of this steel are as follows [4]:

1. The material is double-vacuum melted to insure high metallurgical quality, closly controlled chemical composition, and optimum solidification conditions for aerospace applications;

2. The material has high strength coupled with excellent corrosion resistance and good toughness characteristics;

3. The material has equal fatigue strengths in the longitudinal and transverse directions. This is particularly important for the diaphragms where the maximum stresses are radial in direction (i.e., will occur in both "x" and "y" directions of the diaphragm plane depending on the polar coordinate of a particular diaphragm element).

4. A reasonable amount of relevant fatigue strength test data is available.

5. The material is iron based and probably has a fatigue endurance limit.

Figures 4 and 5 show reversed-bending and reversed-axial fatigue strength data for Armco PH13-8Mo as reported in Armco Product Bulletin S-24 dated Oct, 1986 [4]. This data shows fully-reversed (rotating beam) bending endurance strength of 689.6 MPa (100 ksi) after 100 million cycles. The reversed-axial endurance strength after 10 million cycles is 620 MPa (89.9 ksi), 10% less than the bending endurance strength. The lower axial endurance strength is typical of fatigue test data.

This exact same data is presented in the Aerospace Structural Metals Handbook (Code 1510, pages 28 and 29, June 1988), except that there is a discrepancy in the abscissa axis for the rotating-beam bending data. The cycles-to-failure abscissa of the Aerospace Handbook S-N plot shows a factor of 10 less cycles than does the abscissa of the Armco data. The Aerospace Handbook references Armco Product Bulletin S-33c published in August, 1972.

Figure 6 from MIL-HDBK-5C (September, 1976) also shows reversed-axial fatigue strength data for Armco PH13-8Mo. The source of this data is not stated. The endurance strength at 10 million cycles is 551.5 MPa (80 ksi). This is 11% lower than the reversed-axial value reported by Armco. However, the 0.250-inch diameter test specimens used in these tests were machined from 2-inch by 6-inch bar stock, whereas the 0.250-inch diameter Armco specimens were machined from 0.75-inch diameter bar stock. The difference in endurance strengths may be due to the different product forms from which the specimens were machined, or due to other factors which differed between the sources of test data. It may also be that the MIL-HDBK data represents derated data.

Maximum stresses in the diaphragm occur in the radial direction, and consist of a combination of bending and membrane stresses. Maximum bending stresses are significantly greater than the maximum membrane stresses. Accordingly, fully-reversed bending fatigue data would seem to be the most pertinent data to use. To be most relevant, such data should be obtained using flat bending specimens machined from thin plate stock. However, test data for this type of specimen has not been found and may not currently exist for Armco PH13-8Mo.

All of the fatigue test data referenced above suggests that Armco PH13-8Mo reaches a constant fatigue strength between 10 and 100 million cycles. However, since test data at one-billion or more fatigue cycles has not been found, this conclusion cannot be verified. Armco's reversed-bending data is apparently based on test samples from only one melt heat, whereas their reversed-

axial data was obtained from two different heats with "essentially the same results". MIL-HDBK-5C gives the lowest reported value of reversed-axial fatigue strength. Since we require 14.4-billion cycles of life, and since we must favor conservatism in the absence of additional fatigue or component test data, we will use the MIL-HDBK endurance stress value of 551.5 MPa (80.0 ksi) as the value of S_{et} in the Shigley equation.

Figure 7 shows the assumed Gaussian endurance strength distribution for Armco PH13-8Mo, H1000 steel. The mean endurance stress of 551.5 MPa (80 ksi) applies to polished, unnotched test specimens under fully-reversed axial loading. The assumed standard deviation of this distribution is 44.1 MPa (6.4 ksi). The basis of this assumption is the fact that the coefficient of variation (mean strength/standard deviation) for the fatigue strength of steels is typically found to be about 0.08 [2].

Insofar as the diaphragm components are concerned, we can now bring the required 60% confidence level into the picture. Using Equation 4 we calculate the confidence factor for Equation 1 using $C_{et} = 0.08$, $t_{(\alpha;n-1)} = 0.325$, and n = 2 (Armco tests were run on specimens from two heats with essentially the same results):

$$k_g = L_{et}/S_{et} = 1 - 0.325*0.08/(2)^{\frac{1}{2}} = 0.981.$$

Thus the 60% lower confidence limit of endurance strength for Armco PH13-8Mo (H1000) becomes:

$$L_{et} = 0.981*551.5 = 541.0 \text{ MPa (78.4 ksi).}$$

7.0 Maximum Allowable Design Operating Stress, S_{ed}, for Diaphragms

Factors k_c and k_g for the Shigley equation have been determined to be 0.660 and 0.981, respectively, for 100,000-hour life of the compressor's mechanical subsystem at 97.5% reliability. The 50% probability fatigue endurance strength for Armco PH13-8Mo, S_{et}, has been fixed at 551.5 MPa (80 ksi). The remaining Shigley factors needed to compute the maximum allowable design operating stress for the diaphragms can be specified as follows:

$k_a = 0.85$ (this factor applies to a ground surface finish, p. 189 of [3]; it is intended that the actual diaphragm surface will be polished, resulting in a better-than-ground finish)

$k_b = 1.0$ (this factor does not apply since the diaphragm thickness will be considerably less than the thickness of the fatigue test specimens; p. 190 of [3])

$k_d = 1.0$ (this factor does not apply since operating temperature of the diaphragms will be less than 160 F; p. 191 of [3])

$k_e = 0.95$ (this should be a conservative allowance for stress concentration effects since the diaphragms will be designed without any notches or steps. The integral OD rim of the diaphragm will be smoothly transitioned into the diaphragm's thin plate section by means of a generous fillet radius. Finite-element stress analysis of this transition region has been performed to verify that the transition radius will not produce any stress concentrating effect.)

$k_f = 0.95$ (this should be a conservative allowance for miscellaneous effects such as corrosion or erosion of the diaphragm. All available data and "vendor's opinion" indicate that helium and the selected hydraulic oil should be chemically non-reactive with the diaphragm material. Particulate matter arising from the compressor fabrication process will be controlled by stringent cleanliness requirements. Thus corrosion and/or erosion are not expected to be significant factors.)

We can now evaluate the Shigley equation for the maximum allowable nominal design operating stress in the diaphragm:

$$S_{ed} = (k_a)(k_b)(k_c)(k_d)(k_e)(k_f)(k_g)(S_{et}) \qquad (1)$$

$$S_{ed} = (0.85)(1.0)(0.66)(1.0)(0.95)(.95)(0.981)(551.5)$$

$$S_{ed} = (0.496)(551.5) = 273.5 \text{ MPa} \quad (39.6 \text{ ksi})$$

It must be remembered that the above value of maximum allowable stress is based on simple, uniaxial, alternating stresses. Actual diaphragm stesses are biaxial in nature, being a combination of membrane and bending stresses. Accordingly, the diaphragm stress analysis must predict an equivalent maximum operating stress which can be related to the maximum allowable uniaxial stress, S_{ed}. The maximum shear-strain energy criterion

currently provides the best method for correlating a biaxial fatigue stress condition to uniaxial fatigue test data. This criterion is also variously known as the von Mises, the octahedral-stress, and the distortion-energy criterion.

Figure 8 is a plot of the maximum allowable operating stress distribution for the cryocooler diaphragms based on the life and reliability requirements of Attachment 1, and using the interpretations and methods outlined in the previous sections of this memorandum.

LIST OF FIGURES

REFERENCES

1. Igor Bazovsky, "Reliability Theory and Practice",
   Prentice-Hall, Inc., 1961, p. 33

2. E.B. Haugen and P.H. Wirsching, "Probabilistic
   Design", Parts 1 thru 5, Machine Design, April 17
   thru June 12, 1975, pp. 81 and 85.

3. Shigley, "Mechanical Engineering Design", 3rd edit.

4. Armco Product Bulletin No. S-24, Armco Inc., Oct,
   1981
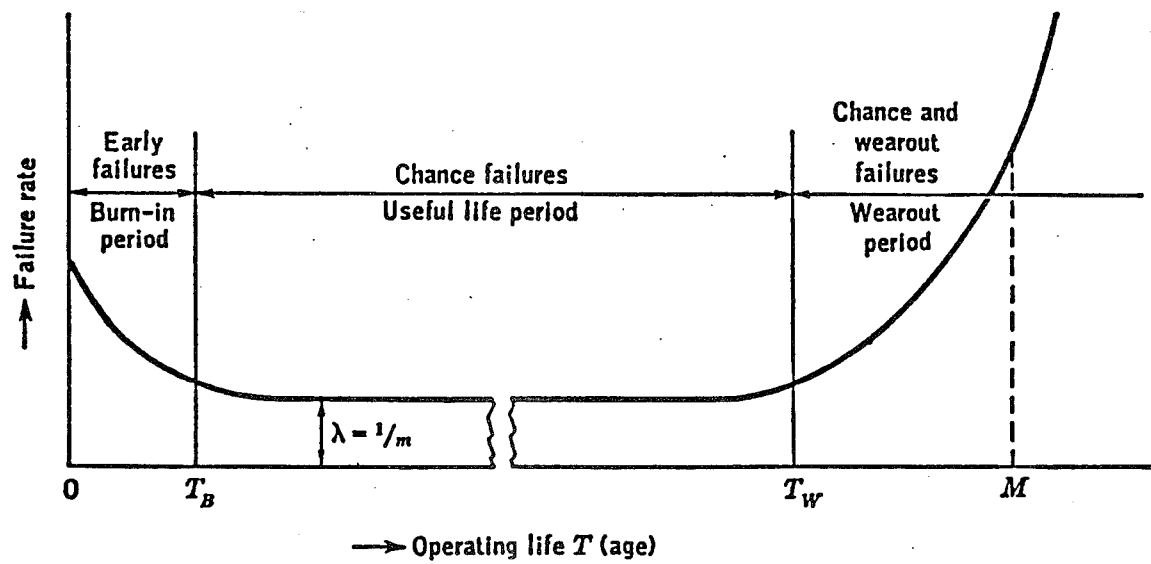
FIGURE 1. - Variation in Component Failure Rate Vs. Time

Fig. 2 Example of Material Strength, Component Stress, and Difference Distributions
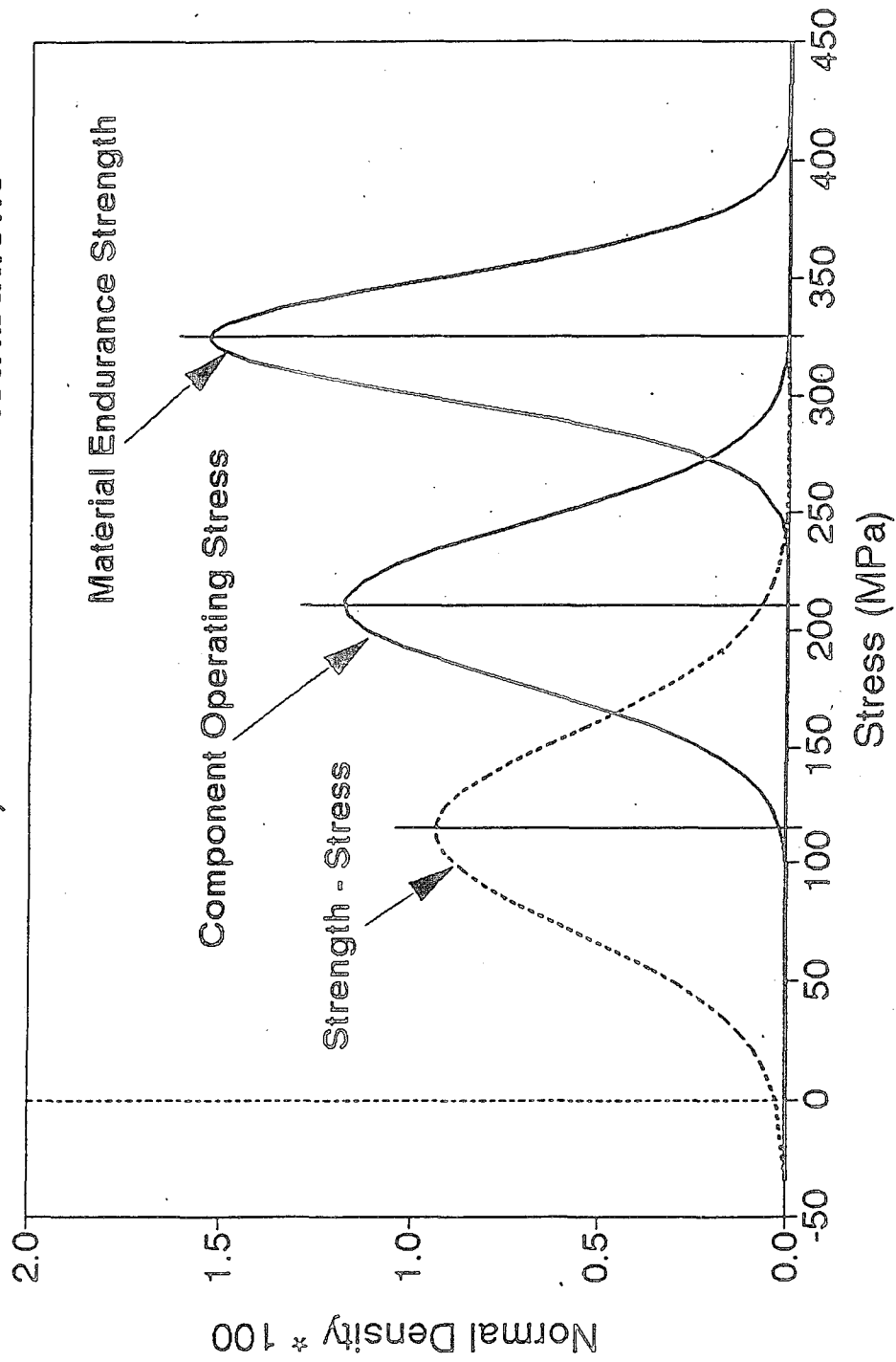
Fig. 3 Kc Vs Probability of Failure
Cet = 0.08; Ced = 0.10
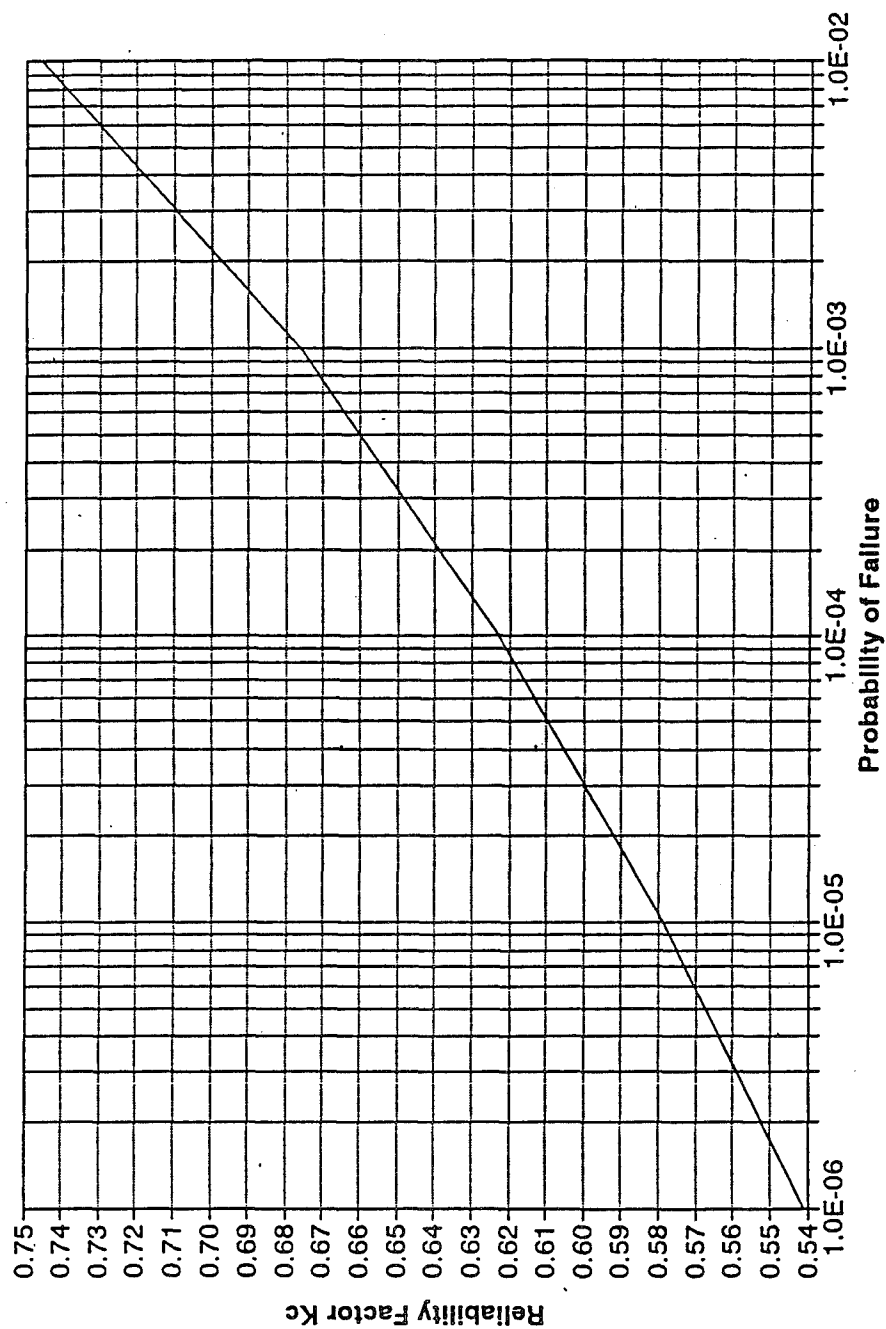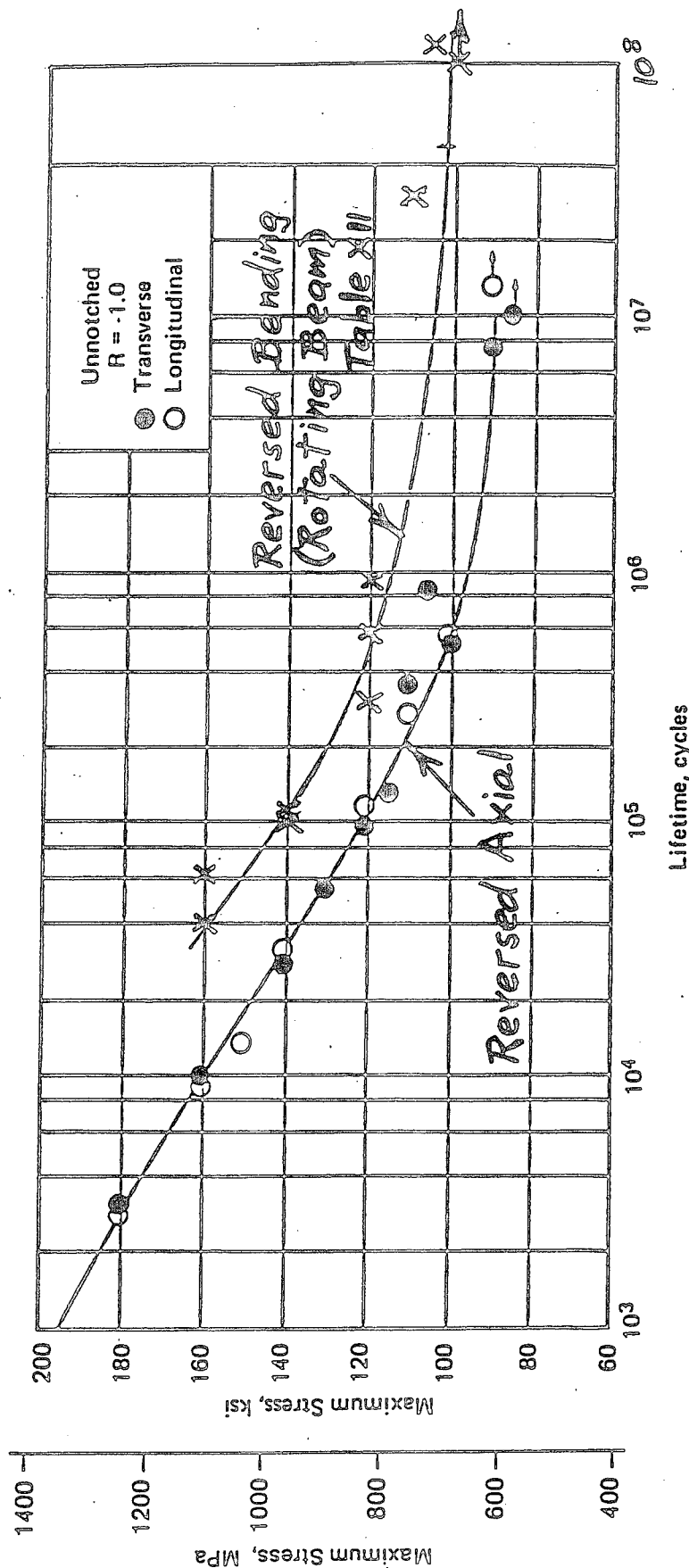
FIGURE 5. — Fatigue test results for unnotched longitudinal and transverse specimens of Condition H 1000 PH 13-8 Mo stainless steel at a stress ratio of R = -1.0 Test values from one heat.

FIGURE 4. - Armco Fatigue Test Results for Unnotched Longitudinal and Transverse Specimens of Condition H1000 PH13-8Mo Stainless Steel at a Stress Ratio of R = -1.0
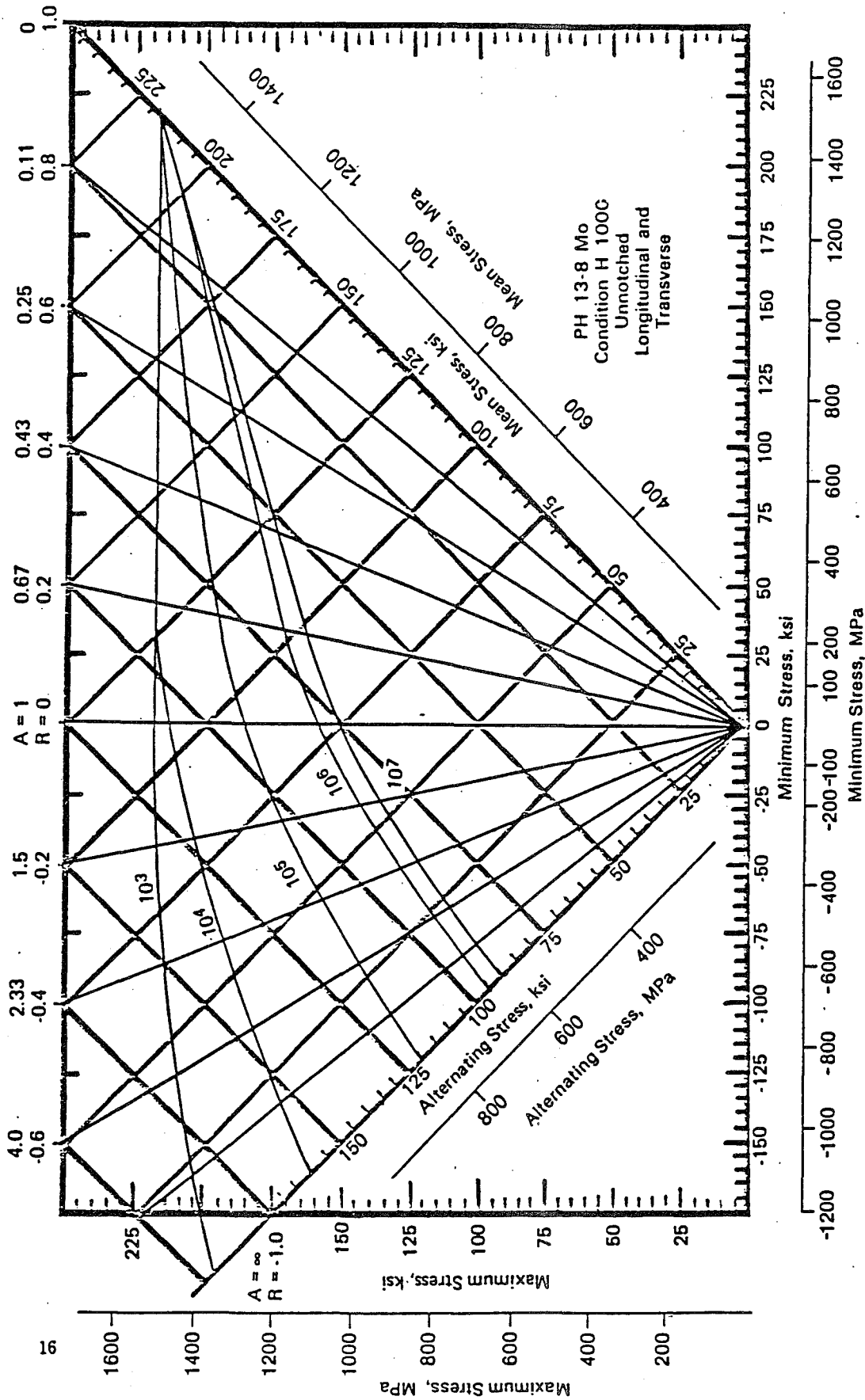
FIGURE 9. — Constant-life diagram for axial-load, unnotched, fatigue behavior of PH 13-8 Mo stainless steel.* Constructed using Figures 3, 4 and 5.

*A DUPLICATE PROGRAM WAS RUN ON ANOTHER HEAT AND RESULTS WERE ESSENTIALLY THE SAME. DATA AVAILABLE UPON REQUEST.

FIGURE 5. - Armco Constant Life Diagram for Axial-Load, Unnotched, Fatigue Behavior of Condition H1000 PH13-8Mo Stainless Steel

115
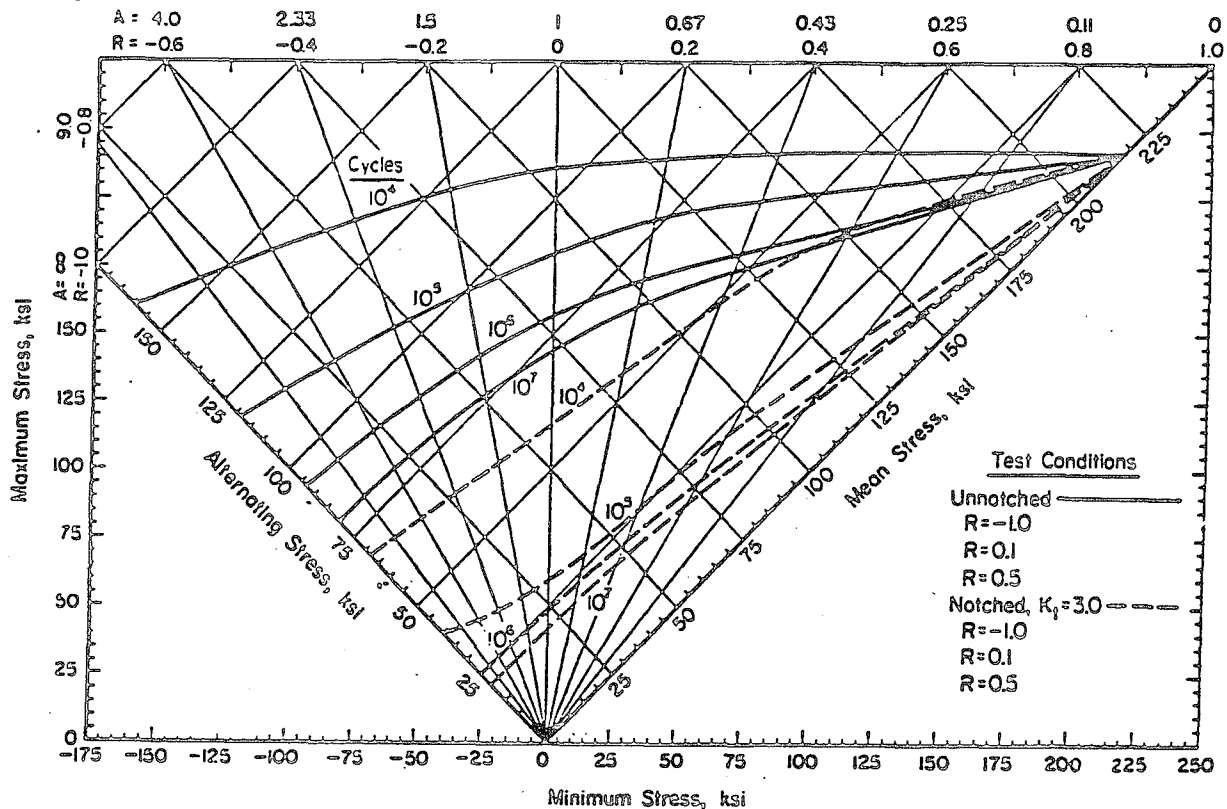
FIGURE 2.6.5.1.8. *Typical constant life fatigue diagram for PH13-8Mo (H1000) stainless steel (bar) at room temperature (longitudinal and long transverse).*

Correlative Information for Figure 2.6.5.1.8

Product Form: Bar, 2x6 inches

Test Parameters:
Loading - Axial
Frequency - 1800 cpm
Temperature - RT
Atmosphere - Air

Properties:

	TUS, ksi	TYS, ksi	Temp, F
	217.0	207.0	RT (Unnotched)

Specimen Details: Unnotched
0.250-inch diameter

Notched, V-Groove, $K_t = 3.0$
0.375-inch gross diameter
0.250-inch net diameter
0.013-inch root radius, r
60°° flank angle, ω

$$K_N = 2.75; \ \rho = 0.00012 \text{ inch, where } K_N = 1 + \frac{K_t - 1}{1 + \frac{\pi}{\pi - \omega}\sqrt{\frac{\rho}{r}}}$$

Surface Condition: Unnotched: Mechanically polished in longitudinal direction.
Notched: Polished mechanically with abrasively charged wire.

FIGURE 6   - Typical Constant Life Fatigue Diagram for
PH13-8Mo (H1000) Stainless Steel (Bar) at
Room Temperature (Longitudinal and Long
Transverse) (MIL-HDBK-5C)

116

Fig. 7   Assumed Endurance Strength Distribution
for Armco PH13-8Mo Stainless (H1000)

Polished, unnotched specimens
subjected to reversed-bending
and reversed-axial loading

Endurance limit strength
distribution assuming
coefficient of variation
(Std Dev/Mean) = 0.08

Mean endurance strength
551.5 MPa
(80 ksi)

Standard Deviation
44.1 MPa
(6.4 ksi)

Lower 60% confidence
limit (one-sided) for mean
endurance strength:
541.0 MPa
(78.4 ksi)

Stress (MPa)

Normal Density * 100

Fig. 8   Diaphragm Material Strength, Operating Stress, and Difference Distributions
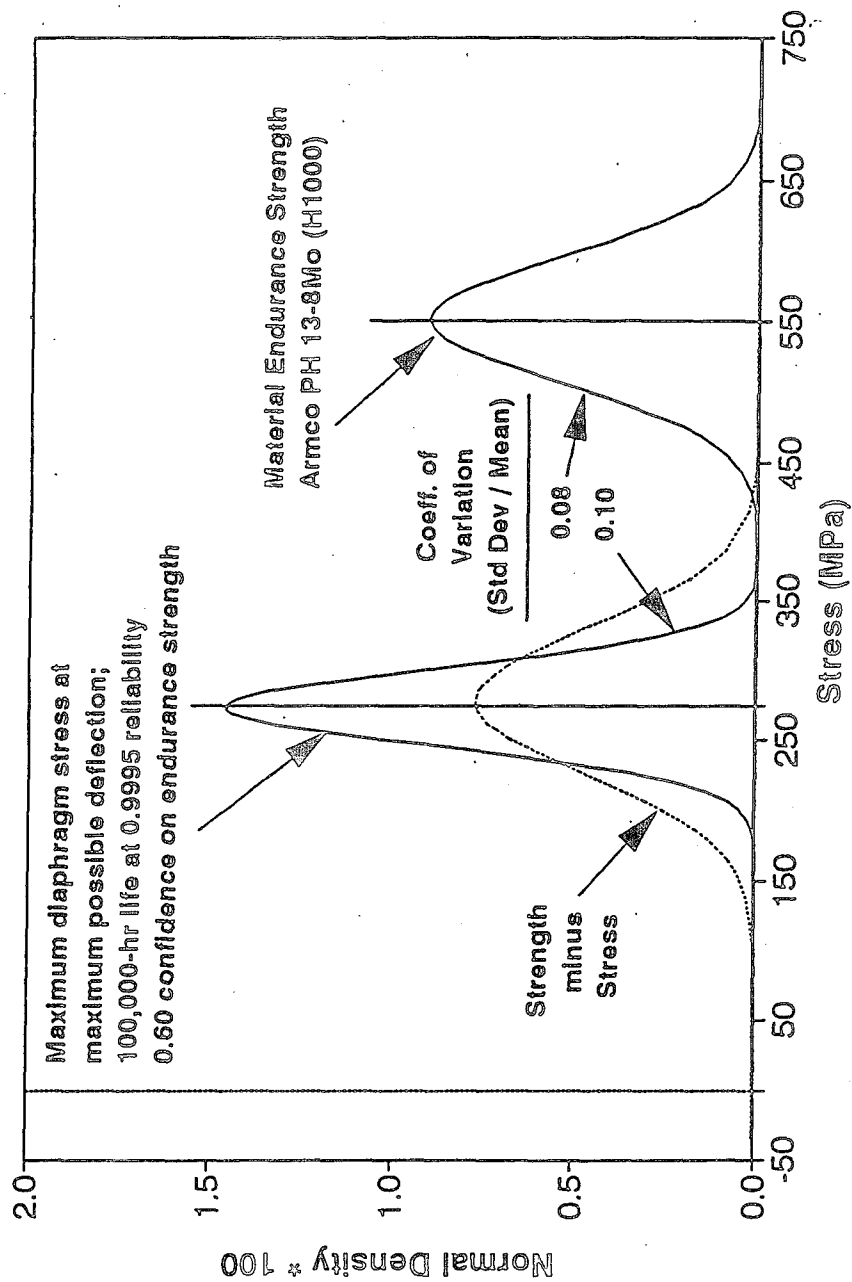
Appendix B
PHILLIPS.TDS
Cryocooler Compressor
Control Program Listing

```
( ****************************************************************
( PHILLIPS.TDS - Compresor Control Program
( ****************************************************************
DECIMAL                                                          `
$20 CONSTANT P5-DDR         ( Address of port 5 DDR
$15 CONSTANT P5             ( Address of Digital Data
$08 CONSTANT P5-DDR-DATA (   0000 1000    0 = IN  1 = OUT
$16 CONSTANT P6-DDR         ( Address of port 6 DDR
$17 CONSTANT P6             ( Address of Digital Data
$0F CONSTANT P6-DDR-DATA (   0000 1111    0 = IN  1 = OUT
( D to A Addresses - 8 bit
$190 CONSTANT DA-FREQ
$200 CONSTANT MFBASE                ( base address of Multi-Function card set by jumper
   0 MFBASE + CONSTANT DDR          ( port 2 data dir. register. Port 1 at next addr
   2 MFBASE + CONSTANT 2PORT        ( port 2 bit 0 is addr line 16 of expanded
                                    ( memory. bit 1 is expanded memory global enable.
   3 MFBASE + CONSTANT 1PORT        ( UPP port 1 bits 0 to 4 connected to address lines
                                    ( 10 to 14 of expanded memory.  Bit 7 connected to
                                    ( address line 15  .
   6 MFBASE + CONSTANT ADCSR        ( A-D converter control register
   7 MFBASE + CONSTANT ADDR0        ( A-D converter data register
$10 MFBASE + CONSTANT UCER          ( pair of UPP contact enable registers
$20 MFBASE + CONSTANT USCR  (
$21 MFBASE + CONSTANT MFNR  (
$22 MFBASE + CONSTANT FNR   (
$23 MFBASE + CONSTANT CMR   (       All these have same names as
$24 MFBASE + CONSTANT RASRA (       on Hitachi HD63140 data sheet.
$25 MFBASE + CONSTANT RASRB (       See this for more detail
$26 MFBASE + CONSTANT IOARA (
$27 MFBASE + CONSTANT IOARB (
$28 MFBASE + CONSTANT IOARC (
$29 MFBASE + CONSTANT IOARD (
( Raw analog data                       ( Scaled data
$800 CONSTANT V-GND         (     You don't scale ground
$802 CONSTANT S-DC-IN       $822 CONSTANT S-DC          ( Channel 1
$804 CONSTANT S-PK-IN       $824 CONSTANT S-PK          ( Channel 2
$806 CONSTANT M-DC-IN       $826 CONSTANT M-DC          ( Channel 3
$808 CONSTANT M-PK-IN       $828 CONSTANT M-PK          ( Channel 4
$80A CONSTANT PEAK-SP-IN    $82A CONSTANT M-PEAK-SP     ( Channel 5
$80C CONSTANT M-DC-SP-IN    $82C CONSTANT M-DC-SP       ( Channel 6
$80E CONSTANT S-DC-SP-IN    $82E CONSTANT S-DC-SP       ( Channel 7
$810 CONSTANT PEAK-DL-IN    $830 CONSTANT PEAK-DL       ( Channel 8
$812 CONSTANT VIBE-IN       $832 CONSTANT VIBE          ( Channel 9
( Trip Data Addresses
$834 CONSTANT HI-VIBE
$836 CONSTANT LO-M-GAP
$838 CONSTANT LO-S-GAP
( Master Stroke PI control    Slave Stroke PI control
$840 CONSTANT M-PK-ERR       $850 CONSTANT S-PK-ERR      ( Stroke Error
$842 CONSTANT M-K-I-S-U      $852 CONSTANT S-K-I-S-U     ( Stroke control new input
$844 CONSTANT M-K-I-S-UZ     $854 CONSTANT S-K-I-S-UZ    ( Stroke control old input
$846 CONSTANT M-K-I-S-X      $856 CONSTANT S-K-I-S-X     ( Stroke control new output
$848 CONSTANT M-K-I-S-XZ     $858 CONSTANT S-K-I-S-XZ    ( Stroke control old output
$84A CONSTANT M-SSAT         $85A CONSTANT S-SSAT        ( SATURATED FLAG
( Master DC PI control        Slave DC PI control
$860 CONSTANT M-DC-ERR       $870 CONSTANT S-DC-ERR      ( Current DC Error
$862 CONSTANT M-K-I-D-U      $872 CONSTANT S-K-I-D-U     ( DC control new input
$864 CONSTANT M-K-I-D-UZ     $874 CONSTANT S-K-I-D-UZ    ( DC control old input
$866 CONSTANT M-K-I-D-X      $876 CONSTANT S-K-I-D-X     ( DC control new output
$868 CONSTANT M-K-I-D-XZ     $878 CONSTANT S-K-I-D-XZ    ( DC control old output
```

```
$86A CONSTANT M-DSAT        $87A CONSTANT S-DSAT        ( SATURATED FLAG
( Odds 'n ends
$880 CONSTANT P6-DATA    ( Port 6 RAM Image
$882 CONSTANT SWTIMER    ( The Timer
$884 CONSTANT CSTATE     ( Control State Variable
$886 CONSTANT LIM-VAL    ( Limited value back from LIMIT
$888 CONSTANT TRIP      ·( Just what it says
$88A CONSTANT S-OLD
$88C CONSTANT RESET-BIT
$88E CONSTANT CLICK      (·Ramp timer loop skipper
( D/A's
$890 CONSTANT S-PK-DEM    ( D/A 10
$892 CONSTANT S-DC-DEM    ( D/A 11
$894 CONSTANT M-PK-DEM    ( D/A 12
$896 CONSTANT M-DC-DEM    ( D/A 13
( Stuff for Gap & Set Point Calcs
$900 CONSTANT M-GAP-SP
$902 CONSTANT S-GAP-SP
$904 CONSTANT M-GAP
$906 CONSTANT S-GAP
$908 CONSTANT S-PEAK-SP
$910 CONSTANT RAMP-TIM
$912 CONSTANT STAB-TIM
$914 CONSTANT TLOAD       ( % Exicution time
$916 CONSTANT M-PK-OLD    . ( Old error values for filter
$918 CONSTANT S-PK-OLD
$91A CONSTANT M-DC-OLD
$91C CONSTANT S-DC-OLD
$920 CONSTANT M-PK-F             ( Filtered values
$922 CONSTANT S-PK-F
$924 CONSTANT M-DC-F
$926 CONSTANT S-DC-F
$928 CONSTANT RAMP-TAR
$92A CONSTANT STAB-TAR
$92C CONSTANT PK-TIM      ( Peak ramp timer    NOT
$92E CONSTANT PK-TAR      ( "      "  target   USED
( SYSTEM CONSTANTS
1 CONSTANT INACTIVE
2 CONSTANT RAMPUP
3 CONSTANT STABILIZE
4 CONSTANT RUN
5 CONSTANT CALIBRATE
40 CONSTANT K-FILTER      ( filter constant
$930 CONSTANT M-K-P-PK    (  Stroke control Kp
$932 CONSTANT S-K-P-PK    (
$934 CONSTANT M-K-I-PK    (   Stroke control Ki
$936 CONSTANT S-K-I-PK    (
$938 CONSTANT M-K-P-DC    (  DC Kp
$93A CONSTANT S-K-P-DC    ( .
$93C CONSTANT M-K-I-DC    (  DC Ki
$93E CONSTANT S-K-I-DC    (
$940 CONSTANT S-ON
$942 CONSTANT M-ON
(  Loop switching timer and target
$944 CONSTANT LOOP-TIM
$946 CONSTANT LOOP-TAR
250 CONSTANT M-PK-LIM     ( Value to stuff into st-dem
250 CONSTANT S-PK-LIM     ( Value to stuff into st-dem
CODE LSR6 PULD, LSRD, LSRD, LSRD, LSRD, LSRD, LSRD, PSHD, END-CODE
( UNIVERSAL PULSE PROCESSOR SUPPORT
```

```
: GFE ( f -    f=0 to stop   f=1 to start Pulse Processor
   2* USCR C! ;
: UPPDR ( n - a   calculate address of UPP Data Register n
   2* $40 MFBASE + + ;
: PP ( n1 n2 n3 n4 n5 n6 n7 fn -    load n1-n7 to function number fn
   FNR C!        IOARD C!    IOARC C!    IOARB C!    IOARA C!
   RASRB C!      RASRA C!    CMR C! ;
: SET-PP
   0 GFE           ( turn off operation
   $FC00 UCER !
   $FFFF DDR !    ( MF card data direction registers set for outputs on
   10 MFNR C!     ( maximum function number reached+1
   ( Pulse Processor program
   ( CMR   RASRA   RASRB   IOARA   IOARB   IOARC   IOARD   FNR
     $40    5       10      $C0     0       10      0       1    PP
     $58    5       16      $C0     0       23      0       2    PP
     $40    6       11      $C0     0       11      0       3    PP
     $58    6       17      $C0     0       23      0       4    PP
     $40    7       12      $C0     0       12      0       6    PP
     $58    7       18      $C0     0       23      0       7    PP
     $40    8       13      $C0     0       13      0       8    PP
     $58    8       19     .$C0     0       23      0       9    PP
   ( Limiting values for the 4 8-bit D/A's
           $100 16 UPPDR !
           $100 17 UPPDR !
           $100 18 UPPDR !
           $100 19 UPPDR !
   1 GFE ( General Function Enable for Pulse Processor) ;
: DA   ( Output the 4 D/A channels
   S-DC-DEM  @ 10 UPPDR !
   S-PK-DEM  @ 11 UPPDR !
   M-DC-DEM  @ 12 UPPDR !
   M-PK-DEM  @ 13 UPPDR !    ;
: MF ( initialise Multi-Function card
   P5-DDR-DATA P5-DDR C! ( set DDR to make P53 MF card reset output
   0 P5 C!         ( reset MF card
   $08 P5 C!       ( end of reset
   $14 DUP C@ 4 OR SWAP C! ( enable external mem. ready function
   $FC00 UCER ! ( allocate bits 0-9 to page select, 10-15 to pulse processor
   0 2PORT ! ;   ( select page 0
( **************************************************************
: DALIMIT ( 0 < stack < 255
        DUP 255 > IF 255 LIM-VAL ! ELSE DUP LIM-VAL !
             THEN
           0 < IF 0 LIM-VAL !
             THEN
             LIM-VAL @ ;
( **************************************************************
: LIMIT ( 0 < stack < 1023 .
        DUP 1023 > IF 1023 LIM-VAL ! ELSE DUP LIM-VAL !
             THEN
           0 < IF 0 LIM-VAL !
             THEN    LIM-VAL @ ;
( **************************************************************
: ACQUIRE
        $0F AND
        DUP $20 OR    ( START CONVERT BIT
        ADCSR C!      ( START CONVERT
        BEGIN    ADCSR C@  ( GET STATUS
        $7F > UNTIL
```

```
            DUP 7 > IF 4 - THEN      ( To shift down the ADDR for ch 8 & 9
            DUP 3 > IF 4 - THEN      ( To    "      "    "   "     "   ch 4 to 7
            2* ADDR0 + @
            LSR6 ;
( *********************************************************************
: ANALOG
            0 ACQUIRE   V-GND                          !   ( Channel 0
            1 ACQUIRE   V-GND @ - S-DC-IN              !   ( Channel 1
            2 ACQUIRE   V-GND @ - S-PK-IN              !   ( Channel 2
            3 ACQUIRE   V-GND @ - M-DC-IN              !   ( Channel 3
            4 ACQUIRE   V-GND @ - M-PK-IN              !   ( Channel 4
            5 ACQUIRE   V-GND @ - PEAK-SP-IN           !   ( Channel 5
            6 ACQUIRE   V-GND @ - M-DC-SP-IN           !   ( Channel 6
            7 ACQUIRE   V-GND @ - S-DC-SP-IN           !   ( Channel 7
            8 ACQUIRE   V-GND @ - PEAK-DL-IN           !   ( Channel 8
            9 ACQUIRE   V-GND @ - VIBE-IN              !   ( Channel 9
            ;
( *********************************************************************
( scale all inputs to eng units using input*m/n+p format
( All inputs are /2 in hdwr and 4.88 mv/bit
( Cap probe cal => 125 mv/mil   5.00VDC offset  .0254 mm/mil
: SCALE             (   m     n       p      - offsets
            S-DC-IN       @ 10    1    */ 1600  - S-DC    !
            S-PK-IN       @ 1     1    */    0  - S-PK    !
            M-DC-IN       @ 10    1    */ 1600  - M-DC    !
            M-PK-IN       @ 1     1    */    0  - M-PK    !
            PEAK-SP-IN    @ 3     2    */    0  + M-PEAK-SP   !
            PEAK-DL-IN    @ 1     1    */    0  + PEAK-DL     !
            M-DC-SP-IN    @ 10    1    */    0  + M-DC-SP     !
            S-DC-SP-IN    @ 10    1    */    0  + S-DC-SP     !
            VIBE-IN       @ 5     1    */    0  + VIBE        !      ;
( *********************************************************************
( Protection and Alarm logic
: PROTECTION
            0 TRIP !
            VIBE      @ 2000 > IF 1 1 TRIP ! HI-VIBE    ! ENDIF
            M-GAP     @   0 < IF 1 1 TRIP ! LO-M-GAP.   ! ENDIF
            S-GAP     @   0 < IF 1 1 TRIP ! LO-S-GAP    ! ENDIF ;
( *********************************************************************
: FILTER                  ( Smooth the error values
            M-PK @ M-PK-OLD @ - K-FILTER 100 */ M-PK-OLD @ + M-PK-F !
                M-PK-F @ M-PK-OLD !
            S-PK @ S-PK-OLD @ - K-FILTER 100 */ S-PK-OLD @ + S-PK-F !
                S-PK-F @ S-PK-OLD !
            M-DC @ M-DC-OLD @ - K-FILTER 100 */ M-DC-OLD @ + M-DC-F !
                M-DC-F @ M-DC-OLD !
            S-DC @ S-DC-OLD @ - K-FILTER 100 */ S-DC-OLD @ + S-DC-F !
                S-DC-F @ S-DC-OLD !            ;
( *********************************************************************
: CALCS          ( Calculate gaps, dc and errors
            FILTER
            700 M-DC-F @ 10 / M-PK-F @ + - M-GAP !   ( 700 bits hits the wall
            700 S-DC-F @ 10 / S-PK-F @ + - S-GAP !
            M-DC-SP @ M-DC-F @ - M-DC-ERR !
            S-DC-SP @ S-DC-F @ - S-DC-ERR !
            M-PEAK-SP @ 100 + PEAK-DL @ - S-PEAK-SP !        ( 100 Offset
            M-PEAK-SP @ M-PK-F @ - M-PK-ERR !
            S-PEAK-SP @ S-PK-F @ - S-PK-ERR ! ;
( *********************************************************************
: INIT4  10 M-K-I-DC    ! 150 M-K-I-PK   !        ( I-DC 7=>5
```

124

```
                3 M-K-P-DC       !    50 M-K-P-PK    !         ( P-DC 2=>2
               10 S-K-I-DC       !   150 S-K-I-PK    !         ( I-DC 7=>5
                3 S-K-P-DC       !    50 S-K-P-PK    ! ;       ( P-DC 3=>2
( *************************************************************************
: M-PK-LOOP          ( Master Stroke Control Loop
          ( Calculate integral part
          ( X = K [ U + UZ ] + XZ
          M-SSAT @ 0= IF
                  M-PK-ERR @ M-K-I-PK @ 1000 */ M-K-I-S-U !
                  M-K-I-S-U @ M-K-I-S-UZ @ M-K-I-S-XZ @ + + M-K-I-S-X !
                  M-K-I-S-U @ M-K-I-S-UZ !
                  M-K-I-S-X @ M-K-I-S-XZ !
          ( Calculate proportional part and sum
          THEN  M-PK-ERR @  M-K-P-PK @ 1000 */ M-K-I-S-X @ + M-PK-DEM !
          ( Limit stroke amplitude if gap is too small
(         M-GAP @ M-GAP-SP @ < IF M-PK-LIM @ M-PK-DEM ! THEN
                  M-PK-DEM @ DUP 254 > SWAP 1 < OR IF
                  1 M-SSAT ! ELSE 0 M-SSAT ! ENDIF
          M-PK-DEM @ DALIMIT M-PK-DEM ! ;
( *************************************************************************
: S-PK-LOOP          ( Slave Stroke Control Loop

          ( Calculate integral part
          ( X = K [ U + UZ ] + XZ
          S-SSAT @ 0= IF
                  S-PK-ERR @ S-K-I-PK @ 1000 */ S-K-I-S-U !
                  S-K-I-S-U @ S-K-I-S-UZ @ S-K-I-S-XZ @ + + S-K-I-S-X !
                  S-K-I-S-U @ S-K-I-S-UZ !
                  S-K-I-S-X @ S-K-I-S-XZ !
          ( Calculate proportional part and sum
          THEN  S-PK-ERR @  S-K-P-PK @ 1000 */ S-K-I-S-X @ + S-PK-DEM !
          ( Limit stroke amplitude if gap is too small
(         S-GAP @ S-GAP-SP @ < IF S-PK-LIM @ S-PK-DEM ! THEN
                  S-PK-DEM @ DUP 254 > SWAP 1 < OR IF
                  1 S-SSAT ! ELSE 0 S-SSAT ! ENDIF
          S-PK-DEM @ DALIMIT S-PK-DEM ! ;
( *************************************************************************
: S-ADDER          (    adds stroke delta pot to master and sends it to slave
          100 PEAK-DL @ - 10 / M-PK-DEM @ + S-PK-DEM !      ;
( *************************************************************************
: M-DC-LOOP          ( Master DC Error Control Loop
        . ( Calculate integral part
          M-DSAT @ 0= IF
          CSTATE @ STABILIZE = IF 4 M-K-I-DC ! 1 M-K-P-DC ! ELSE INIT4 THEN
                  M-DC-ERR @ M-K-I-DC @ 2000 */ M-K-I-D-U !
                  M-K-I-D-U @ M-K-I-D-UZ @ M-K-I-D-XZ @ + + M-K-I-D-X !
                  M-K-I-D-U @ M-K-I-D-UZ !
                  M-K-I-D-X @ M-K-I-D-XZ !
          ( Calculate proportional part and sum
          THEN  M-DC-ERR @  M-K-P-DC @ 2000 */ M-K-I-D-X @ + M-DC-DEM !
                  M-DC-DEM @ DUP 254 > SWAP 1 < OR IF
                  1 M-DSAT ! ELSE 0 M-DSAT ! ENDIF
          M-DC-DEM @ DALIMIT M-DC-DEM ! ;
( *************************************************************************
: S-DC-LOOP          ( Slave DC Error Control Loop
          ( Calculate integral part
          S-DSAT @ 0= IF
          CSTATE @ STABILIZE = IF 4 S-K-I-DC ! 1 S-K-P-DC ! ELSE INIT4 THEN
                  S-DC-ERR @ S-K-I-DC @ 2000 */ S-K-I-D-U !
                  S-K-I-D-U @ S-K-I-D-UZ @ S-K-I-D-XZ @ + + S-K-I-D-X !
```

```
                    S-K-I-D-U @ S-K-I-D-UZ !
                    S-K-I-D-X @ S-K-I-D-XZ !
            ( Calculate proportional part and sum
            THEN   S-DC-ERR @  S-K-P-DC @ 2000 */ S-K-I-D-X @ + S-DC-DEM !
                    S-DC-DEM @ DUP 254 > SWAP 1 < OR IF
                    1 S-DSAT ! ELSE 0 S-DSAT ! ENDIF
            S-DC-DEM @ DALIMIT S-DC-DEM ! ;
( ************************************************************************
: INIT1 DIS
        P5-DDR-DATA P5-DDR C!    ( Init port 5
        P6-DDR-DATA P6-DDR C!    ( Init port 6
        3 DUP CFIGM ! $01F0 C!   ( Set Ports A&B to Output
        MF
        SET-PP
        0 TRIP !                 ( Clear TRIP word
        INACTIVE CSTATE !        ( Init state to INACTIVE
        $01 P6 C!                ( State action
        10 SWTIMER     !         ( Setup the timer
        IBM                      ( Setup for pc terminal
        0  M-PK-ERR   !  0  M-DC-ERR   !   0  LO-M-GAP  !   0  LO-S-GAP  !
        0  S-PK-ERR   !  0  S-DC-ERR   !   0  M-GAP-SP  !   0  M-PEAK-SP !
        0  M-K-I-S-U  !. 0  M-K-I-S-X` !   0  S-GAP-SP  !   0  S-PEAK-SP !
        0 .M-K-I-D-U  !  0` M-K-I-D-X  !   0  M-GAP     !   0  S-GAP     !
        0  S-K-I-S-U  !  0  S-K-I-S-X  !   0 RAMP-TIM   !   0  STAB-TIM  !
        0  S-K-I-D-U  !  0  S-K-I-D-X  !   1 M-PK-DEM   !   1  M-DC-DEM  !
        0  HI-VIBE    !  0  RESET-BIT  !   1 S-ON       !  -1  M-ON      !
        1  S-PK-DEM   !  1 S-DC-DEM    !   0 LOOP-TIM   !   9  LOOP-TAR  !
        0  M-DC-OLD   !  0 M-PK-OLD    ! 140 RAMP-TAR   ! 250  STAB-TAR  !
        0  S-DC-OLD   !  0 S-PK-OLD    !  50 PK-TAR     !   0  CLICK     !
        EIS                      ( Enable Interrupts
        $08 @ $08 OR $08 C!  ;   ( Enable output compare interrupt
( ************************************************************************
: INIT2
        0  M-K-I-S-UZ  !  0  S-K-I-S-UZ  !  0  M-SSAT    !  0  S-SSAT     !
        0  M-K-I-S-XZ  !  0  S-K-I-S-XZ  !  0  M-DSAT    !  0  S-DSAT     !
        0  M-K-I-D-UZ  !  0  S-K-I-D-UZ  !  0  M-DC-DEM  !  0  S-DC-DEM   !
        0  M-K-I-D-XZ  !  0  S-K-I-D-XZ  !  0  M-PK-DEM  !  0  S-PK-DEM   !
        0  M-K-I-D-X   !  0  S-K-I-D-X   !
        0  M-K-I-S-X   !  0  S-K-I-S-X   !  ;
( ************************************************************************
(               Digital I/O Set-up   1 = ON
( Bit 7 6 5 4 3 2 1 0 Port6  Pin
( Out - - - - - - - 1  01H   C11  E-stop
( Out - - - - - - 1 -  02H.  C10  Flash
( Out - - - - - 1 - -  04H   C9   Run
( Out - - - - 1 - - -  08H   C8
( In  - - - 1 - - - -  10H   C7
( In  - - 1 - - - - -  20H   C6
( In  - 1 - - - - - -  40H . C5   Calibrate
( In  1 - - - - - - -  80H   C4   E-stop
( ************************************************************************
: INACTIVE-ACTION
        ( Test For State Transition
                ( calibrate switch on ?
        P6 C@ $40 AND $40 = IF
                CALIBRATE CSTATE ! 5 SWTIMER !
                THEN
                ( Do mode action
                ( E-stop on or trip flag set ?
        P6 C@ $80 AND $80 = TRIP @ 1 = OR IF $01 P6 C! ( E-stop out
```

126

```
                    INIT2                ( now check for e-stop sw cycling
        P6 C@ $80 AND $80 = TRIP @ 1 = AND IF 1 RESET-BIT ! THEN
        P6 C@ $80 AND $00 = RESET-BIT @ 1 = AND IF 0 TRIP ! THEN
                ELSE $00 P6 C! RAMPUP CSTATE !  0 RESET-BIT !
                0 SWTIMER !  0 RAMP-TIM !
                0 HI-VIBE !  0 LO-M-GAP !  0 LO-S-GAP !  PAGE THEN ;
( ************************************************************************
: RAMPUP-ACTION
        ( Test For State Transition
                ( E-stop on or trip flag set ?
        P6 C@ $80 AND $80 = TRIP @ 1 = OR IF
                INACTIVE CSTATE ! 0 SWTIMER !
                THEN
                ( calibrate switch on ?
        P6 C@ $40 AND $40 = IF
                CALIBRATE CSTATE ! 5 SWTIMER !
                THEN
        ( Do Mode Action
        CSTATE @ RAMPUP = IF
        CLICK @ 2 < IF CLICK @ 1 + CLICK ! ELSE 0 CLICK !
        RAMP-TIM @ 1 + RAMP-TIM !
            M-DC-DEM @ 32  > IF
                ELSE M-DC-DEM @ 1 + M-DC-DEM ! THEN
            S-DC-DEM @ 32  > IF
                ELSE S-DC-DEM @ 1 + S-DC-DEM ! THEN
            M-PK-DEM @ 124 > IF
                ELSE M-PK-DEM @ 1 + M-PK-DEM ! THEN
            S-PK-DEM @ 124 > IF
                ELSE S-PK-DEM @ 1 + S-PK-DEM ! THEN
        RAMP-TIM @ RAMP-TAR @ = IF
            32  M-K-I-D-UZ !    32  S-K-I-D-UZ !
            STABILIZE CSTATE !  0 SWTIMER  !
                0 RAMP-TIM !  0 STAB-TIM !  0 CLICK  !
        THEN THEN THEN ;
( ************************************************************************
: STABILIZE-ACTION
        ( Test For State Transition
                ( E-stop on or trip flag set ?
        P6 C@ $80 AND $80 = TRIP @ 1 = OR IF
                INACTIVE CSTATE ! 0 SWTIMER !
                THEN
                ( calibrate switch on ?
        P6 C@ $40 AND $40 = IF
                CALIBRATE CSTATE ! 5 SWTIMER !
                THEN
        ( Do Mode Action   New & improved
        CSTATE @ STABILIZE = IF
                4 LOOP-TAR !    ( loop switch timer
                S-ON @ 1 = IF S-DC-LOOP   THEN
                M-ON @ 1 = IF M-DC-LOOP   THEN
        SWTIMER @ 250 = IF       ( wait a while before finishing ramp
                CLICK @ 2 < IF CLICK @ 1 + CLICK ! ELSE 0 CLICK !
                        ( only ramp to sp-50
                M-PEAK-SP @ 50 - M-PK-F @ < IF
                    ELSE M-PK-DEM @ 1 + M-PK-DEM !
                        S-PK-DEM @ 1 + S-PK-DEM ! THEN
                THEN                ( the timers almost up ,so finish the ramp
                STAB-TAR @ 30 - STAB-TIM @ < IF
                M-PK-F @ S-PK-F @ > IF  ( see whose biggest
                M-PEAK-SP @ 10 - M-PK-F @ > IF M-PK-DEM @ 1 + M-PK-DEM !
```

```
                                                 S-PK-DEM @ 1 + S-PK-DEM ! THEN
                    ELSE    ( push em both until one is close to m-sp
                M-PEAK-SP @ 10 - S-PK-F @ > IF S-PK-DEM @ 1 + S-PK-DEM !
                                             M-PK-DEM @ 1 + M-PK-DEM ! THEN
                    THEN   THEN       ( now finish the timer
            STAB-TIM @ 1 + DUP STAB-TIM ! STAB-TAR @ = IF
            RUN CSTATE ! 0 STAB-TIM !  0 CLICK !
            M-PK-DEM @ M-K-I-S-UZ !   S-PK-DEM @ S-K-I-S-UZ !
            THEN
        ELSE SWTIMER @ 1 + SWTIMER !   THEN   THEN   ;
( *****************************************************************
: RUN-ACTION
        ( Test For State Transition
                ( E-stop on or trip flag set ?
        P6 C@ $80 AND $80 = TRIP @ 1 = OR IF
            INACTIVE CSTATE ! 0 SWTIMER !
            THEN
            ( calibrate switch on ?
        P6 C@ $40 AND $40 = IF
            CALIBRATE CSTATE ! 5 SWTIMER !
            THEN
        ( Do Mode Action
        CSTATE @ RUN = IF
            2 LOOP-TAR !       ( loop switch timer
            10 SWTIMER !       ( new & improved w/adder
            $04 P6 C!          ( turn on run led
        PROTECTION
        S-ON @ 1 = IF S-DC-LOOP S-ADDER    THEN
        M-ON @ 1 = IF M-DC-LOOP M-PK-LOOP THEN   THEN   ;
( *****************************************************************
: CALIBRATE-ACTION
                ( calibrate switch on ?
        P6 C@ $40 AND 0= IF
            INACTIVE CSTATE ! 0 SWTIMER !
            THEN
            ( Do mode action
        CSTATE @ CALIBRATE = IF
            140 M-PK-DEM ! 40 M-DC-DEM !
            140 S-PK-DEM ! 40 S-DC-DEM !   THEN ;
( *****************************************************************
: LOOP-SWITCH
        LOOP-TIM @ LOOP-TAR @ > IF S-ON @ -1 * S-ON !   M-ON @ -1 * M-ON !
        0 LOOP-TIM !   THEN ;
( *****************************************************************
: SUPER          ( Supervisor State Machine
        CSTATE @ CASE
                INACTIVE  OF   INACTIVE-ACTION   ENDOF
                RAMPUP    OF   RAMPUP-ACTION      ENDOF
                STABILIZE OF   STABILIZE-ACTION ENDOF
                RUN       OF   RUN-ACTION        ENDOF
                CALIBRATE OF   CALIBRATE-ACTION ENDOF
        ENDCASE ;
( *****************************************************************
: CONTROL                ( Main loop
        OTIME   ANALOG  SCALE  CALCS  SUPER   LOOP-SWITCH
        ?TIME TLOAD !   DA   ;
( *****************************************************************
: SHOW
        HOME
        " x           Mode: " 1 SPACES
```

128

```
        CSTATE @ CASE
                INACTIVE  OF  ." INACTIVE   "   0 3 .R 3 SPACES ENDOF
                CALIBRATE OF  ." CALIBRATE  "                     ENDOF
                RAMPUP    OF  ." RAMP UP    "
                        RAMP-TAR @ RAMP-TIM @ - 3 .R 3 SPACES ENDOF
                STABILIZE OF  ." STABILIZE  "
                        STAB-TAR @ STAB-TIM @ - 3 .R 3 SPACES
                        STAB-TAR @ SWTIMER  @ - 4 .R 3 SPACES ENDOF
                RUN       OF  ." RUN        "   0 3 .R 3 SPACES ENDOF
        ENDCASE   CR
(                              TLOAD @ 10 5333 */   .  4 SPACES CR
        CSTATE @ CASE
                STABILIZE OF  17 SPACES  ." DC  loops active " ENDOF
                RUN       OF  17 SPACES  ." All loops active " ENDOF
                INACTIVE  OF  17 SPACES  ."                 " ENDOF
        ENDCASE    CR     CR
        ." Master DC SP  : " M-DC-SP @ 10 / 4 .R 3 SPACES
        ." Peak SP  : "      M-PEAK-SP    @ 4 .R 3 SPACES
            M-ON @ 1 = IF ." On " ELSE ."      " THEN   CR
        ."            Pos : " M-DC-F  @ 10 / 4 .R 3 SPACES
        ."       Pos : "      M-PK-F      @ 4 .R 3 SPACES
        ." Gap : "     .      M-GAP       @ 4 .R 3 SPACES CR
        ."           Dem : " -M-DC-DEM    @ 4 .R 3 SPACES
        ."       Dem : "      M-PK-DEM    @ 4 .R 3 SPACES CR
        CR
        ." Slave  DC SP  : " S-DC-SP @ 10 / 4 .R 3 SPACES
        ." Peak SP  : "      S-PEAK-SP    @ 4 .R 3 SPACES
            S-ON @ 1 = IF ." On " ELSE ."      " THEN CR
        ."            Pos : " S-DC-F  @ 10 / 4 .R 3 SPACES
        ."       Pos : "      S-PK-F      @ 4 .R 3 SPACES
        ." Gap : "            S-GAP       @ 4 .R 3 SPACES CR
        ."           Dem : " S-DC-DEM     @ 4 .R 3 SPACES
        ."       Dem : "      S-PK-DEM    @ 4 .R 3 SPACES CR
(       CR
        ." Vibration : "     VIBE         @ 4 .R 3 SPACES CR
(       4  SPACES ." M-DSAT   :   " M-DSAT    @ U. 4 SPACES
(       4  SPACES ." M-SSAT   :   " M-SSAT    @ U. 4 SPACES CR
        LO-M-GAP     @ 1 = IF ." LO-M-GAP " ELSE 10 SPACES THEN
        LO-S-GAP     @ 1 = IF ." LO-S-GAP " ELSE 10 SPACES THEN CR
        HI-VIBE      @ 1 = IF ." HI VIBE  " ELSE 10 SPACES THEN CR
        TRIP         @ 1 = IF ." Tripped.....turn E-stop on to reset " THEN CR
        RESET-BIT    @ 1 = IF ." Resetting...turn E-stop off to run  " THEN CR
        LOOP-TIM @ 1 + LOOP-TIM ! ;
( ***********************************************************************
88 USER %CTR   ( an 8 bit variable)
90 USER %TIMER
: +TIME        ( Interrupting word that increments %TIMER
        $08 C@ $09 @ 2DROP     ( Clear timer 1 overflow flag
        1 %TIMER +!            ( increment variable
        RETURN;
: INIT3  DIS
        $04 $08 C!             ( enable overflow interrupt
        $8 C@ $8 OR $8 C!      ( new line
        0 %TIMER !  0 $09  !   ( clear timer
        EIS ;
TOI ASSIGN +TIME              ( set up task switch
( ***********************************************************************
: X
   DIS ;
: INTWORK          ( one pass through a regularly occurring sequence
```

```
   1 %CTR C+!                    ( increment a byte variable)
   %CTR C@ 0=    IF              ( true every 256 'loops'
   DIS SHOW EIS                  ( Display page
   THEN  4800 LATER RETURN;      ( 4800 = 0.8138us * 256 * 480 = 1 sec

 OCI ASSIGN INTWORK
( ***********************************************************************
: GO         ( foreground program
   INIT1 INIT2 INIT3 INIT4
   PAGE                  ( Send Clear Screen to terminal
        BEGIN  CONTROL
        300 MS
   ?TERMINAL UNTIL ;   ( stop on cntrl/c
   SET GO                  (   USE THIS LINE IN FINAL VERSION
```

DISTRIBUTION LIST

AUL/LSE
Bldg 1405 - 600 Chennault Circle
Maxwell AFB, AL 36112-6424   1 cy

DTIC/OCC
Cameron Station
Alexandria, VA 22304-6145   2 cys

AFSAA/SAI
1580 Air Force Pentagon
Washington, DC 20330-1580   1 cy

PL/SUL
Kirtland AFB, NM 87117-5776   2 cys

PL/HO
Kirtland AFB, NM 87117-5776   1 cy

Official Record Copy

  PL/VTPT/Capt Jeffrey Wiese   2 cys

Dr. R. V. Wick   1 cy
PL/VT
Kirtland, AFB, NM 87117-5776